creative commons
COMMONS DEED

저작자표시-비영리-변경금지 2.0 대한민국

이용자는 아래의 조건을 따르는 경우에 한하여 자유롭게

- 이 저작물을 복제, 배포, 전송, 전시, 공연 및 방송할 수 있습니다.

다음과 같은 조건을 따라야 합니다:

저작자표시. 귀하는 원저작자를 표시하여야 합니다.

비영리. 귀하는 이 저작물을 영리 목적으로 이용할 수 없습니다.

변경금지. 귀하는 이 저작물을 개작, 변형 또는 가공할 수 없습니다.

- 귀하는, 이 저작물의 재이용이나 배포의 경우, 이 저작물에 적용된 이용허락조건을 명확하게 나타내어야 합니다.
- 저작권자로부터 별도의 허가를 받으면 이러한 조건들은 적용되지 않습니다.

저작권법에 따른 이용자의 권리는 위의 내용에 의하여 영향을 받지 않습니다.

이것은 이용허락규약(Legal Code)을 이해하기 쉽게 요약한 것입니다.

Disclaimer

dCollection

工學博士 學位論文

A New Reactive Power Control Method of Intermittent Distributed Generators for Conservation Voltage Reduction

Conservation voltage reduction을 위한 새로운

分散電源의 無效電力 制御技法에 대한 硏究

2014年 8月

서울大學校 大學院

電氣·컴퓨터工學部

黃 玶 益

A New Reactive Power Control Method of Intermittent Distributed Generators for Conservation Voltage Reduction

指導敎授 文 承 逸

이 論文을 工學博士 學位論文으로 提出함

2014 年 4月

서울大學校 大學院

電氣・컴퓨터工學部

黃 玶 益

黃玶益의 工學博士 學位論文을 認准함

2014 年 6月

委 員 長 _____ (인)

副委員長 _____ (인)

委 員 _____ (인)

委 員 _____ (인)

委 員 _____ (인)

Abstract

A New Reactive Power Control Method of Intermittent Distributed Generators for Conservation Voltage Reduction

Pyeong-Ik Hwang

School of Electrical Engineering and Computer Science

The Graduate School

Seoul National University

This dissertation proposes a network-model-based conservation voltage reduction (CVR) method considering distributed generators (DGs) and a novel reactive power controller for intermittent DGs to achieve reliable and economical CVR.

CVR is a concept linked to reductions in energy consumption through reduced voltage amounts supplied to customers. The network-model-based CVR method implements CVR in a centralized manner and determines the references for volt/var control devices based on an optimization scheme. The impacts of DGs on the network-model-based CVR method were analyzed. The result showing that the inaccuracies of the DG model and intermittent active power can degrade the CVR effect. Moreover, intermittent active power can increase the operation cost of a distribution system by causing frequent switching operations of tap changes and shunt capacitors. Because the CVR function is periodically executed with a certain time interval in a distribution management system (DMS), these problems cannot be solved by using only

the CVR function. In other words, both the CVR function and the local control system should be utilized.

This dissertation proposes unified models for a three-wire voltage source converter (VSC), which is widely used in DG interface systems, for an unbalanced steady-state analysis. In a steady state, the active and reactive power supplied by a DG depends on the terminal voltage, output filter, voltage and current sensor positions, and power control strategy. Considering these factors, two equivalent circuit models consisting of an equivalent three-phase current source (ETCS) and some of filter impedances are proposed. In addition, the current output of each ETCS is formulated as a function of the active and reactive power reference, the terminal voltage, and the impedances of the output filter. With unified models, 35 different three-wire VSC types can be represented. The accuracy of the models are verified by comparing the results of a power flow study to results obtained from a PSCAD simulation.

In order to reduce the adverse effects of the intermittent DG on CVR, this dissertation proposes a new reactive power control method which it terms the "*two-segment active power versus reactive power (Q–P) droop method*". The reactive power is controlled based only on the measured active power; thus, the proposed method corresponds to the general interconnection requirements for DGs. The relationship between the active and reactive power is represented by two line segments given by the active and reactive power references and the lower and upper droop constants. If the active power is lower than its reference, the lower droop determines the reactive power. Otherwise, the upper droop constant does. The droop constants are not fixed; they are determined by the CVR function in the DMS.

This dissertation proposes a network-model-based CVR method. In order to

prevent frequent switching operations, the expected value of the active power for an intermittent DG, which changes slowly over time, is used to formulate the optimization problem. By solving the optimization problem, the references for the volt/var control devices are determined. Finally, the droop constants are determined based on the optimal state. In order to reduce the computational burden, the droop constants are calculated with the sensitivities. The droop constants are initially estimated under the assumption that only the active power output of a DG changes. Later, the droop constants are corrected considering the active power variations of multiple DGs.

In a case study using the modified IEEE 123-node test feeder with three DGs, it is shown that the effect of CVR is improved with the proposed models and methods. Specifically, with the proposed reactive power control method for an intermittent DG, the CVR effect can be remarkably improved.

Keywords:

Voltage and var control, Conservation voltage reduction, Distributed generator, Reactive power control, Droop control

Student Number: 2006-21324

Contents

Abstract I
Contents IV
List of Tables VIII
List of Figures X

Chapter 1 Introduction 1
1.1 Motivation and purpose 1
1.2 Highlights and contributions 4
1.3 Dissertation organization 5

Chapter 2 Technical Issues in CVR Considering DGs 9
2.1 Conservation voltage reduction 9
2.1.1 Concept and effects 9
2.1.2 Volt/var control devices 12
2.1.3 Methods for implementing CVR 14
2.1.4 Effect of DGs on a network-model-based CVR 16
2.2 Three-phase steady-state models for a DG 19
2.2.1 Synchronous generator 20
2.2.2 Induction generator 21
2.2.3 Voltage source converter 21
2.3 Reactive power control method 23
2.3.1 Passive methods 24
2.3.2 Active methods 25

Chapter 3 Three-phase Steady-State Models for a Three-Wire VSC 29
3.1 Power output characteristics of a VSC 29
3.2 Voltage and current sensor positions.....31
3.3 Power control strategy 33
3.3.1 Voltage-controlled method..... 34
3.3.2 Current-controlled method..... 36
3.4 Proposed models 42
3.4.1 Equivalent circuit models 42
3.4.2 Voltage-controlled VSC models..... 43
3.4.3 Current-controlled VSC models..... 48
3.4.4 Unified models..... 54
3.5 Verification of the proposed models 57
3.5.1 Single node system 58
3.5.2 Modified IEEE 13-node test feeder 62

Chapter 4 Reactive Power Control Method for Intermittent DGs.....65
4.1 Characteristics of conventional reactive power control methods.....65
4.2 Two-segment reactive power versus active power control ...70
4.2.1 Basic concept 70
4.2.2 Operational characteristics..... 71

Chapter 5 CVR Function for a DMS 75
5.1 Active power determination for intermittent DGs 77

5.2 Reference determination for volt/VAr control devices 79
5.2.1 Load modeling 79
5.2.2 OPF problem formulation 80
5.2.3 Solution method for the OPF 82
5.3 Droop constants determination for intermittent DGs.....84
5.3.1 Estimation of initial droop constants 84
5.3.2 Correction of droop constants 89
5.4 Illustrative example.....98
5.4.1 Test system..... 98
5.4.2 CVR results..... 100
5.4.3 Droop constants determination method ..... .103

Chapter 6 Case Study.....107
6.1 Introduction to the test system 107
6.2 Effect of the DG model.....109
6.3 Effect of the two-segment *Q*–*P* droop control method.....111
6.4 Effect of the active power determination method.....116

Chapter 7 Conclusions and Future Extensions 119
7.1 Conclusions.....119
7.2 Future Extensions.....123

Bibliography.....125

Appendix A. Results of VSC Model Verification.....135
A.1 Single node system 135

A.2 Modified IEEE 13-node test feeder 138

Appendix B. Voltage Sensitivity Matrices.....141

B.1 Power injection sensitivity matrices with respect to the three-phase power of a DG.....141

B.2 Voltage sensitivity matrices with respect to the three-phase power of a DG.....146

Appendix C. Detailed Data of Case Study 149

C.1 Initial state of the volt/var control devices.....149

C.2 References of the volt/var control devices for the effect of the DG model.....150

C.2.1 Balanced model..... 150

C.2.2 Proposed model..... 151

C.3 References of the volt/var control devices for the effect of the two-degment *Q*–*P* droop control method 152

C.3.1 Fixed reactive power control 152

C.3.2 Fixed voltage control 153

C.3.3 Two-segment *Q*–*P* droop control..... .154

국문초록.....157

감사의 글.....161

List of Tables

Table 2.1 Effect of CVR 11
Table 2.2 Grid interface systems for DGs 19
Table 3.1 Coefficients of unified models for a voltage-controlled VSC 55
Table 3.2 Coefficients of unified models for a current-controlled VSC..... 56
Table 3.3 Main DG parameters 57
Table 4.1 Voltages of the base case 66
Table 4.2 Voltage variations according to reactive power control methods 68
Table 5.1 Volt/var control devices and corresponding variables determined by the CVR function..... 76
Table 5.2 Step voltage regulator in the IEEE 13-node test feeder..... 98
Table 5.3 Shunt capacitors in the IEEE 13-node test feeder..... 98
Table 5.4 Active power consumption changes of the loads..... 103
Table 6.1 Loads in the IEEE 123-node test feeder 108
Table 6.2 Tap changers in the IEEE 123-node test feeder..... 108
Table 6.3 Shunt capacitors in the IEEE 123-node test feeder..... 108
Table A.1 Maximum differences of DG output currents between the PSCAD simulation and the power flow: Cases 1 and 2 for the single node system..... 135
Table A.2 Maximum differences of DG output currents between the PSCAD simulation and the power flow: Cases 3 and 4 for the single node system..... 136
Table A.3 Maximum differences of DG output currents between the PSCAD simulation and the power flow: Cases 5 and 6 for the single node system..... 137
Table A.4 Maximum current and voltage differences between the PSCAD

simulation and the power flow: Case 1 for the modified IEEE 13-node test feeder 138
Table A.5 Maximum current and voltage differences between the PSCAD simulation and the power flow: Case 2 for the modified IEEE 13-node test feeder 139
Table A.6 Maximum current and voltage differences between the PSCAD simulation and the power flow: Case 3 for the modified IEEE 13-node test feeder 140
Table C.1 Initial reactive power outputs of DGs 149
Table C.2 Initial state of ShC 1 149
Table C.3 Initial tap positions 149
Table C.4 Reactive power references for DGs: balanced model 150
Table C.5 References for ShC 1: balanced model 150
Table C.6 References for tap changers: balanced model 150
Table C.7 Reactive power references for DGs: proposed model 151
Table C.8 References for ShC 1: proposed model 151
Table C.9 References for tap changers: proposed model 151
Table C.10 Reactive power references for DGs: fixed reactive power control 152
Table C.11 References for ShC 1: fixed reactive power control 152
Table C.12 References for tap changers: fixed reactive power control 152
Table C.13 Voltage references for DGs: fixed voltage control 153
Table C.14 References for ShC 1: fixed voltage control 153
Table C.15 References for tap changers: fixed voltage control 153
Table C.16 References for DGs: two-segment *Q*–*P* droop control 154
Table C.17 References for ShC 1: two-segment *Q*–*P* droop control 154
Table C.18 References for tap changers: two-segment *Q*–*P* droop control 154

List of Figures

Figure 1.1 Dissertation organizations 7
Figure 2.1 Voltage ranges of ANSI C84.1 10
Figure 2.2 Voltage dependency of loads 10
Figure 2.3 Interconnection points of volt/var control devices 12
Figure 2.4 Effect of DGs on the minimum voltage limit for CVR 17
Figure 2.5 Configuration of a synchronous-generator-interfaced DG 20
Figure 2.6 Configuration of an induction-generator-interfaced DG 21
Figure 2.7 Configuration of a VSC-interfaced DG 22
Figure 2.8 Reactive power characteristics of a variable power factor control 25
Figure 2.9 Fixed voltage controller 26
Figure 2.10 Reactive power characteristic of Q–V droop control 26
Figure 2.11 Reactive power characteristics of a Volt/Var control 27
Figure 3.1 Overall configuration of a DG with a VSC interface 30
Figure 3.2 Output filter and possible voltage and current measurements 32
Figure 3.3 Power control strategies for a VSC 33
Figure 3.4 Equivalent circuit of a voltage-controlled VSC 34
Figure 3.5 Power control system for a voltage-controlled VSC 36
Figure 3.6 Power controller based on SRFPIC 41
Figure 3.7 Classification of the VSC models 42
Figure 3.8 Equivalent-circuit models for VSCs 43
Figure 3.9 VSC with an LCL filter 43
Figure 3.10 Single node system 58
Figure 3.11 Three-phase reactive power output for different sensor positions 60
Figure 3.12 Phase power outputs for different power control strategies 60

Figure 3.13 Maximum differences of the DG output currents between the PSCAD simulation and the power flow: single node system 61
Figure 3.14 Modified IEEE 13-node test feeder 62
Figure 3.15 Difference between the PSCAD simulation and the power flow: modified IEEE 13-node test feeder 64
Figure 4.1 Reactive power outputs of conventional reactive power control methods 69
Figure 4.2 Voltage variations with the conventional reactive power control methods 69
Figure 4.3 Relationship between the active and reactive powers of two-segment *Q*–*P* droop control 71
Figure 4.4 Reactive power output and voltage of node 652 according to R^- 73
Figure 4.5 Reactive power output and voltage of node 634 according to R^+ 73
Figure 4.6 Reactive power output and voltages with $R^- = 0.5$ and $R^+ = 0.15$ 73
Figure 5.1 Probability density functions of intermittent DGs 77
Figure 5.2 Flow chart for determining the initial droop constants 88
Figure 5.3 Voltage variations with the initial lower droop constants 90
Figure 5.4 Node voltage variation with respect to the active power output change of a DG with two-segment *Q*–*P* droop controller 90
Figure 5.5 Possible trajectory of the node voltage with the two-segment *Q*–*P* droop controller 93
Figure 5.6 Flow chart for the droop constant correction 97
Figure 5.7 PDF of the active power output for DGs 99
Figure 5.8 Voltage magnitude changes of the load nodes 102
Figure 5.9 Minimum voltages with zero droop constants 105
Figure 5.10 Minimum voltages with initial droop constants 105

Figure 5.11 Minimum voltages with corrected droop constants 105
Figure 6.1 Modified IEEE 123-node test feeder 107
Figure 6.2 Reduction of the active power supplied according to the DG model 110
Figure 6.3 PDFs for active power output of the DGs..... 112
Figure 6.4 Flow chart of the CVR function for the fixed reactive power control method and the fixed voltage control method 114
Figure 6.5 Reduction of the active power supplied according to reactive power control method 114
Figure 6.6 Active power consumption of the loads 117
Figure 6.7 Active power output of the intermittent DGs 117
Figure 6.8 References for SVRs: Case 1..... 117
Figure 6.9 References for SVRs: Case 2..... 117
Figure B.1 Structure of power injection sensitivity matrices..... 142

Chapter 1. Introduction

1.1 Motivation and purpose

General motivation for studying conservation voltage reduction

The integration of distributed generators (DGs) into distribution systems is increasing owing to their various environmental and economic advantages. Theoretically, DGs can improve the reliability of the power supplied to the customers, reduce transmission and distribution losses, and save investment costs [1]. However, the high penetration of intermittent DGs, of which the active power is non-dispatchable and varies rapidly compared to the load, causes a new problem for voltage management because the conventional voltage-control devices used in a distribution system are designed to compensate for slow and gradual changes [2–4].

Driven by the advances in information and communications technology, various next-generation distribution management systems (DMSs) have been proposed for more reliable and efficient operation of the distribution system with DGs, e.g., advanced DMSs and smart DMSs [5–8]. In next-generation DMSs, the state of the distribution system can be estimated accurately from measured data using various applications. Moreover, operation resources can be controlled remotely via the communications infrastructure.

Volt/VAr control (VVC), one of the key technologies required for a DMS, maintains the voltages of the distribution system within specific bounds, such as those stated by the American National Standards Institute (ANSI) and

Canadian Standards Association (CSA) [9–10]. Conservation voltage reduction (CVR) is an expanded objective for VVC and one of the easiest ways to reduce the peak load and total annual energy consumption [4, 11]. The basic idea of CVR is that the active and reactive power demands of a load generally decrease as the voltage decreases. The reduction of the reactive power demand decreases the line loss of the distribution system. Consequently, both the active power demand and the line loss can be reduced by lowering the voltages of the distribution system. Conventional CVR uses step voltage regulators (SVRs) and shunt capacitors (ShCs) on distribution feeders and on-load tap changers (OLTCs) on substation transformers.

The first wide-scale CVR was implemented by the American Electric Power (AEP) in 1973 [12]. Since then, numerous electric utilities have implemented CVR and evaluated its practical effects [13–21]. It has been reported that energy consumption can be reduced by 0.3–1.0% by reducing the voltage by 1.0%. The Korea Electric Power Corporation (KEPCO) established a CVR strategy that utilizes OLTCs to reduce peak loads for short periods, and has performed nationwide CVR several times. With the strategy, loads can be reduced up to 668 MW [22].

Due to the recent increase in the interconnection of DGs that can control reactive power, a DG is also considered as a controllable resource for CVR [23–25]. However, an intermittent DG can degrade the CVR effect [26]. Therefore, developing a CVR method that considers DGs is consistent with current technical trends.

Specific topics of this dissertation

This dissertation concentrates on two CVR topics that consider DGs: a network-model-based CVR method and a reactive power control method for an intermittent DG.

A network-model-based method can be used to implement CVR in a centralized manner. First, the state of the distribution system is estimated in the DMS by using applications such as state estimate and real-time power flow programs. Then, the references for the volt/var control devices are determined by solving an optimization problem. The network-model-based method has received attention as the CVR method for the next-generation DMS because it enables optimized operation of the distribution system [4].

The optimization problem is formulated by using a base case and network models. The base case consists of the voltage of the substation node, power consumption of the loads, power output of the DGs, and status of the volt/var control devices. If the measured active power output of an intermittent DG, which varies randomly, is used directly, the references for devices based on a mechanical switch, such as an OLTC, SVR, or ShC, can be changed frequently. As a result, the system operating costs increase because the switching operation reduces the device lifetime [27]. Therefore, to prevent frequent switching, instead of the measured value, an appropriate value is used as the active power output of the DG for the base case.

Meanwhile, accurate network models should be used in the CVR function to achieve reliable and economical CVR. A distribution system is an inherently unbalanced system due to unbalanced loads, single- and two-phase

lines, and untransposed lines. Therefore, accurate DG models considering unbalanced operations are needed.

The CVR function is executed periodically in the DMS because it takes time to gather the states of the distribution system and to determine the references. While waiting for execution of the CVR function, the local control system of the volt/var control devices must control the voltages within an acceptable range. If an intermittent DG is connected to the distribution system, the voltage varies rapidly owing to the active power variation of the DG. In the worst case, an under-voltage violation might occur. Unfortunately, the problem cannot be solved with conventional volt/var control devices because their response times are slow [28–29]. Therefore, the rapid voltage variation caused by the DG should be compensated for by the reactive power controller of the DG itself.

1.2 Highlights and contributions

This dissertation proposes a novel network-model-based CVR method that considers DGs. Its contributions can be divided into three areas, described as follows.

Three-wire voltage source converter model for a three-phase steady-state analysis

A voltage source converter (VSC) is used to interface the primary energy source of a DG to the main gird since the primary energy source resembles a

voltage source [30]. Under unbalanced operating conditions, the power output of the VSC depends on the voltage of the connected node, the power control strategy used, and the sensor position. Considering these, detailed three-wire VSC models for three-phase steady-state analysis are proposed.

Reactive power control method for intermittent DGs

In order to reduce the adverse effects of an intermittent DG, this dissertation proposed a novel reactive power control method, the "*two-segment reactive power versus active power (Q–P) droop control method*". This method is passive, does not use the measured voltage, and meets the general interconnection requirements [31–32]. In addition, a method to determine the control parameters is proposed.

Active power determination for intermittent DGs

A method to determine the active power output of the intermittent DG used to generate a base case for the optimization problem is proposed to prevent frequent switching and to reduce operating costs.

1.3 Dissertation organization

Chapter 1 consists of the general introduction, motivation and purpose, and highlights and contributions, and describes the organization of this dissertation.

Chapter 2 introduces the concept and effect of CVR. The impact of the DG

on CVR is described. Previous research on the DG modeling and the reactive power control method are summarized.

Chapter 3 reviews factors that determine the output of the three-wire VSC. Considering these factors, three-phase steady-state models for the VSC are proposed. The accuracy of the proposed models is verified by comparing the results of the power flow study using the proposed models with the results of a PSCAD simulation.

Chapter 4 investigates the operating characteristics of conventional reactive power control methods for an intermittent DG in terms of CVR. The requirements to improve the CVR effect with the DG are identified, and a two-segment *Q*–*P* droop control method is proposed.

Chapter 5 describes the CVR function for a DMS. Methods to determine the active power output of the intermittent DG for the base case of the optimization problem and the control parameters for the two-segment *Q*–*P* droop controller are presented. The effects of the proposed methods are verified in numerical studies using the power flow.

Chapter 6 presents case studies. The improvement of the CVR effect using the proposed methods is identified.

Chapter 7 concludes this dissertation and discusses future extensions.

In addition, Appendix A presents a method for calculating the voltage sensitivity with respect to the output power of the DG.

The organization of this dissertation is summarized in Fig. 1.1.

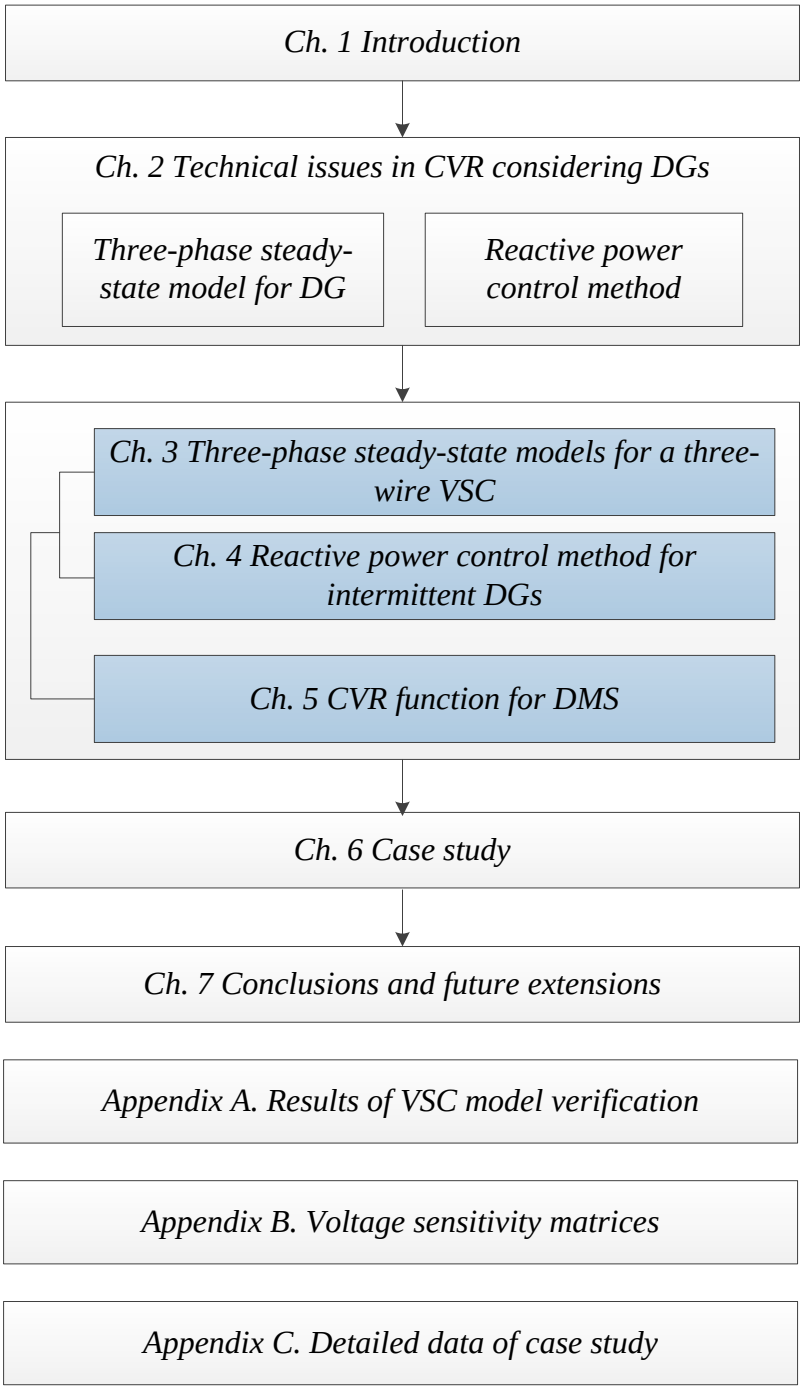

Fig. 1.1 Dissertation organizations.

Chapter 2. Technical Issues in CVR considering DGs

2.1 Conservation voltage reduction

2.1.1 Concept and effects

The distribution utilities are responsible for maintaining the voltage supplied to customers within specific ranges. For example, Fig. 2.1 shows the voltage ranges of the American National Standards Institute (ANSI) standard [9]. The voltage supplied by the utility has to be in the range denoted by the ‘Service Voltage’. Typically, utilities maintain the supplied voltage in the upper portion of this range [11].

The active and reactive power consumption of an electrical load depends on the supplied voltage. Considering this dependency, the load can be classified into a constant power, current, and impedance load [33]. The power consumption of a constant power load is constant, regardless of the voltage, as shown in Fig. 2.2, while the power consumptions of the constant current and impedance loads decrease with the voltage. According to the ANSI standard, electrical devices should be operated in the range denoted by the ‘Utilization Voltage’ in Fig. 2.1.

Therefore, the active power consumption of loads can be reduced by maintaining the voltage supplied to the customer in the lower portion of the acceptable range. In addition, a reduction in the reactive power consumption

decreases the line loss of the distribution system. Consequently, the energy consumption can be reduced without any adverse effect on customers. This is the basic concept of conservation voltage reduction (CVR).

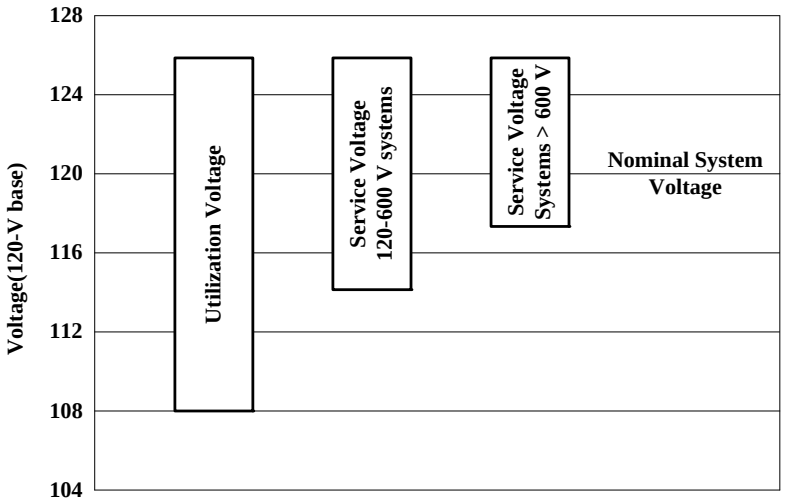

Fig. 2.1 Voltage ranges of ANSI C84.1.

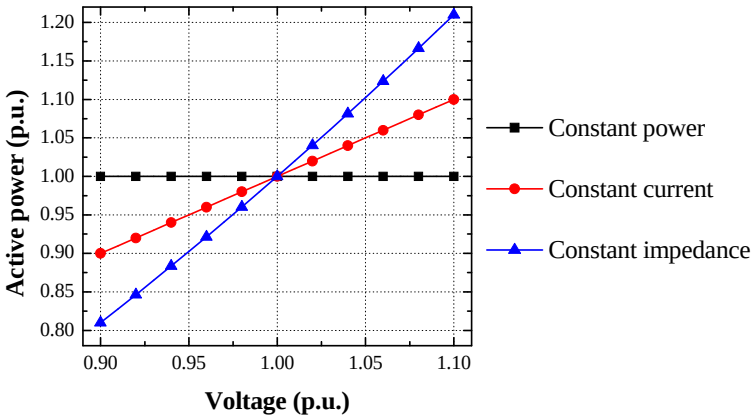

Fig. 2.2 Voltage dependency of loads.

The earliest study on a wide-scale CVR was performed by American Electric Power in 1973 [12]. Subsequently, various utilities and institutes have implemented CVR and analyzed its effects. The major findings are summarized in Table 2.1. The conservation voltage reduction factor (*CVRf*) is used to quantify the CVR effect, and is defined as

$$CVRf = \frac{\Delta E\%}{\Delta V\%}, \tag{2.1}$$

where $\Delta E\%$ is the percentage of energy saved and $\Delta V\%$ is the percentage of voltage reduction.

Table 2.1 Effect of CVR

Reference	**Year**	***CVRf***
American Electric Power [12]	1978	0.62
Northeast Utilities [13]	1987	1
Bonneville Power Administration [14]	1990	0.99
Commonwealth Edison [15]	1990	1
Snohomish [16]	1991	0.5
BC Hydro [17]	1995	0.7
Southern California Edison [18]	1995	1
Northwest Energy Efficiency Alliance [19]	2007	0.84
Electric Power Research Institute [20]	2011	0.7
Electric Power Research Institute [21]	2012	0.61

Reducing the voltage by 1% generally reduces the energy consumption by 0.5–1%. A simulation-based study showed that if CVR was implemented for all distribution feeders in the United States, 3.04% of the annual national energy consumption would be saved [34].

In addition, CVR can be used to reduce peak load for short periods. The Korea Electric Power Corporation has performed nationwide CVR to reduce peak load several times and obtained load reduction by up to 668 MW [22].

2.1.2 Volt/var control devices

Conventionally, on-load tap changers (OLTCs) on substation transformers, and step voltage regulators (SVRs) and shunt capacitors (ShCs) on distribution lines, are used for CVR. Due to a recent increase in the interconnection of distributed generators (DGs) that can control the reactive power output, the reactive power output of DGs is also considered as a resource for CVR [23–25]. The interconnection points of the devices are shown in Fig. 2.3.

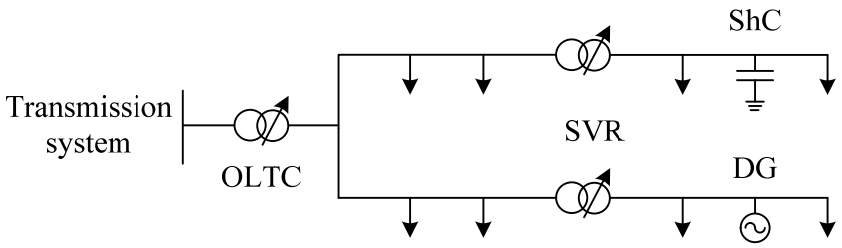

Fig. 2.3 Interconnection points of volt/var control devices.

A) On-load tap changers

Substation transformers are equipped with on-load tap changers (OLTCs), which control the voltage magnitude of the secondary side of the transformer by adjusting the turn ratio. The voltage is controlled discretely according to the tap step. Generally, an OLTC can correct the voltage by ±10% in 16 steps, with each step representing a 1.25% change in the voltage. Since the feeder lines are all connected to the secondary side of the substation transformer, the voltages in the distribution system all change similarly with changes in the tap position.

B) Step voltage regulators

A step voltage regulator (SVR) is a 1:1 autotransformer with tap changer on the series winding. Typically, an SVR can control the voltage by ±10 % in 32 steps, with each step representing a 0.625% change of the voltage. Only the voltages of nodes downstream from the SVR are changed by the tap.

C) Shunt capacitors

A shunt capacitor (ShC) is connected in parallel to a distribution line through a mechanical switch. By supplying reactive power via the ShC, the reactive power flow on the distribution line can be decreased. As a result, the voltage drop on the distribution line is reduced and the voltages of the distribution system are increased. However, the voltage changes of nodes differ to each other. In addition, the line loss of the distribution system can be reduced.

D) Distributed generators

Distributed generators (DGs), of which the gird interface system is a synchronous generator or converter, can control the reactive power output. The effects of the reactive power injection are similar to those of a ShC. However, the reactive power output can be controlled continuously, unlike with an ShC.

2.1.3 Methods for implementing CVR

The methods used for implementing CVR can be classified into open-loop methods and close-loop feedback methods [4].

A) Open-loop methods

Open-loop methods have been widely used to implement CVR. With these methods, volt/var control devices are operated based on the voltage estimated from local measurements. Since no real-time communication infrastructure is needed, open-loop methods are simple and economical ways to implement CVR. However, the CVR is not optimized for all operating conditions. In addition, the method cannot adapt to an unexpected topology change in the distribution system.

The simplest and easiest way to implement CVR with an open-loop method is by utilizing the line drop compensator (LDC) of the OLTC and SVR. The LDC estimates the voltage of a specific node from local measurements, i.e., the voltage and current. If the estimated voltage is outside the acceptable range for a certain time, the LDC changes the tap position. For CVR, the reference

voltage for the LDC is set as low as possible.

When the ShC is also used for CVR, the OLTCs, SVRs, and ShCs should be controlled in a coordinated manner. A two-step optimization algorithm based on day-ahead forecasting data was proposed to achieve an optimal coordinated control [35]. In the first step, the commitment schedule for ShCs is determined to correct power factor and to flatten the voltage profile. The second step is to determine the tap position of the OLTC and SVR to maintain the voltage profile as low as possible.

Many utilities have implemented CVR using open-loop methods utilizing OLTCs, SVRs, and/or ShCs [16, 22, 36–37].

B) Close-loop feedback method

The actual voltages of the distribution system are used for CVR in close-loop feedback methods. The voltage can be measured by using the supervisory control and data acquisition (SCADA) system and/or the advanced metering infrastructure (AMI). Based on the measured voltage, the CVR function of the distribution management system (DMS) periodically determines the references for the volt/var control devices, and these are sent to each device via a communication infrastructure. Since more reliable and optimal CVR can be achieved by using the actual voltages, close-loop feedback methods will likely be adopted for next-generation DMSs. Currently, some utilities have implemented CVR with the close-loop feedback method [19, 38–40].

According to the reference determination method in the CVR function, close-loop feedback methods can be classified into rule-based and network-model-

based methods. With rule-based methods, the references are determined based on specific rules, such as presented in [41–42]. With network-model-based methods, the references are calculated by solving the optimal power flow (OPF) representing CVR. A network-model-based CVR algorithm based on the oriented discrete coordinate descent method was proposed in [43]. Considering conventional volt/var control devices and DGs, two-timescale optimization method proposed in [23]. A slow-timescale control determines references for conventional volt/VAr control devices, while the fast-timescale control determines references for DGs. In [24], the OPF problem for CVR with respect to the DG was formulated and solutions were proposed. In [25], real-time adaptive CVR was implemented using a multi-agent system.

2.1.4 Effect of DGs on a network-model-based CVR

The OPF problem for the network-model-based CVR function is formulated using the power consumption of loads, power generation by DGs, voltages at substation nodes, and network models. The objective function of the OPF problem is to minimize the energy consumption. The voltage operational bound is represented as a constraint. In order to prevent an unexpected under-voltage by using inaccurate data to formulate the OPF problem, the minimum voltage limit used for the OPF problem must exceed the actual minimum voltage limit. This offset is called a safety margin. For a distribution system without a DG, the safety margin is determined by considering the load variation between the execution of the CVR function, the measurement error, the network model error,

etc.

If a dispatchable DG is connected to the distribution system, the safety margin may be increased to consider a possible error in the DG model, as shown in Fig. 2.4. In addition, if an intermittent DG is connected, the safety margin is increased further to consider the variation in the active power output of the DG. Consequently, interconnection of DGs can degrade the effect of CVR because the lower bound limit of the voltage is increased. Therefore, in order to minimize the adverse effects of DGs on CVR, accurate DG models should be used in the CVR function, and an appropriate reactive power control method that can reduce the adverse effects of inconsistent active power should be adopted for intermittent DGs.

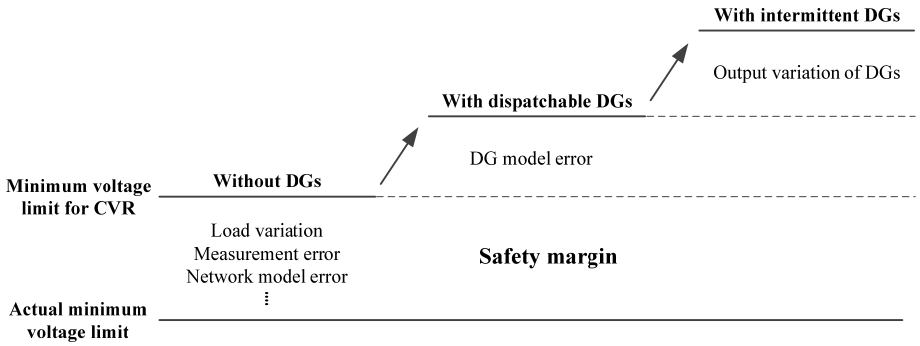

Fig. 2.4 Effect of DGs on the minimum voltage limit for CVR.

Because references for volt/var control devices are determined by solving the OPF problem, the references are sensitive to the base case of the OPF problem. If active power outputs of the intermittent DG, which vary rapidly and randomly with time, the references can be changed frequently and thus the number of switching operations can increase. The increase in the switching operations of the conventional volt/var control devices decreases lifetime of the devices and increases maintenance costs. Consequently, overall operating costs increase. To prevent frequent change in the references for the conventional volt/var control devices, a modified active power output of the intermittent DG, which varies slowly over time, should be used.

2.2 Three-phase steady-state models for a DG

The primary energy source of a DG is connected to the distribution system via an interface system, as summarized in Table 2.2. The preferred interfacing system is a synchronous generator and power electronic converter, because these can control their reactive power output. As power electronic converters, voltage source converters (VSCs) are widely used because the primary energy sources resemble a voltage source [30].

Since a distribution system is an unbalanced system inherently, accurate three-phase DG models that consider the unbalanced operation conditions should be used to achieve more reliable and economical CVR. In the steady state, the phase outputs of a DG depend on the interface system and terminal voltage. Therefore, a DG can be represent by using a model for the interface system in the steady-state analysis

Table 2.2 Grid interface systems for DGs

Interface system	Types of DGs
Synchronous generator	biomass, combined cycle gas turbine, gas turbine, geothermal, internal combustion engine, solar thermal
Induction generator	small hydropower, wind power
Power electronic converter	battery, fuel cell, micro-turbine, solar photovoltaic, wind power

2.2.1 Synchronous generator

The active and reactive powers of a synchronous-generator-interfaced DG are controlled by a governor and exciter, respectively, as shown in Fig. 2.5 [33]. The governor adjusts the active power output calculated from the sensed voltage (v_s) and current (i_s) by controlling the mechanical power output (P_{mech}) of the primary energy source. In order to achieve stable operation involving various synchronous generators, the governor generally includes a power–frequency (P–f) droop controller. The exciter controls the reactive power by adjusting the excitation voltage for field winding. Alternatively, the exciter can control the terminal voltage.

To analyze three-phase steady-state operation, the synchronous generator can be represented by the model presented in [45–46].

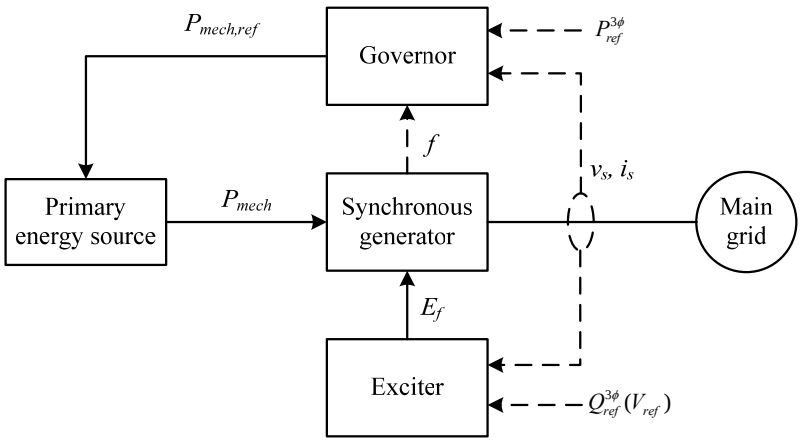

Fig. 2.5 Configuration of a synchronous-generator-interfaced DG.

2.2.2 Induction generator

The active power output of a DG can be controlled in a manner similar to the synchronous generator, as shown in Fig. 2.6. Generally, the reactive power output is not controllable, although it can be controlled in some special induction generators, such as a double-fed induction generator (DFIG).

In [47], an induction generator model for a three-phase steady-state analysis was proposed. A model for a DFIG has also been proposed and its accuracy verified [48].

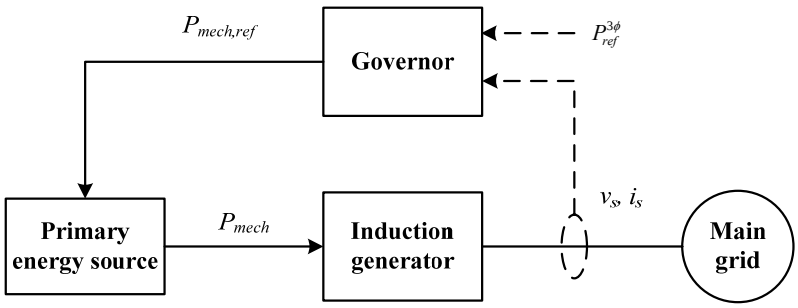

Fig. 2.6 Configuration of an induction-generator-interfaced DG.

2.2.3 Voltage source converter

Figure 2.7 shows the general configuration of a VSC-interfaced DG. The VSC is connected to the primary energy source via a direct current (DC) link and to the main grid via an output filter. The control system maintains the three-phase active and reactive power outputs calculated from the measured voltage and current at their desired values by controlling the states of the semiconductor

switches. If the primary energy source is non-dispatchable, it operates in maximum power-point tracking (MPPT) mode, and the power control system controls the DC link voltage rather than the active power.

In [49], the VSC-interfaced DG was modeled as a three-phase voltage source. Models represented in the positive–negative–zero sequence frame have been proposed [46, 50]. To verify the accuracy of the models, the power flow obtained using a model was compared to that of a PSCAD simulation. The maximum voltage difference was 0.008 p.u. (0.8%). Phase-frame-based power flow models for a VSC utilizing the vector control method were proposed in [51].

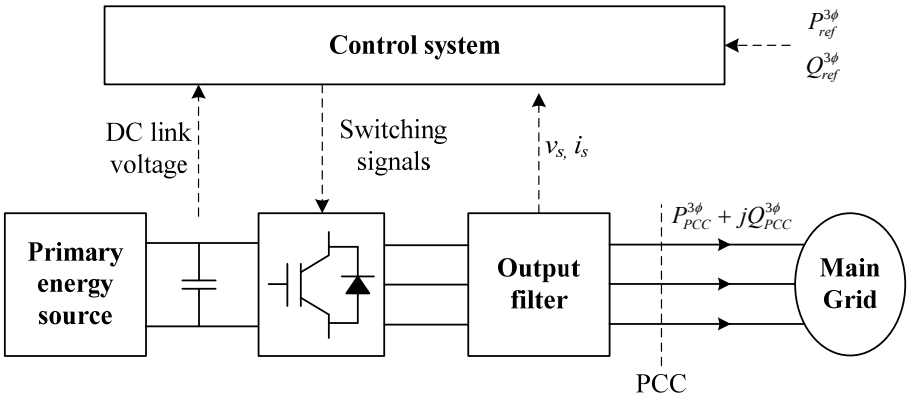

Fig. 2.7 Configuration of a VSC-interfaced DG.

2.3 Reactive power control methods

The CVR function is executed periodically in the DMS because it takes time to gather the states of the distribution system and to determine references for the volt/var control devices. While waiting for execution of the CVR function, the local controllers of the volt/var control devices are in charge of controlling the voltages of the distribution system within an acceptable range. When an intermittent DG is connected to the distribution system, the voltages are varied quickly in random directions by the inconsistent output of the DG. Unfortunately, conventional volt/var control devices, such as ShCs, SVRs, and OLTCs, cannot control this rapid random variation of the voltage due to their slow response times. Therefore, an intermittent DG must be used to compensate for the voltage variation, as the interface system is capable of controlling the reactive power quickly.

Various reactive power control methods have been proposed to determine the reactive power reference for a power controller. The methods can be classified into active methods and passive methods according to whether the voltage is used. Active methods, which use the voltage, are the simplest methods for compensating for the voltage variation introduced by either a change in the active power output of the DG or a change in the load demand. However, active voltage control of a DG can have adverse interactions with other voltage control devices. This is the one of the reasons why active methods are prohibited in IEEE standard 1547 [31]. In addition, the owner of the DG might be unwilling to adopt an active method because compensating for the voltage variation

caused by the load incurs an additional loss that reduces the benefits.

2.3.1 Passive methods

A. Fixed reactive power control

Regardless of the active power output and terminal voltage, the reactive power reference is kept constant:

$$Q_{ref}^{3\phi} = \text{constant} . \tag{2.2}$$

Therefore, the voltage variation cannot be compensated for.

B. Fixed power factor control

To maintain the power factor at the desired value (PF_{ref}), the reactive power reference is determined as follows from the measured active power output ($P_{out}^{3\phi}$):

$$Q_{ref}^{3\phi} = \begin{cases} P_{out}^{3\phi} \tan\left(\cos^{-1}(PF_{ref})\right) & \text{for lagging power factor} \\ -P_{out}^{3\phi} \tan\left(\cos^{-1}(PF_{ref})\right) & \text{for leading power factor} \end{cases} . \tag{2.3}$$

If a leading power factor reference is used, the voltage variation caused by the active power change might be reduced, while a lagging power factor increases the voltage variation.

C. Variable power factor control

The reactive power reference is determined as in equation (2.3). However, the power factor reference is not a constant, and is given by a function of the

active power. For example, if the power factor reference is determined as shown in Fig. 2.8(a), the reactive power reference varies as shown in Fig. 2.8(b) according to the active power. Alternatively, the active power versus the reactive power curve can be given directly [52].

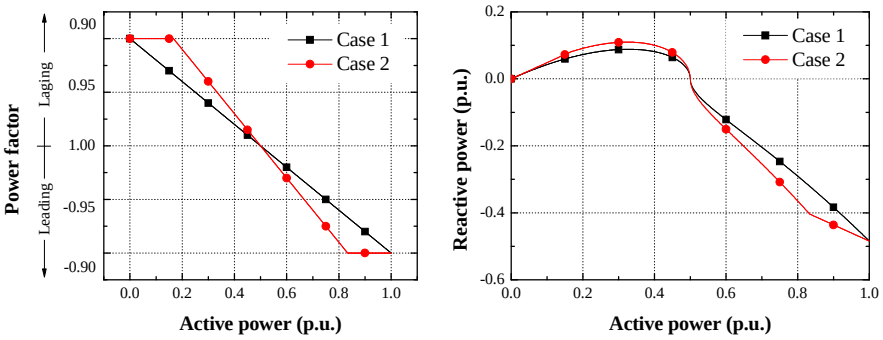

(a) Power factor (b) Reactive power

Fig. 2.8 Reactive power characteristics of a variable power factor control.

2.3.2 Active methods

A. Fixed voltage control

This control method maintains the terminal voltage of the DG at a desired value, V_{ref}. Since the reactive power used to control the voltage cannot be calculated directly from an equation, a proportional–integral (PI) controller is used to determine the reactive power reference, as shown in Fig. 2.9. Under unbalanced operating conditions, the positive-sequence component of the voltage is generally controlled.

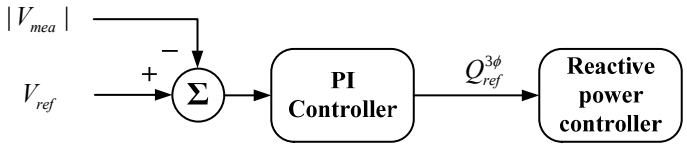

Fig. 2.9 Fixed voltage controller.

B. Reactive power versus voltage droop control

With the reactive power versus voltage (Q–V) droop control method, the reactive power reference is determined as

$$Q_{ref}^{3\phi} = \frac{1}{R}\left(V_{ref} - |V_{mea}|\right), \tag{2.4}$$

where R is the Q–V droop constant. As shown in Fig. 2.10, the reactive power decreases linearly as the voltage increases.

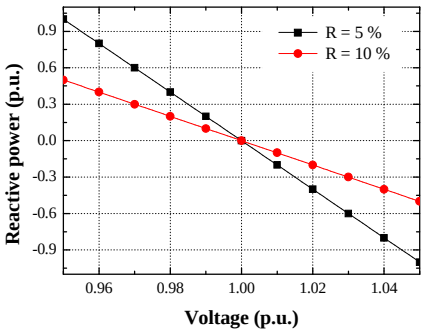

Fig. 2.10 Reactive power characteristic of Q–V droop control.

C. Advanced volt/var control

The relationship between the reactive power and voltage is determined as a piecewise linear function defined by (V, Q) pairs [53]. According to (V, Q) pairs,

various operation modes can be predetermined, and the DMS can change the operation mode. Figure 2.11 shows an example, which is referred to as 'Normal mode' in [53]. If the voltage is between V_1 and V_2 or between V_3 and V_4, the operational characteristics are identical to those of Q–V droop control. Otherwise, the characteristics are identical to those of fixed reactive power control.

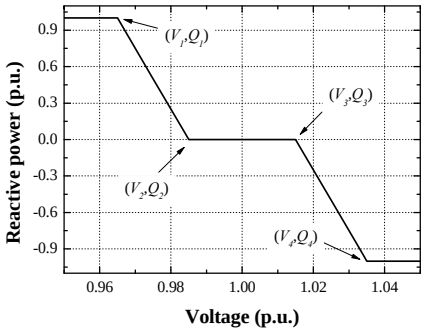

Fig. 2.11 Reactive power characteristics of a Volt/Var control.

Chapter 3. Three-phase Steady-State Models for a Three-Wire VSC

VSCs are widely used to connect renewable energy sources, such as wind turbines and photovoltaics, with a distribution system. This is because the primary energy sources resemble a voltage source [30]. In this chapter, three-phase steady-state models for the three-wire VSC are proposed. The proposed models can be used to represent a DG with a three-wire VSC interface for a three-phase steady-state analysis. The accuracy of the proposed models is verified by comparing the results of the power flow with those obtained from the PSCAD simulation.

3.1 Power output characteristics of a VSC

Figure 3.1 shows the general configuration of a DG with a VSC interface. The VSC is connected to the primary energy source via a DC link, and to the main grid via an output filter. The control system maintains the three-phase active and reactive power outputs at their desired values, $P_{ref}^{3\phi}$ and $Q_{ref}^{3\phi}$, by controlling the states of semiconductor switches. If the power output of the primary energy source is non-dispatchable, the primary energy source operates in maximum power-point tracking (MPPT) mode, and the power control system controls the DC link voltage rather than the active power output.

Even though the references are identical, the three phases injected into the

main grid at the point of common connection (PCC), i.e., $P_{PCC}^{3\phi}$ and $Q_{PCC}^{3\phi}$, may differ depending on the positions of the voltage and current sensors. This is because the power control system controls the power output based on the measured voltage and current. On the other hand, the phase outputs are determined by the power control strategy. Therefore, both the location of the sensor and the power control strategy should be taken into account in the three-phase steady-state models for VSCs.

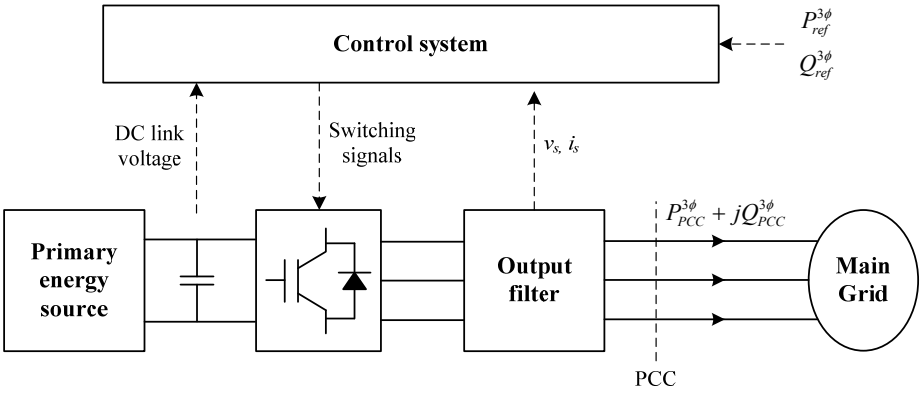

Fig. 3.1 Overall configuration of a DG with a VSC interface.

3.2 Voltage and current sensor positions

For the VSC, an *L* filter, *LC* filter, or *LCL* filter can be used to reduce the harmonics generated by switching operations, as shown in Fig. 3.2. In general, either the grid voltage (v_g) or the capacitor voltage (v_c), together with either the grid current (i_g) or the converter current (i_{VSC}), are sensed and used in the power control system [54]. Based on these sensed voltage and current data, the VSCs can be classified into four varieties. For each, the active and reactive references and the sensed voltage and current have the following steady-state relationship:

- Grid voltage and grid current (GVGC) sensing: *L*, *LC*, or *LCL* filter

$$P_{ref}^{3\phi} + jQ_{ref}^{3\phi} = V_g^t I_g^* \tag{3.1}$$

- Grid voltage and converter current (GVCC) sensing: *LC* or *LCL* filter

$$P_{ref}^{3\phi} + jQ_{ref}^{3\phi} = V_g^t I_{VSC}^* \tag{3.2}$$

- Capacitor voltage and gird current (CVGC) sensing: *LCL* filter

$$P_{ref}^{3\phi} + jQ_{ref}^{3\phi} = V_c^t I_g^* \tag{3.3}$$

- Capacitor voltage and converter current (CVCC) sensing: *LCL* filter

$$P_{ref}^{3\phi} + jQ_{ref}^{3\phi} = V_c^t I_{VSC}^* \tag{3.4}$$

where V_g and V_c are the grid and capacitor voltage phasor vectors, I_g and I_{VSC} are the grid and converter current phasor vectors, and the superscript * denotes the complex conjugate. Therefore, at steady state, the three-phase active and

reactive powers injected into the main grid at the PCC are equal to $P_{ref}^{3\phi}$ and $Q_{ref}^{3\phi}$ only if the grid voltage and current are sensed, i.e., with GVGC sensing.

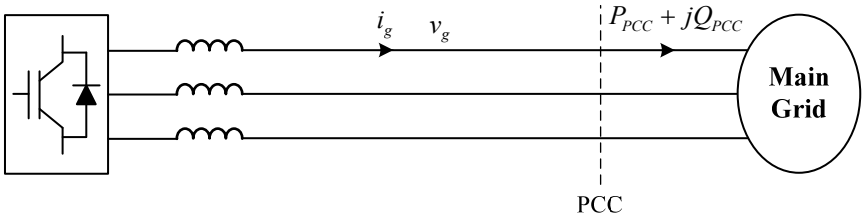

(a) *L* filter

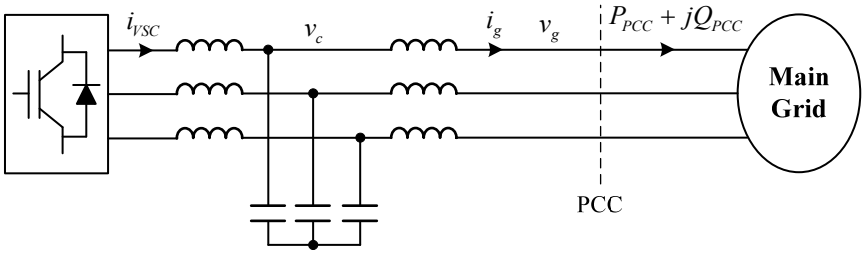

(b) *LC* filter

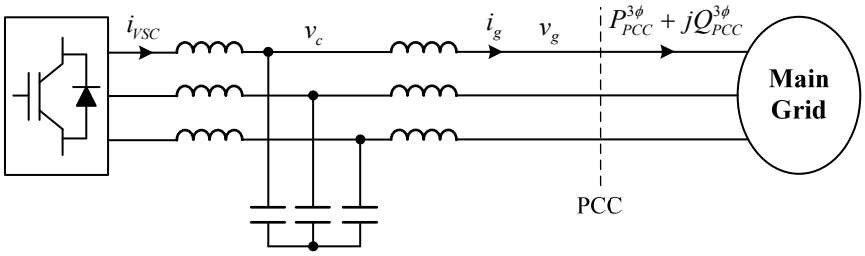

(c) *LCL* filter

Fig. 3.2 Output filter and possible voltage and current measurements.

3.3 Power control strategy

The power control strategies for VSCs used for DG applications can be classified into voltage-controlled and current-controlled methods. In a voltage-controlled method, the voltage references for the modulator that controls the state of the semiconductor switches are directly determined in the power controller as shown in Fig. 3.3(a). On the other hand, in a current-controlled method, the power controller determines the current references for the current controller that generates the voltage references for the modulator, Fig. 3.3(b). Current-controlled methods are more widely used for grid-connected DGs due to the potential advantages of improved power quality, better capability to decouple active and reactive power control, and inherent overcurrent protection [30].

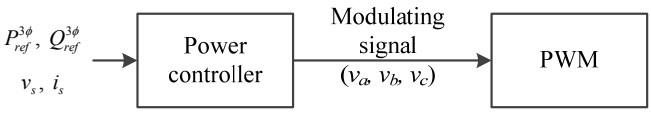

(a) Voltage-controlled method

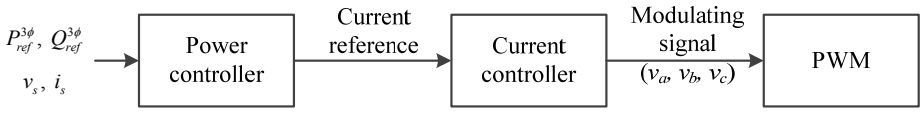

(b) Current-controlled method

Fig. 3.3 Power control strategies for a VSC.

3.3.1 Voltage-controlled method

Figure 3.4 shows an equivalent circuit of a grid-connected converter system to explain the operating principle of the voltage-controlled method. It is assumed that the angle of the grid voltage is zero.

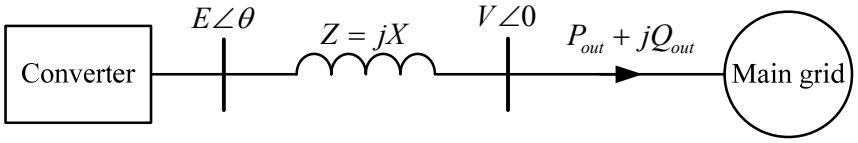

Fig. 3.4 Equivalent circuit of a voltage-controlled VSC.

The active and reactive powers injected into the main grid are given by

$$P_{out} = \frac{EV}{X}\sin\theta \tag{3.5}$$

and

$$Q_{out} = \frac{V\left(E\cos\theta - V\right)}{X}, \tag{3.6}$$

respectively, where E and θ are the magnitude and angle of the terminal voltage of the converter, V is the magnitude of the grid voltage, and X is a reactance of the line. Because θ is typically sufficiently small to make the approximations $\sin\theta \approx \theta$ and $\cos\theta \approx 1$, P_{out} and Q_{out} can be approximated as follows:

$$P_{out} \approx \frac{EV}{X}\theta \tag{3.7}$$

and

$$Q_{out} \approx \frac{V}{X}(E - V). \tag{3.8}$$

Therefore, the angle of the output voltage can be used to control the active power output, and the magnitude of the output voltage can be used control the reactive power output.

The power control system of a voltage-controlled VSC based on these characteristics is shown in Fig. 3.5 [55]. The voltage angle and magnitude references, θ_{ref} and E_{ref}, are determined by the active and reactive power controllers, respectively. The system frequency, f, is calculated from the measured ac voltage, V_{ac}, using a phase locked loop (PLL). In the reference voltage generator, the instantaneous voltage references are determined as follows:

$$e_{a,ref} = E_{ref} \cos(2\pi ft + \theta_{ref}), \tag{3.9}$$

$$e_{b,ref} = E_{ref} \cos(2\pi ft + \theta_{ref} - \frac{2}{3}\pi), \tag{3.10}$$

and

$$e_{c,ref} = E_{ref} \cos(2\pi ft + \theta_{ref} + \frac{2}{3}\pi), \tag{3.11}$$

where t is time. The switching signals for the VSC, S_{VSC}, are determined using a pulse width modulator (PWM).

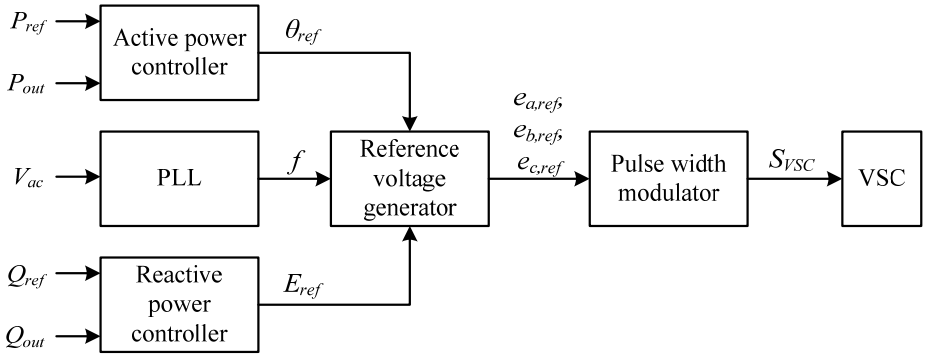

Fig. 3.5 Power control system for a voltage-controlled VSC.

3.3.2 Current-controlled method

The current-controlled method is based on instantaneous power theory, whereby the instantaneous active and reactive powers, p and q, are given by

$$p = v_{abc} \cdot i_{abc} \tag{3.12}$$

and

$$q = v_{abc\perp} \cdot i_{abc}, \tag{3.13}$$

where v_{abc} and i_{abc} are the instantaneous voltage and current vectors expressed in the *a-b-c* reference frame, '$\cdot$' is the inner product operator, and $v_{abc\perp}$ is an orthogonal version of v_{abc} (i.e., with a 90° leading phase shift). The orthogonal voltage vector is given by

$$v_{abc\perp} = M v_{abc}, \tag{3.14}$$

where the transformation matrix M is

$$M = \frac{1}{\sqrt{3}}\begin{bmatrix} 0 & 1 & -1 \\ -1 & 0 & 1 \\ 1 & -1 & 0 \end{bmatrix}. \tag{3.15}$$

When the voltages and currents of the three phases are sinusoidal but not balanced, the instantaneous active and reactive powers can be represented by positive- and negative-sequence quantities, and divided into average terms, P and Q, and oscillatory terms, $\tilde{p}$ and $\tilde{q}$, i.e.,

$$p = (v^+ + v^-)\cdot(i^+ + i^-) = \underbrace{v^+ \cdot i^+ + v^- \cdot i^-}_{P} + \underbrace{v^+ \cdot i^- + v^- \cdot i^+}_{\tilde{p}} \tag{3.16}$$

and

$$q = (v_\perp^+ + v_\perp^-)\cdot(i^+ + i^-) = \underbrace{v_\perp^+ \cdot i^+ + v_\perp^- \cdot i^-}_{Q} + \underbrace{v_\perp^+ \cdot i^- + v_\perp^- \cdot i^+}_{\tilde{q}}, \tag{3.17}$$

where the superscripts + and – denote the positive- and negative-sequence component vectors of the corresponding instantaneous vector.

The instantaneous current reference used to track the active and reactive power references can be divided into the active and reactive current references, $i_{p,ref}$ and $i_{q,ref}$, because any current vector aligned with v and any current vector orthogonal to v determine the instantaneous active and reactive powers, respectively, i.e.,

$$i_{p,ref} = g v_{abc} \tag{3.18}$$

and

$$i_{q,ref} = b v_{abc\perp}, \tag{3.19}$$

where g is the instantaneous conductance and b is the instantaneous susceptance. Various methods have been proposed to determine g and b with unbalanced operating conditions [56–60]. The methods can be classified into two groups depending on the performance. With the first group, the oscillatory terms of the instantaneous active and reactive powers can be eliminated, regardless of the desired values; however, the instantaneous current references are not sinusoidal. With second group, the instantaneous current references are sinusoidal; however, the oscillatory terms cannot be eliminated. Since the DG should satisfy the requirements for harmonic current distortions (e.g., IEEE 1547 [31]), the application of the first group to DGs connected to a distribution system (which is an inherently unbalanced system) appears to be limited [61]. Therefore, only power control strategies that generate sinusoidal current references will be considered here, i.e., positive- and negative-sequence control (PNSC), average active–reactive control (AARC), and balanced positive-sequence control (BPSC) [58–60]. In addition, synchronous reference-frame proportional–integral control (SRFPIC) will be considered because SRFPIC is widely used for DGs, even though unbalanced operating conditions are not accounted for.

A) Positive- and negative-sequence control

PNSC was initially proposed for a VSC that delivers only active power to the grid. From equation (3.16), the current reference should satisfy the following relations in order to inject the desired active power and zero reactive power without any oscillatory components:

$$v^+ \cdot i^+_{p,ref} + v^- \cdot i^-_{p,ref} = P^{3\phi}_{ref} \tag{3.20}$$

and

$$v^+ \cdot i^-_{p,ref} + v^- \cdot i^+_{p,ref} = 0\,, \tag{3.21}$$

where $i^+_{p,ref}$ and $i^-_{p,ref}$ are the positive- and negative-sequence components of $i_{p,ref}$. Similarly, the constraints for $i_{q,ref}$ in order to eliminate the oscillatory part of the instantaneous reactive power are given by

$$v^+_{\perp} \cdot i^+_{q,ref} + v^-_{\perp} \cdot i^-_{q,ref} = Q^{3\phi}_{ref} \tag{3.22}$$

and

$$v^+_{\perp} \cdot i^-_{q,ref} + v^-_{\perp} \cdot i^+_{q,ref} = 0\,, \tag{3.23}$$

where $i^+_{q,ref}$ and $i^-_{q,ref}$ are the positive- and negative-sequence components of $i_{q,ref}$. From equations (3.14) and (3.20)–(3.23), the current reference can be found:

$$i_{ref} = i^+_{p,ref} + i^+_{p,ref} + i^+_{q,ref} + i^-_{q,ref} = \frac{1}{|v^+|^2 - |v^-|^2}(P^{3\phi}_{ref} + Q^{3\phi}_{ref} M)(v^+ - v^-)\,. \tag{3.24}$$

In the control system, a special PLL or frequency-locked loop (FLL) is used to obtain v^+ and v^- from the measured instantaneous voltage, v, such as a decoupled double synchronous reference-frame PLL (DDSRF-PLL) or a double second-order generalized integrator FLL (DSOGI-FLL) [54].

B) Average active–reactive control

According to instantaneous active–reactive control (IARC), the current

reference is given by

$$i_{ref} = \frac{P_{ref}^{3\phi}}{|v|^2} v + \frac{Q_{ref}^{3\phi}}{|v|^2} v_{\perp} . \tag{3.25}$$

With unbalanced operating conditions, the current reference is not sinusoidal due to the oscillatory component of $|v|$. AARC can be used to generate a sinusoidal current reference from the average of $|v|$ rather than the instantaneous value of $|v|$. For a three-wire system, the average can be calculated from the positive- and negative-sequence components as

$$\frac{1}{t_f - t_0} \int_{t_0}^{t_f} |v|^2 \, dt = |v^+|^2 + |v^-|^2 . \tag{3.26}$$

By substituting equation (3.26) into equation (3.25), the current reference generated using AARC can be described by

$$i_{ref} = \frac{1}{|v^+|^2 + |v^-|^2} (P_{ref}^{3\phi} + Q_{ref}^{3\phi} M) v . \tag{3.27}$$

C) Balanced positive-sequence control

The objective of BPSC is to generate a balanced sinusoidal current reference. Since the positive-sequence voltage is balanced and sinusoidal, and is greater than the negative-sequence voltage with unbalanced operating conditions, the current reference can be determined as follows:

$$i_{ref} = \frac{1}{|v^+|^2} (P_{ref}^{3\phi} + Q_{ref}^{3\phi} M) v^+ . \tag{3.28}$$

D) Synchronous reference-frame proportional–integral control

In SRFPIC, the voltage and current vectors are represented in the rotating *d*-*p* frame of reference, in which the *d*-axis is aligned with the rotating voltage vector and the *q*-axis is 90° ahead of the *d*-axis. As shown in equations (3.12) and (3.13), the current aligned with the voltage vector (i.e., the *d*-axis current) determines the active power, and the current orthogonal to the voltage vector (i.e., the *q*-axis current) determines the reactive power. Therefore, the active and reactive power outputs can be independently controlled by adjusting the *d*- and *q*-axis currents, respectively. With SRFPIC, the *dq*-axis current references, $i_{ref,d}$ and $i_{ref,q}$, are determined from the measured three-phase active and reactive power outputs, P_{mea} and Q_{mea}, using proportional–integral (PI) controllers, as shown in Fig. 3.6.

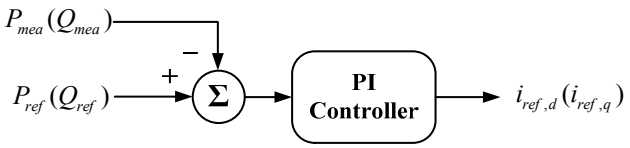

Fig. 3.6 Power controller based on SRFPIC.

3.4 Proposed models

The VSC can be classified into 20 categories, according to the voltage and current sensor positions and the power control strategy used, as shown in Fig. 3.7. The models for the VSC equipped with an *LCL* filter are described first. The unified models are presented at the end of this section.

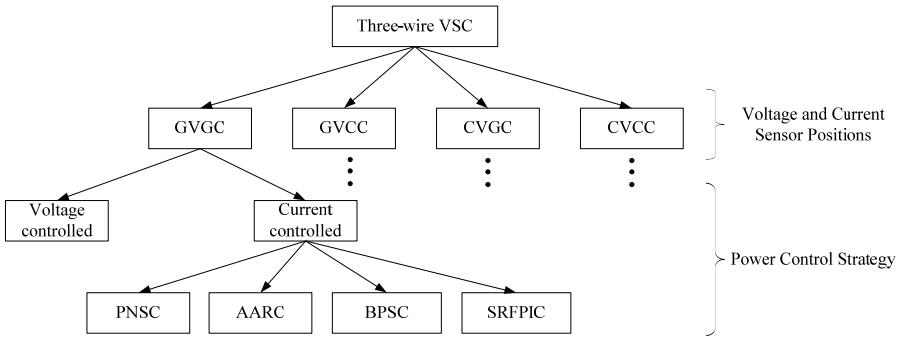

Fig. 3.7 Classification of the VSC models.

3.4.1 Equivalent circuit models

Figure 3.8 shows the proposed equivalent-circuit models for the three-phase analysis. Since the power output is calculated using the sensed voltages, the location of the sensing point is included in the equivalent circuits. In other words, the DGs that sense the grid voltage (both GVGC and GVCC types) are modeled as a single node connected to an equivalent three-phase current source (ETCS). For the others, the DG is modeled as two nodes connected via the grid-side impedance of the LCL filter. In both equivalent-circuit models, the location

of the voltage-sensing point is the ETCS-connected node, and the current output of the ETCS is equal to the grid-side current of the original system (see Fig. 3.2).

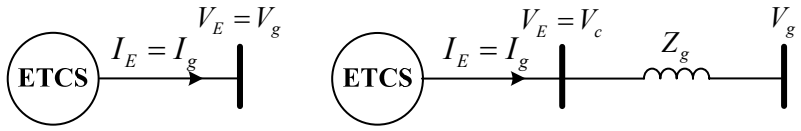

(a) GVGC and GVCC (b) CVGC and CVCC

Fig. 3.8. Equivalent-circuit models for VSCs.

3.4.2 Voltage-controlled VSC models

Figure 3.9 shows the configuration of the VSC based on an *LCL* filter.

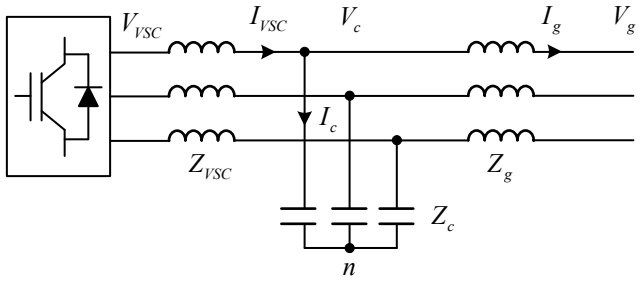

Fig. 3.9 VSC with an LCL filter.

Since the voltage references of the voltage-controlled VSC for the modulator are balanced (see equations (3.9)–(3.11)), the phasor vector of the converter phase-to-neutral voltage, $V_{VSC,p\text{-}n}$, can be expressed as

$$V_{VSC,p-n} = V^a E\,, \tag{3.29}$$

where V^a is a complex constant that corresponds to the voltage phasor of phase A and E is a 1×3 row vector given by

$$E = \begin{bmatrix} 1 & e^{-j\frac{2}{3}\pi} & e^{j\frac{2}{3}\pi} \end{bmatrix}^t\,. \tag{3.30}$$

A) GVGC sensing

With a three-wire system, the current phasors shown in Fig. 3.9 can be formulated with phase-to-neutral voltages as follows:

$$I_{VSC} = \frac{V_{VSC,p-n} - V_{c,p-n}}{Z_{VSC}}\,, \tag{3.31}$$

$$I_c = \frac{V_{c,p-n}}{Z_c} = \frac{V_{g,p-n} + Z_g I_g}{Z_c}\,, \tag{3.32}$$

and

$$I_g = I_{VSC} - I_c\,, \tag{3.33}$$

where $V_{c,p\text{-}n}$ is the capacitor voltage phasor vector (phase-to-neutral), $V_{g,p\text{-}n}$ is the grid voltage phasor vector (phase-to-neutral), Z_{VSC} is the equivalent impedance of the converter side components of the filter and the semiconductor switch, Z_c is the impedance of the capacitor side components of the filter, and Z_g is the impedance of the grid-side components of the filter. By substituting equations (3.31) and (3.32) into equation (3.33) and re-arranging the subsequent expression, the grid current can be written as

$$I_g = \frac{Z_c}{Z_c Z_g + Z_c Z_{VSC} + Z_g Z_{VSC}} V_{VSC,p-n} - \frac{Z_c + Z_{VSC}}{Z_c Z_g + Z_c Z_{VSC} + Z_g Z_{VSC}} V_{g,p-n} \quad . (3.34)$$

In a power control system, the voltage references are controlled in order to maintain the power outputs calculated using the grid voltage and current in case of GVGC sensing. Because the phase-to-neutral voltages are measured in the three-wire VSC, the active and reactive power references can be expressed as

$$P_{ref}^{3\phi} + jQ_{ref}^{3\phi} = V_{g,p-n}^{t} I_g^{*} . \quad (3.35)$$

By substituting equations (3.29) and (3.34) into equation (3.35), V^a can be written as

$$V^a = \frac{\left(Z_c Z_g + Z_c Z_{VSC} + Z_g Z_{VSC}\right)\left(P_{ref}^{3\phi} - jQ_{ref}^{3\phi}\right) + \left(Z_c + Z_{VSC}\right) V_{g,p-n}^{t} V_{g,p-n}^{*}}{Z_c \left(V_{g,p-n}^{*}\right)^{t} E} . \quad (3.36)$$

The phase-to-ground voltages are generally used in steady-state analysis methods. Since the grid-side voltage is equal to the voltage of the ETCS-connected node, the phase-to-neutral voltage vector can be calculated from the phase-to-ground voltage of the ETCS-connected node, i.e.,

$$V_{g,p-n} = TV_E , \quad (3.37)$$

where V_E is a phase-to-ground voltage phasor vector of the ETCS-connected node, and the transformation matrix T is given by

$$T = \frac{1}{3}\begin{bmatrix} 2 & -1 & -1 \\ -1 & 2 & -1 \\ -1 & -1 & 2 \end{bmatrix} . \quad (3.38)$$

The grid current can then be formulated as a function of the three-phase active and reactive power references, the phase-to-ground voltage vector of the ETCS-connected node, and the impedances of the filter by substituting equation (3.37) into equation (3.36), and then substituting equations (3.29) and (3.36) into equation (3.34), i.e.,

$$I_g = \frac{P_{ref}^{3\phi} - jQ_{ref}^{3\phi}}{\left(V_E^*\right)^t E} E + Z_1 \frac{V_E^t T V_E^*}{\left(V_E^*\right)^t E} E - Z_1 T V_E , \tag{3.39}$$

where

$$Z_1 = \frac{Z_c + Z_{VSC}}{Z_c Z_g + Z_c Z_{VSC} + Z_g Z_{VSC}} . \tag{3.40}$$

B) GVCC sensing

From equations (3.31)–(3.33), the converter current is given by

$$I_{VSC} = \frac{\left(Z_c + Z_g\right) V_{VSC,p-n} - Z_c V_{g,p-n}}{Z_c Z_g + Z_c Z_{VSC} + Z_g Z_{VSC}} . \tag{3.41}$$

Since the method with GVCC sensing controls the output powers based on the grid voltage and the converter current, the active and reactive power references are given by

$$P_{ref}^{3\phi} + jQ_{ref}^{3\phi} = V_{g,p-n}^t I_{VSC}^* . \tag{3.42}$$

Similar to the GVGC sensing case, V^a can be calculated as follows:

$$V^a = \frac{\left(Z_c Z_g + Z_c Z_{VSC} + Z_g Z_{VSC}\right)\left(P_{ref}^{3\phi} - jQ_{ref}^{3\phi}\right) + Z_c V_{g,p-n}^t V_{g,p-n}^*}{\left(Z_c + Z_g\right)\left(V_{g,p-n}^*\right)^t E}. \quad (3.43)$$

The grid current can then be formulated as

$$I_g = \frac{Z_c}{Z_c + Z_g}\frac{P_{ref}^{3\phi} - jQ_{ref}^{3\phi}}{\left(V_E^*\right)^t E}E + \frac{Z_c Z_2}{Z_c + Z_g}\frac{V_E^t T V_E^*}{\left(V_E^*\right)^t E}E - \frac{Z_c Z_2 + 1}{Z_c + Z_g}TV_E, \quad (3.44)$$

where

$$Z_2 = \frac{Z_c}{Z_c Z_g + Z_c Z_{VSC} + Z_g Z_{VSC}}. \quad (3.45)$$

C) CVGC sensing

The grid current is given by equation (3.33), and the three-phase active and reactive power references can be expressed as

$$P_{ref}^{3\phi} + jQ_{ref}^{3\phi} = V_{c,p-n}^t I_g^*. \quad (3.46)$$

Therefore, V^a is given by

$$V^a = \frac{\left(Z_c Z_g + Z_c Z_{VSC} + Z_g Z_{VSC}\right)\left(P_{ref}^{3\phi} - jQ_{ref}^{3\phi}\right) + \left(Z_c + Z_{VSC}\right)V_{c,p-n}^t V_{c,p-n}^*}{Z_c\left(V_{c,p-n}^*\right)^t E}. \quad (3.47)$$

Because the node connected to the capacitor is the ETCS-connected node, the capacitor voltage is

$$V_{c,p-n} = TV_E. \quad (3.48)$$

Consequently, the equation of the grid current is identical to that with GVGC

sensing case, i.e., equation (3.38). However, the equivalent circuit models with GVGC and CVGC sensing are different, as shown in Fig. 3.8, and thus the grid currents are different, even though the grid voltages are identical.

D) CVCC sensing

The converter current is given by equation (3.31), and the three-phase active and reactive power references can be expressed as

$$P_{ref}^{3\phi} + jQ_{ref}^{3\phi} = V_{c,p-n}^{t} I_{VSC}^{*} . \tag{3.49}$$

Therefore, V^a can be obtained as

$$V^{a} = \frac{Z_{VSC}\left(P_{ref}^{3\phi} - jQ_{ref}^{3\phi}\right) + V_{c,p-n}^{t} V_{c,p-n}^{*}}{\left(V_{c,p-n}^{*}\right)^{t} E} . \tag{3.50}$$

With CVCC sensing, the grid current is given by

$$I_g = \frac{P_{ref}^{3\phi} - jQ_{ref}^{3\phi}}{\left(V_E^{*}\right)^{t} E} E + \frac{1}{Z_{VSC}} \frac{V_E^{t} T V_E^{*}}{\left(V_E^{*}\right)^{t} E} E - \frac{Z_c + Z_{VSC}}{Z_c Z_{VSC}} T V_E . \tag{3.51}$$

3.4.3 Current-controlled VSC models

The instantaneous voltage and current vectors can be replaced with corresponding phasor vectors for the steady-state analysis. Therefore, the current references can be written as follows:

- PNSC

$$I_{ref} = \frac{1}{|V_s^+|^2 - |V_s^-|^2}\left(P_{ref}^{3\phi} + Q_{ref}^{3\phi} M\right)(V_s^+ - V_s^-), \tag{3.52}$$

- AARC

$$I_{ref} = \frac{P_{ref}^{3\phi}}{|V_s^+|^2 + |V_s^-|^2} V_s + \frac{Q_{ref}^{3\phi}}{|V_s^+|^2 + |V_s^-|^2} M V_s, \tag{3.53}$$

- BPSC

$$I_{ref} = \frac{P_{ref}^{3\phi}}{|V_s^+|^2} V_s^+ + \frac{Q_{ref}^{3\phi}}{|V_s^+|^2} M V_s^+, \tag{3.54}$$

where V_s is the phasor vector of the sensed voltage, and V_s^+ and V_s^- are the positive- and negative-sequence components of V_s, respectively. V_s^+ and V_s^- can be calculated directly from V_s as follows:

$$V_s^+ = A V_s \tag{3.55}$$

and

$$V_s^- = A^t V_s, \tag{3.56}$$

where

$$A = \frac{1}{3}\begin{bmatrix} 1 & e^{j\frac{2}{3}\pi} & e^{-j\frac{2}{3}\pi} \\ e^{-j\frac{2}{3}\pi} & 1 & e^{j\frac{2}{3}\pi} \\ e^{j\frac{2}{3}\pi} & e^{-j\frac{2}{3}\pi} & 1 \end{bmatrix}. \tag{3.57}$$

With SRFPIC, the current reference is not given directly since it is generated using PI controllers. However, it can be assumed that the *dq*-axis current reference and the angular velocity of the *dq* reference frame are constant because the high-frequency oscillating terms are negligible for a steady-state fundamental frequency analysis. Therefore, the current reference can be assumed to be balanced. Because the current reference of the BPSC is balanced, the current reference written in phasor form is identical to equation (3.54).

The three-wire VSC operates based on the phase-to-neutral voltage. Since the phase-to-ground voltage of the voltage-sensed node is the voltage of the ETCS-connected node, V_E, the sensed voltage is given by

$$V_s = TV_E . \tag{3.58}$$

From equations (3.55)–(3.58), the following relations can be obtained:

$$|V_s^+|^2 = \left(ATV_E\right)^t \left(ATV_E\right)^* = V_E^t A^t V_E^*, \tag{3.59}$$

$$|V_s^-|^2 = \left(A^tTV_E\right)^t \left(A^tTV_E\right)^* = V_E^t AV_E^*, \tag{3.60}$$

$$|V_s^+|^2 - |V_s^-|^2 = V_E^t \left(A^t - A\right)V_E^* = -jV_E^t MV_E^*, \tag{3.61}$$

$$|V_s^+|^2 + |V_s^-|^2 = V_E^t \left(A^t + A\right)V_E^* = V_E^t TV_E^*, \tag{3.62}$$

$$V_s^+ - V_s^- = \left(A - A^t\right)TV_E = jMV_E, \tag{3.63}$$

$$M\left(V_s^+ - V_s^-\right) = jM^2V_E = -jTV_E, \tag{3.64}$$

$$MV_s = MTV_E = MV_E, \tag{3.65}$$

$$MV_s^+ = MATV_E = -jAV_E \tag{3.66}$$

Finally, the current reference phasors can be written with respect to the voltage of the ETCS connected bus as follows:

- PNSC

$$I_{ref} = \frac{-1}{V_E^t M V_E^*}\left(MP_{ref}^{3\phi} - TQ_{ref}^{3\phi}\right)V_E, \tag{3.67}$$

- AARC

$$I_{ref} = \frac{1}{V_E^t T V_E^*}\left(TP_{ref}^{3\phi} + MQ_{ref}^{3\phi}\right)V_E, \tag{3.68}$$

- BPSC and SRFPIC

$$I_{ref} = \frac{1}{V_E^t A^t V_E^*}\left(AP_{ref}^{3\phi} - jAQ_{ref}^{3\phi}\right)V_E. \tag{3.69}$$

A) GVGC sensing

The grid current is identical to the reference current because the methods with GVGC sensing control the grid current. Therefore, the grid currents are as follows.

- GVGC sensing and PNSC

$$I_g = \frac{-1}{V_E^t M V_E^*}\left(MP_{ref}^{3\phi} - TQ_{ref}^{3\phi}\right)V_E \tag{3.70}$$

- GVGC sensing and AARC

$$I_g = \frac{1}{V_E^t T V_E^*}\left(TP_{ref}^{3\phi} + MQ_{ref}^{3\phi}\right)V_E \tag{3.71}$$

- GVGC sensing and BPSC (or SRFPIC)

$$I_g = \frac{1}{V_E^t A^t V_E^*}\left(AP_{ref}^{3\phi} - jAQ_{ref}^{3\phi}\right)V_E \tag{3.72}$$

B) GVCC sensing

Using equations (3.32)–(3.33), the grid current can be written as

$$I_g = \frac{Z_c}{Z_c + Z_g} I_{VSC} - \frac{1}{Z_c + Z_g} V_{g,p-n}\,. \tag{3.73}$$

With GVCC sensing, the grid voltage is measured and the converter current is maintained at the reference value. Therefore, the grid current can be obtained by substituting equation (3.37) into equation (3.73) and replacing I_{VSC} with the current reference as follows.

- GVCC sensing and PNSC

$$I_g = \frac{Z_c}{Z_c + Z_g}\frac{-1}{V_E^t M V_E^*}\left(MP_{ref}^{3\phi} - TQ_{ref}^{3\phi}\right)V_E - \frac{1}{Z_c + Z_g}TV_E \tag{3.74}$$

- GVCC sensing and AARC

$$I_g = \frac{Z_c}{Z_c + Z_g}\frac{1}{V_E^t T V_E^*}\left(TP_{ref}^{3\phi} + MQ_{ref}^{3\phi}\right)V_E - \frac{1}{Z_c + Z_g}TV_E \tag{3.75}$$

- GVCC sensing and BPSC (or SRFPIC)

$$I_g = \frac{Z_c}{Z_c + Z_g}\frac{1}{V_E^t A^t V_E^*}\left(AP_{ref}^{3\phi} - jAQ_{ref}^{3\phi}\right)V_E - \frac{1}{Z_c + Z_g}TV_E \tag{3.76}$$

C) CVGC sensing

Since the CVGC sensing method also controls the grid current, the equations for the grid current are identical to those with GVGC sensing, i.e., equations (3.70)–(3.72). Note that the equations for the grid current are identical; however, the equivalent circuit models differ, as shown in Fig. 3.8.

D) CVCC sensing

Because the converter current is controlled, the grid current can be expressed by combining equations (3.31) and (3.32) as follows:

$$I_g = I_{ref} - I_c = I_{ref} - \frac{1}{Z_c} V_{c,p-n} \,. \tag{3.77}$$

By substituting the current reference phasors and equation (3.48) into equation (3.77), the grid currents can be obtained as follows.

- CVCC sensing PNSC

$$I_g = \frac{-1}{V_E^t M V_E^*} \left(M P_{ref}^{3\phi} - T Q_{ref}^{3\phi} \right) V_E - \frac{1}{Z_c} T V_E \tag{3.78}$$

- CVCC sensing AARC

$$I_g = \frac{1}{V_E^t T V_E^*} \left(T P_{ref}^{3\phi} + M Q_{ref}^{3\phi} \right) V_E - \frac{1}{Z_c} T V_E \tag{3.79}$$

- CVCC sensing BPSC (or SRFPIC)

$$I_g = \frac{1}{V_E^t A^t V_E^*} \left(A P_{ref}^{3\phi} - j A Q_{ref}^{3\phi} \right) V_E - \frac{1}{Z_c} T V_E \tag{3.80}$$

3.4.4 Unified models

The grid current output for the VSCs equipped with an *L* filter or an *LC* filter can be formulated using the same procedure as described in the previous section. According to the power control strategy, the current output can be represented as follows. The coefficients α, β, and γ, are determined by the sensor positions and output filter, and are listed in Tables 3.1 and 3.2. Note that the equivalent circuit model is different according to the sensor location, as shown in Fig. 3.8.

- Voltage-controlled VSC

$$I_g = \alpha \frac{P_{ref}^{3\phi} - jQ_{ref}^{3\phi}}{\left(V_E^*\right)^t E} E + \beta \frac{V_E^t T V_E^*}{\left(V_E^*\right)^t E} E - \gamma T V_E \tag{3.81}$$

- Current-controlled VSC with PNSC

$$I_g = \alpha \frac{-1}{V_E^t M V_E^*} \left(M P_{ref}^{3\phi} - T Q_{ref}^{3\phi} \right) V_E - \beta T V_E \tag{3.82}$$

- Current-controlled VSC with AARC

$$I_g = \alpha \frac{1}{V_E^t T V_E^*} \left(T P_{ref}^{3\phi} + M Q_{ref}^{3\phi} \right) V_E - \beta T V_E \tag{3.83}$$

- Current-controlled VSC with BPSC or SRFPIC

$$I_g = \alpha \frac{1}{V_E^t A^t V_E^*} \left(A P_{ref}^{3\phi} - jA Q_{ref}^{3\phi} \right) V_E - \beta T V_E \tag{3.84}$$

Table 3.1 Coefficients of unified models for a voltage-controlled VSC

Filter	Sensor Positions	Coefficients		
		α	β	γ
L	GVGC	1	1	1
LC	GVGC	1	$\frac{Z_c + Z_{VSC}}{Z_c Z_{VSC}}$	$\frac{Z_c + Z_{VSC}}{Z_c Z_{VSC}}$
	GVCC	1	$\frac{1}{Z_{VSC}}$	$\frac{Z_c + Z_{VSC}}{Z_c Z_{VSC}}$
LCL	GVGC CVGC	1	$\frac{Z_c + Z_{VSC}}{Z_c Z_g + Z_c Z_{VSC} + Z_g Z_{VSC}}$	$\frac{Z_c + Z_{VSC}}{Z_c Z_g + Z_c Z_{VSC} + Z_g Z_{VSC}}$
	GVCC	$\frac{Z_c}{Z_c + Z_g}$	$\frac{Z_c^2}{(Z_c + Z_g)(Z_c Z_g + Z_c Z_{VSC} + Z_g Z_{VSC})}$	$\frac{Z_c^2 + Z_c Z_g + Z_c Z_{VSC} + Z_g Z_{VSC}}{(Z_c + Z_g)(Z_c Z_g + Z_c Z_{VSC} + Z_g Z_{VSC})}$
	CVCC	1	$\frac{1}{Z_{VSC}}$	$\frac{Z_c + Z_{VSC}}{Z_c Z_{VSC}}$

Table 3.2 Coefficients of unified models for a current-controlled VSC

Filter	**Sensor positions**	**Coefficients**	
		α	β
L	GVGC	1	0
LC	GVGC	1	0
	GVCC	1	$\frac{1}{Z_c}$
LCL	GVGC CVGC	1	0
	GVCC	$\frac{Z_c}{Z_c+Z_g}$	$\frac{1}{Z_c+Z_g}$
	CVCC	1	$\frac{1}{Z_c}$

3.5 Verification of the proposed models

In this section, the accuracy of the proposed models is investigated by comparing the results calculated using the power flow with those obtained from the PSCAD simulation. Additionally, the results of the power flow using models presented in previous studies were also compared [46, 49]. For the power flow, the forward/backward sweep method was used [62]. To filter out the oscillatory components in the measurements of the PSCAD model, averaged data from 1 s following the onset of steady-state conditions were compared. Two test systems with different sizes, a single node system and a modified IEEE 13-node test feeder, and two DGs of which the main parameters are summarized in Table 3.3 were used. The *LCL* filters were designed using the method presented in [63].

Table 3.3 Main DG parameters

Parameter	0.5-MW DG	1-MW DG
AC voltage (Line-to-line)	380 V	690 V
System frequency	60 Hz	60 Hz
DC link voltage	700 V	1,300 V
Switching frequency	10 kHz	5 kHz
Z_{VSC}	j0.0368 Ω	j0.1242 Ω
Z_g	j0.0012 Ω	j0.0082 Ω
Z_c	0.0278−j5.7760 Ω	0.0904−j9.5220 Ω

In the PACAD simulation, the DG was modeled as a three-wire two-level VSC with the sinusoidal pulse-width modulation (SPWM) switching technique. The proportional plus resonant scheme was used for the current controller. To obtain the instantaneous positive and negative voltage components, a DDSRF-PLL was utilized [54]. The PSCAD simulation was carried out with time steps of 1×10^{-6} s.

3.5.1 Single node system

In the single node system, the VSC-interfaced DG is directly connected to the slack node as shown in Fig. 3.10. The voltages of phase A, B, and C for the slack node were $1.03\angle 0°$, $1.00\angle -120°$, and $0.97\angle 120°$, respectively. According to the rating of the DG, $P_{rating}^{3\phi}$, and the active and reactive power references, the following six cases were examined.

Case 1: $P_{rating}^{3\phi} = 500$ kW, $P_{ref}^{3\phi} = 500$ kW, $Q_{ref}^{3\phi} = -240$ kVAr
Case 2: $P_{rating}^{3\phi} = 500$ kW, $P_{ref}^{3\phi} = 500$ kW, $Q_{ref}^{3\phi} = 0$ kVAr
Case 3: $P_{rating}^{3\phi} = 500$ kW, $P_{ref}^{3\phi} = 500$ kW, $Q_{ref}^{3\phi} = 240$ kVAr
Case 4: $P_{rating}^{3\phi} = 1{,}000$ kW, $P_{ref}^{3\phi} = 1{,}000$ kW, $Q_{ref}^{3\phi} = -480$ kVAr
Case 5: $P_{rating}^{3\phi} = 1{,}000$ kW, $P_{ref}^{3\phi} = 1{,}000$ kW, $Q_{ref}^{3\phi} = 0$ kVAr
Case 6: $P_{rating}^{3\phi} = 1{,}000$ kW, $P_{ref}^{3\phi} = 1{,}000$ kW, $Q_{ref}^{3\phi} = 480$ kVAr

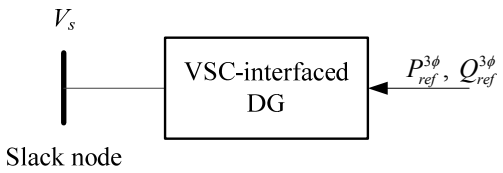

Fig. 3.10 Single node system.

If the reactive power reference is not zero, the power factor is 0.9. Because the *LCL* filter was utilized, the VSCs can be classified into 20 types according to the sensor position and the power control strategy used. For each case, results for each type of VSC were observed and compared.

The power outputs of the DG, which were obtained from the PSCAD simulations, varied depending on the locations of the sensors and on the power control strategy as discussed in the previous section. Figure 3.11 shows the three-phase reactive power output of the DG for Case 2, in which the reactive power reference was zero. In the figure, 'VC' denotes the voltage-controlled VSC. When the locations of the voltage and current sensors were the same, the three-phase reactive power outputs were almost identical, regardless of the power control strategy. However, when the locations of the sensors were varied, the reactive power varied between −2.4 kVAr and 25.0 kVAr. If only the grid voltage and grid current were sensed (GVGC sensing), the three-phase reactive power output was identical to the reference value.

The phase active and reactive power outputs of the DG sensing GVGC for Case 3 are shown in Fig. 3.12. Because of the unbalanced operating conditions, the phase power outputs differed according to power control strategies. However, the results obtained using BPSC and SRFPIC were almost identical as assumed in the previous section.

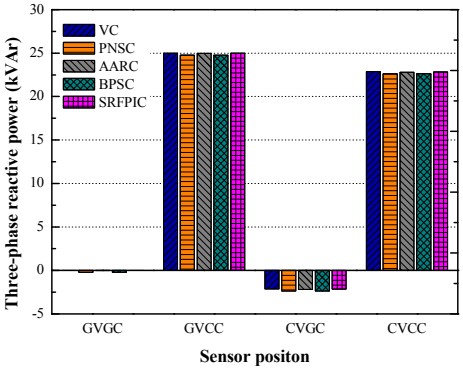

Fig. 3.11 Three-phase reactive power output for different sensor positions.

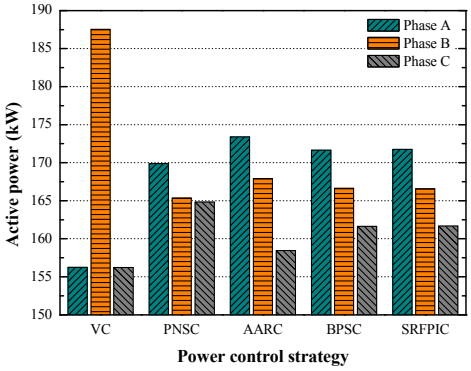

(a) Active power

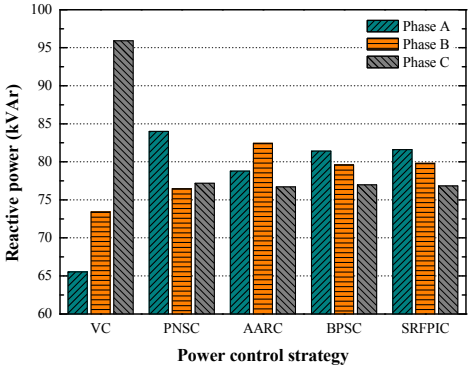

(b) Reactive power

Fig. 3.12 Phase power outputs for different power control strategies.

The maximum differences of the DG output currents between the PSCAD simulation and the power flow are shown in Fig. 3.13, and the detailed results are shown in Appendix A.1. The current difference, ΔI_{DG}, was calculated as

$$\Delta I_{DG} = \left| \frac{|I_{DG,PSCAD}| - |I_{DG,PF}|}{|I_{DG,PSCAD}|} \right| \times 100 \tag{3.85}$$

where $I_{DG,PSCAD}$ is the current obtained from the PSCAD simulation and $I_{DG,PF}$ is the current calculated by using the power flow. In the figure, Model 1 and Model 2 denote the models presented in [49] and [46], respectively.

When the DG was represented by using Model 1 in the power flow, the maximum current difference was 12.7% in the worst case. The maximum difference was up to 14.5% with Model 2. However, with the proposed models, the current outputs of the DG were calculated accurately with difference less than 0.4% for all cases and VSC types.

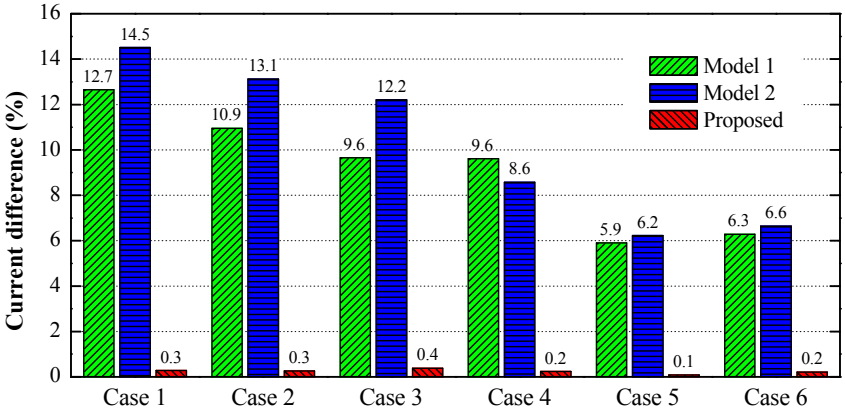

Fig. 3.13 Maximum differences of the DG output currents between the PSCAD simulation and the power flow: single node system.

3.5.2 Modified IEEE 13-node test feeder

The modified IEEE 13-node test feeder are shown in Fig. 3.14 [63]. It consisted of ten lines with a variety of phasing, and nine loads with a total demand of 3,466 + *j*1,986 kVA. Three 1-MW DGs were connected to the original system via transformers (1.5 MVA, 4.16/0.69 kV, 0+*j*1 %). The active power references of the DGs were set to 500 kW, and so approximately 43% of the load was supplied by the DGs. Considering the active power output of the DGs, the tap positions of the voltage regulator between nodes 1 and 650 were reduced by 7 steps from the original tap positions. According to the reactive power references for the DGs, the following three cases were considered.

Case 1: $Q^{3\phi}_{DG\,1,\,ref} = Q^{3\phi}_{DG\,2,\,ref} = Q^{3\phi}_{DG\,3,\,ref} = -240$ kVAr

Case 2: $Q^{3\phi}_{DG\,1,\,ref} = Q^{3\phi}_{DG\,2,\,ref} = Q^{3\phi}_{DG\,3,\,ref} = 0$ kVAr

Case 3: $Q^{3\phi}_{DG\,1,\,ref} = Q^{3\phi}_{DG\,2,\,ref} = Q^{3\phi}_{DG\,3,\,ref} = 240$ kVAr

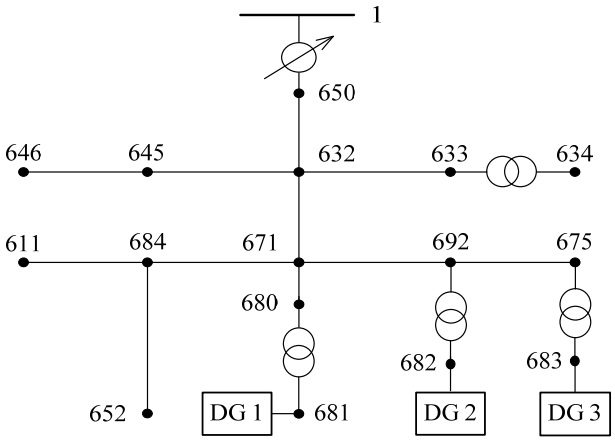

Fig. 3.14 Modified IEEE 13-node test feeder.

Figure 3.15 shows the maximum differences between the PSCAD simulation and the power flow. The detailed results are shown in Appendix A.2. The voltage difference, ΔV, was calculated as

$$\Delta V = \left| \frac{|V_{PSCAD}| - |V_{PF}|}{|V_{PSCAD}|} \right| \times 100 \tag{3.86}$$

where V_{PSCAD} is the voltage obtained from the PSCAD simulation and V_{PF} is the voltage calculated by using the power flow.

The maximum differences of the DG output currents were up to 11.3 % for Model 1 and 12.7% for Model 2. Due to these differences, the node voltages calculated by using the power flow were different from those obtained from the PSCAD simulation. When Model 1 was used to represent the VSC-interfaced DGs in the power flow, the maximum difference of the node voltages was 1.01% (0.0101 p.u.). The difference was up to 1.02% (1.0102 p.u.) when Model 2 was used. These voltage differences are not negligible value in terms of CVR considering that the voltage reduction range of CVR is generally less than 5 %. However, with the proposed models, the DG output currents and the node voltages were calculated accurately with difference less than 0.4% and 0.02% (0.0002 p.u.), respectively.

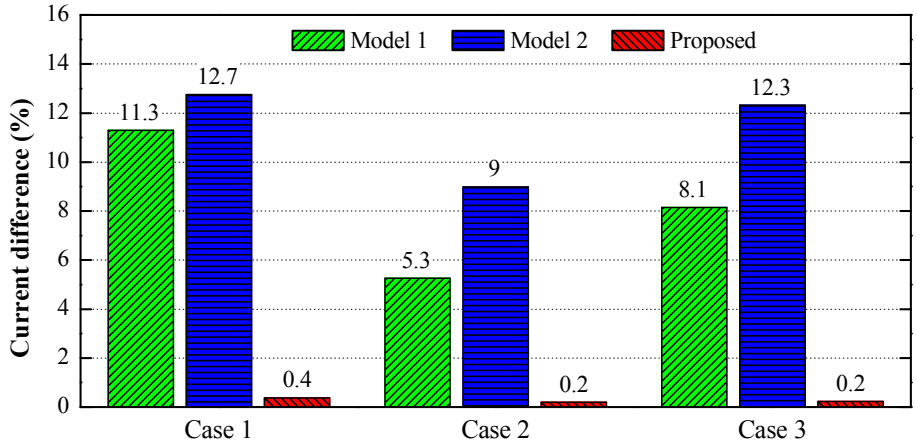

(A) DG output currents

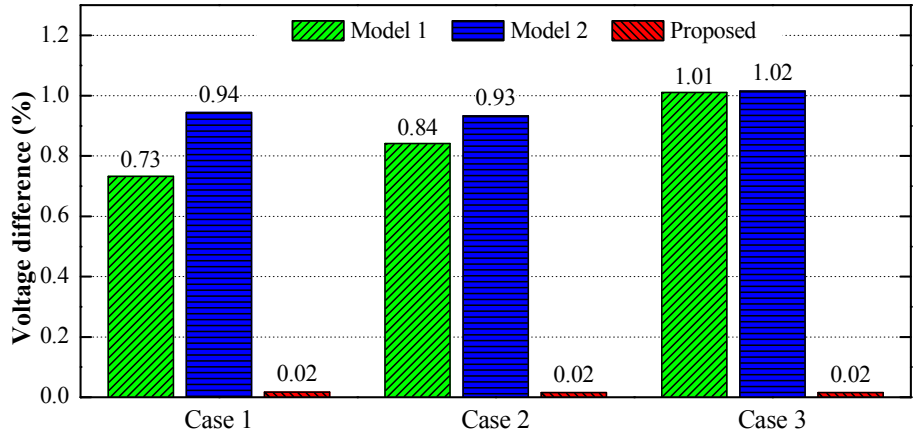

(B) Node voltages

Fig. 3.15 Difference between the PSCAD simulation and the power flow: modified IEEE 13-node test feeder.

Chapter 4. Reactive Power Control Method for Intermittent DGs

In this chapter, the effects of the intermittent outputs of DGs on the voltage profile of the distribution system are analyzed within the framework of CVR. To overcome the adverse effect and improve the CVR effect, a novel reactive power control method is proposed.

4.1 Characteristics of conventional reactive power control methods

The modified IEEE 13-node test feeder used in the previous chapter was used to analyze the effect of inconsistent active power output on CVR. All DGs were interfaced to the distribution system via the GVCC sensing and BPSC VSC. The active power outputs of all DGs were 500 kW. It is assumed that the node voltages have to be maintained higher than 0.96 p.u. The status of the volt/var control devices were as follows; the value in parentheses refers to the phase.

- Tap position of the voltage regulator: 6 (A), 0 (B), 5 (C)
- Capacitors at node 675: open (A), open (B), close (C)
- Capacitor at node 611: closed (C)
- Reactive power output of DG 1: 100 kVAr
- Reactive power output of DG 2: −81.76 kVAr
- Reactive power output of DG 3: −100 kVAr

The minimum voltage of the test system was slightly higher than the minimum limit, as shown in Table 4.1. Because the variation in the load demand was slow, only a slight change in the voltage was observed until the next execution of the CVR function if the DGs were dispatchable.

Table 4.1 Voltages of the base case

Node	Phase Voltage (p.u.)		
	Phase A	**Phase B**	**Phase C**
1	1.0000	1.0000	1.0000
650	1.0375	1.0000	1.0312
632	0.9983	0.9819	0.9934
633	0.9952	0.9798	0.9907
634	0.9707	0.9603	0.9714
645	–	0.9723	0.9915
646	–	0.9706	0.9894
671	0.9680	0.9834	0.9660
680	0.9703	0.9849	0.9682
684	0.9659	–	0.9638
611	–	–	0.9617
652	0.9600	–	–
692	–	–	–
675	0.9623	0.9848	0.9650
681	0.9712	0.9860	0.9692
682	0.9677	0.9832	0.9657
683	0.9618	0.9845	0.9646

To investigate the effect of inconsistent DG active power, the active power output of DG 2 was gradually increased from 0 to 1,000 kW, whereas the active power outputs of DGs 1 and 3 were unchanged. The voltages of three nodes were observed using the power flow analysis: phase A of node 652, phase B of node 634, and phase C of node 611. The following four methods were considered for reactive power control method for DG 2 and the reference are calculated based on the initial state.

- Fixed reactive power control: $Q_{ref}^{3\phi} = -81.76$ kVAr
- Fixed power factor control: $PF_{ref} = 0.9869$ (leading).
- Fixed voltage control: $V_{ref} = 0.9721$ p.u
- *Q*-*V* droop control: $V_{ref} = 0.9639$ p.u and $R = 1$ %

The minimum and maximum voltages of the observed nodes are listed in Table 4.2. For each reactive power control method, the reactive power output and the voltage variation according to the active power output of the DG are shown in Figs. 4.2 and 4.3, respectively. The voltages varied, regardless of the control method used. The voltage variations could be reduced by adjusting the reactive power based on either the active power output or the terminal voltage (i.e., fixed power factor control, fixed voltage control, or *Q*–*V* droop control). When the fixed voltage control method was utilized, the voltage variation was minimized. However, the minimum voltages were less than the lower bound limit, 0.96 p.u.

From these observations, we identified the following two causes as contributing to the degradation of the CVR effect by the intermittent DG:

- Under-voltage violation: to prevent an under-voltage violation, the minimum voltage limit used for the CVR function must increase.

- Voltage increase: when an under-voltage violation does not occur, the voltages increase more than those expected by the CVR function

For these reasons, the voltages are maintained at higher values than when the DG is not intermittent; consequently, the CVR effect decreases.

Table 4.2 Voltage variations according to reactive power control methods

Control method	**Voltage (p.u.)**		
	Minimum	**Maximum**	**Variation**
Fixed reactive power	0.9532	0.9677	0.0145
Fixed power factor	0.9554	0.9650	0.0096
Fixed voltage	0.9570	0.9634	0.0065
Q-V droop	0.9542	0.9666	0.0124

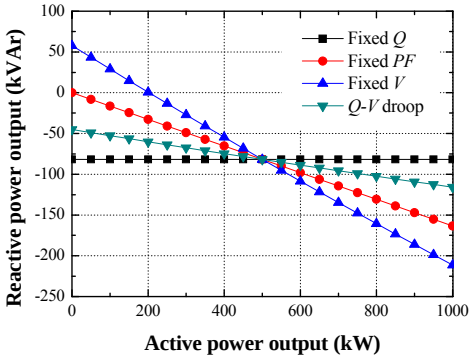

Fig. 4.1 Reactive power outputs of conventional reactive power control methods.

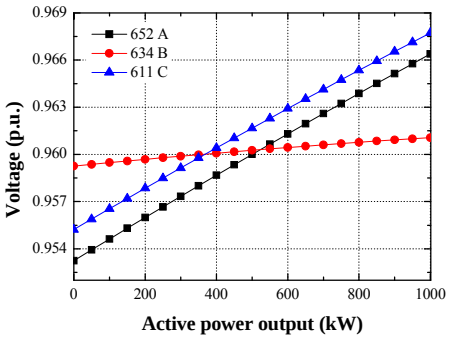

(a) Fixed reactive power control

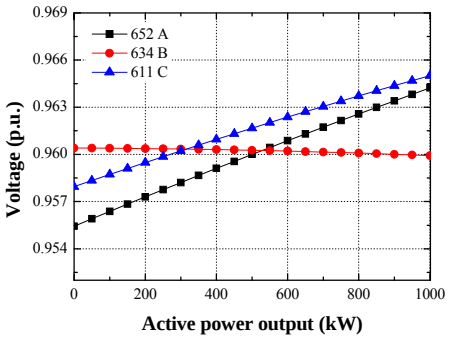

(b) Fixed power factor control

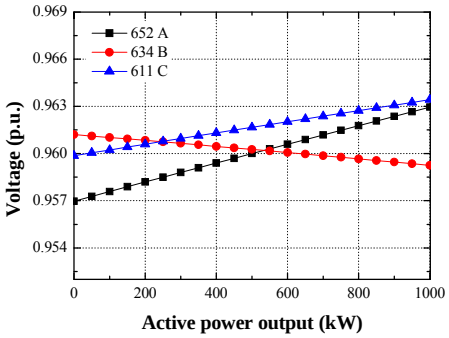

(c) Fixed voltage control

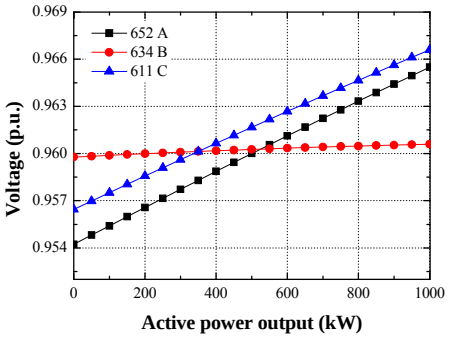

(d) Q–V droop control

Fig. 4.2 Voltage variations with the conventional reactive power control methods.

4.2 Two-segment reactive power versus active power droop control

4.2.1 Basic concept

To reduce the adverse effects of the intermittent DG on CVR, the DG should be able to maintain the voltages of the distribution system as low as possible, but higher than the lower limit. If the DG maintains the reactive power output at a specific value (i.e., fixed reactive control), the voltages of the distribution system increase with the active power output, as shown in Fig. 4.2(a). Therefore, the objective of the reactive power control should be changed based on a specific active power output that sets the minimum voltage of the distribution system equal to the lower bound limit. If the active power output is less than this specific value, the DG should increase the reactive power output to prevent an under-voltage violation. Otherwise, the reactive power output should be reduced to improve the CVR effect by lowering the voltages.

The two-segment reactive power versus active power (*Q*–*P*) droop control method can satisfy this requirement in a passive manner. With this method, the reference for the reactive power controller, $Q_{ref}^{3\phi}$, is given by

$$Q_{ref}^{3\phi} = \begin{cases} Q_{ref}^{Q-P} - R^{+}(P_{out}^{3\phi} - P_{ref}^{Q-P}) & \text{If } P_{out}^{3\phi} > P_{ref}^{Q-P} \\ Q_{ref}^{Q-P} - R^{-}(P_{out}^{3\phi} - P_{ref}^{Q-P}) & \text{Otherwise} \end{cases} \tag{4.3}$$

where P_{ref}^{Q-P} and Q_{ref}^{Q-P} are the three-phase active and reactive power references for the two-segment *Q*–*P* droop controller, respectively, and R^{+} and R^{-} are the upper and lower droop constants, respectively.

The relationship between the active and reactive powers are illustrated in Fig. 4.3. If the active power output is larger than the reference value, the upper droop constant determines the reactive power; otherwise, the lower droop constant does. Therefore, the aforementioned objectives to reduce the adverse effects can be achieved by determining the appropriate droop constants.

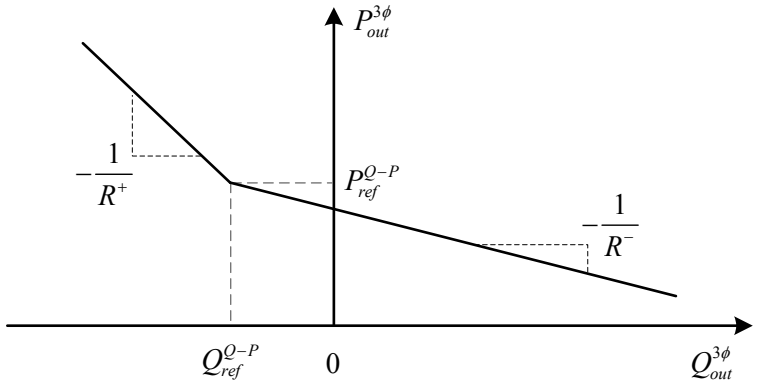

Fig. 4.3 Relationship between the active and reactive powers of two-segment Q–P droop control.

4.2.2 Operational characteristics

To identify the operational characteristics of the proposed method, the test scenario described in the previous section was used. The active and reactive references were 500 kW and −81.76 kVAr, respectively. Figure 4.4 shows the reactive power output of the DG and the voltage of node 652 for phase A, according to R^{-}. The reactive power output and voltage increased with R^{-}. When R^{-} was 0.5, the voltage was maintained at a value almost identical to the minimum limit. In contrast, the reactive power output and the voltage of node

634 for phase B decreased as R^+ increased, as shown in Fig. 4.5. The voltage was close to the minimum limit when R^+ was 0.15. If R^- and R^+ were set to 0.5 and 0.15, respectively, then the reactive power output and the voltages changed in response to the active power, as shown in Fig. 4.6. The minimum voltage was maintained close to the lower bound limit. Therefore, the adverse effect of the intermittent DG can be reduced by using the two-segment *Q*–*P* droop control method.

Because the operation conditions of the distribution system change over time, the droop constants should be modified considering the changed conditions. Unfortunately, the DG is unable to know the overall status of the distribution system; thus, it is impossible for the DG to determine the appropriate droop constants. Therefore, the droop constants should be determined by the CVR function of the DMS.

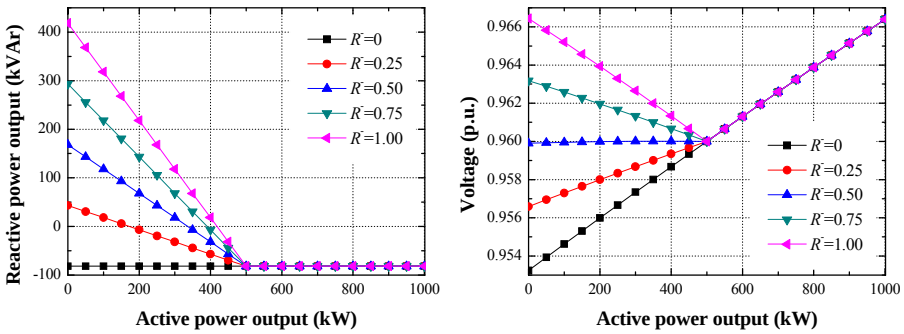

Fig. 4.4 Reactive power output and voltage of node 652 according to R^-.

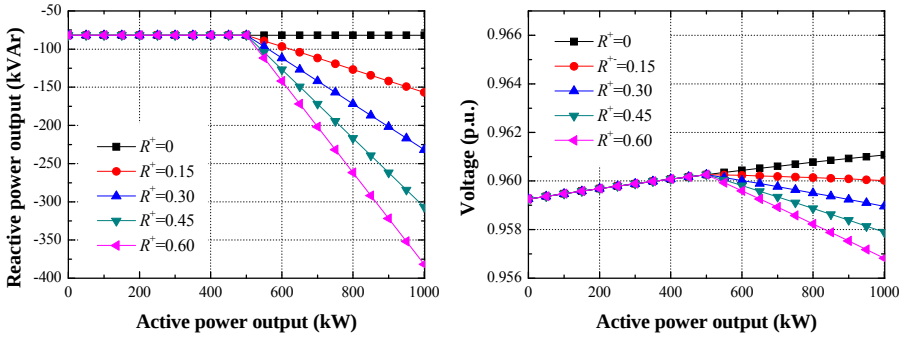

Fig. 4.5 Reactive power output and voltage of node 634 according to R^+.

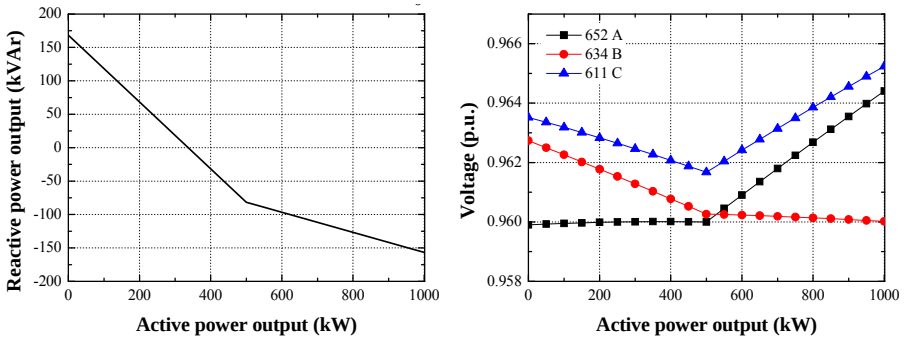

Fig. 4.6 Reactive power output and voltages with $R^- = 0.5$ and $R^+ = 0.15$.

Chapter 5. CVR Function for a DMS

The proposed CVR function is based on a network-model-based method. A stochastic approach should be used to maximize the CVR effect with intermittent DGs. However, the stochastic method is time consuming, and thus not appropriate for CVR, a real-time application requiring the determination of references within a specific time. Therefore, a deterministic approach is adopted for the proposed method, i.e., references are determined using an optimal power flow (OPF).

Various objective functions for the OPF have been proposed [23–25, 43–44]. The objective functions can be classified into two groups. The first group focuses on minimizing the active power consumption of the loads, while the second group minimizes the active power injected from the transmission system. When the strategy of the first group is used, reactive power control devices, such as a capacitor and DG, can supply or absorb too much reactive power to reduce the voltages of the distribution system. As a result, the line loss can increase and thus the active power delivered by the transmission system can increase under a worst-case scenario, even though the power consumption of the loads is minimized. Therefore, the CVR strategy of the second group is adopted. In other words, the objective of the CVR function is to reduce the active power supplied from the transmission system, while maintaining the voltages of the distribution system within an acceptable range.

In the CVR function, references for volt/var control devices, which are listed

in Table 5.1, are obtained using the following three steps:

- Active power determination: considering the intermittency, the active power output of the DG for the base case of the OPF problem and the minimum and maximum active power outputs are determined.

- Reference determination: the OPF problem is formulated, and then the references of the volt/var control devices are obtained by solving the OPF problem.

- Droop constant determination: the droop constants are calculated based on the optimal state.

Table 5.1 Volt/var control devices and corresponding variables determined by the CVR function

Device	Variables
OLTC	Tap position reference
SVR	Tap position reference
ShC	State reference(open/closed)
Dispatchable DG	Reactive power reference
Intermittent DG	Active and reactive power references for two-segment *Q*–*P* droop controller, droop constants

5.1 Active power determination for intermittent DGs

Various probabilistic forecasting methods have been proposed to predict the probability density function (PDF) for the active power output of the intermittent DG, such as that shown in Fig. 5.1 [65]. With these methods, not only the expected value of the active power, but also the possible minimum and maximum active powers, can be determined. These values can also be obtained from historical data.

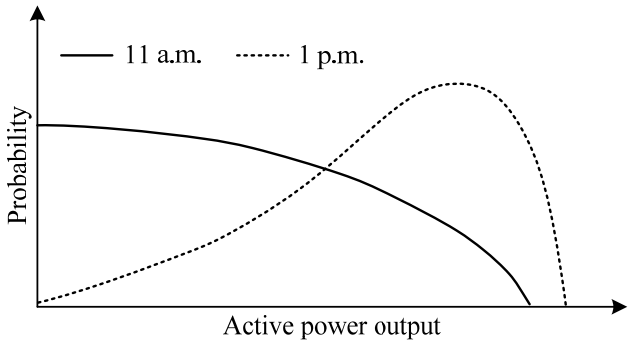

(a) Photovoltaic

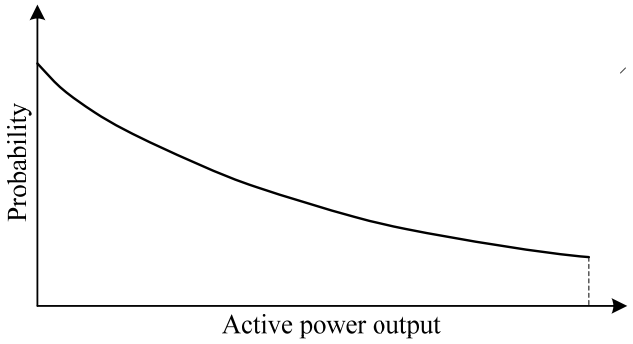

(b) Wind turbine

Fig. 5.1 Probability density functions of intermittent DGs.

Because the references are determined by solving an OPF problem, the references are sensitive to a base case of the OPF problem. If the measured active power output of the intermittent DG, which varies rapidly and randomly, is used to generate the base case, the reference value for the volt/var control device based on a mechanical switch, such as an OLTC and ShC, can be changed frequently. Because the switching operation of the device reduces its lifetime, the system operation cost can increase. In order to prevent the increase in the operation cost by frequent switching operations, an appropriate value that changes slowly and gradually over time should be used as the active power output of the DG for the base case.

The change in the expected value with respect to time is slow and gradual. Thus, the expected value of the active power output of the intermittent DG is used for the base case in the proposed method, i.e., the active power output for the base case is given by

$$P_k^{3\phi} = E[P_{k,out}^{3\phi}], \tag{5.1}$$

where $P_k^{3\phi}$ is the active power output of DG k for the base case of the OPF.

The maximum and minimum active power outputs that will be used to calculate droop constants are also determined from the PDF or historical data, where

$P_{k,min}^{3\phi}$ = Possible minimum active power output of DG k at a given time

$P_{k,max}^{3\phi}$ = Possible maximum active power output of DG k at a given time.

5.2 Reference determination for volt/var control devices

5.2.1 Load modeling

To improve the accuracy and effectiveness of CVR, the loads should be represented with exact models considering their voltage dependency, *e.g.*, the ZIP model and exponential model. However, it is difficult to estimate the parameters for the load models accurately because the loads connected to the distribution system are continuously changing in the real world. If incorrect parameters are used for the load models, under-voltage violations are more likely to occur. To ensure that the voltages of the distribution system are maintained above their minimum bounds, in the proposed method, the loads are modeled as a constant power load, in which the power consumption of the load is independent of the voltage. Even though some of loads are represented by incorrect models, an under-voltage violation is hard to occur because the voltages of the distribution system are maintained at a higher value than those calculated in the CVR function as follows:

- The voltages of the distribution system decrease when the reference values determined by the CVR function are applied.
- Due to the decrease in the voltage, the power consumptions of the loads are reduced. Thus, the voltage drop caused by the loads is smaller than that calculated in CVR.
- Consequently, the voltages of the distribution system are higher than those estimated by the CVR function.

5.2.2 OPF problem formulation

The decision variables for OPF consists of the following: 1) the voltage magnitudes of the nodes, 2) the voltage angles of the nodes, 3) the tap positions of the tap changes, 4) the states of the capacitors, and 5) the reactive power outputs of the DGs. The known values are the active and reactive power consumption of the loads, the active power outputs of the DGs, the voltage of the substation node. The objective function is to reduce the active power supplied from the transmission system.

The active power supplied by the transmission system, $P_{supplied}$, can be expressed as

$$P_{supplied} = \sum_i P^*_{LDs,i} + P^*_{loss} - \sum_i P_{DGs,i} \ , \tag{5.2}$$

where $P^*_{LDs,i}$ is the actual active power consumption of the loads connected to node i, P^*_{loss} is the actual line loss of the distribution system, and $P_{DGs,i}$ is the total active power outputs of DGs connected to node i. Because the exact load models are unknown, the supplied active power is approximated as

$$P_{supplied} \approx \sum_i \left(P_{LDs,i} + wP_{LDs,i}(|V_i| - |V_{i,mea}|) \right) + P_{loss} - \sum_i P_{DGs,i} \ , \tag{5.3}$$

where $P_{LDs,i}$ is the measured active power consumption of loads connected to node i, w is a positive constant that corresponds to the average CVR factor of the distribution system, V_i is the voltage of node i, $V_{i,mea}$ is the measured voltage of node i, and P_{loss} is the line loss when the loads are modeled as a constant power model.

Because the active power output of the DGs and the measured data are constant in the OPF problem, the OPF problem can be formulated as

$$min \qquad \sum_i \left(wP_{LDs,i} \left| V_i \right| \right) + P_{loss} \tag{5.4}$$

subject to

$$P_i = \left| V_i \right| \sum_k \left| V_k \right| \left(G_{ik} \cos(\theta_i - \theta_k) + B_{ik} \sin(\theta_i - \theta_k) \right) \qquad \text{for all node } i \tag{5.5}$$

$$Q_i = \left| V_i \right| \sum_k \left| V_k \right| \left(G_{ik} \sin(\theta_i - \theta_k) - B_{ik} \cos(\theta_i - \theta_k) \right) \qquad \text{for all node } i \tag{5.6}$$

$$V_{i,min} \le \left| V_i \right| \le V_{i,max} \qquad \text{for all node } i \tag{5.7}$$

$$\theta_{i,min} \le \theta_i \le \theta_{i,max} \qquad \text{for all node } i \tag{5.8}$$

$$tap_{m,min} \le tap_{m,ref} \le tap_{m,max} \qquad \text{for all tap changer } m \tag{5.9}$$

$$S_{n,ref} = 1 \ \ or \ \ 0 \qquad \text{for all capacitor } n \tag{5.10}$$

$$-P_k^{3\phi} \tan(\cos^{-1}(PF_{k,min}^{leading})) \le Q_{k,ref}^{3\phi} \le P_k^{3\phi} \tan(\cos^{-1}(PF_{k,min}^{lagging})) \quad \text{for all DG } k \tag{5.11}$$

where

P_i : active power injected into node i by loads and DGs

Q_i : reactive power injected into node i by loads and DGs

θ_i : voltage angle of node i

G_{ik} : real part of the admittance matrix

B_{ik} : imaginary part of the admittance matrix

$tap_{m,ref}$: tap position reference for tap changer m

$tap_{m,min}$: minimum tap position of tap changer m

$tap_{m,max}$: maximum tap position of tap changer m

$S_{n,ref}$: state reference for capacitor n (0=open, 1=closed)

$Q_{k,ref}^{3\phi}$: reactive power reference for DG k

$PF_{k,min,leading}$: minimum leading power factor of DG k

$PF_{k,min,lagging}$: minimum lagging power factor of DG k

Note that this optimization problem is an OPF due to the presence of the power flow equations, equations (5.5) and (5.6) [66]. The reactive power limits for a DG are represented using the power factor, equation (5.11), because the German grid code specifies that a DG shall maintain the power factor at a specific value given by the distribution system operator [67].

The active and reactive powers injected into node i are given by

$$P_i = P_{DGs,i} - P_{LDs,i} \tag{5.12}$$

and

$$Q_i = Q_{DGs,i} - Q_{LDs,i}, \tag{5.13}$$

where $Q_{LDs,i}$ and $Q_{DGs,i}$ are the total reactive power consumption of loads and total reactive power output of the DGs connected to node i, respectively.

5.2.3 Solution method for the OPF

The OPF problem is a non-convex mixed integer nonlinear programming (MINLP) problem; some of the decision variables are integers, and the power

balance constraints, equations (5.5) and (5.6), are non-convex and non-linear. Various global optimization algorithms can be used to find a global solution to the problem. However, these algorithms are very time-consuming, and may be inappropriate for CVR, a real-time application that requires calculation of the reference values within a limited timeframe. Therefore, convex MINLP algorithms can also be used to find a solution. With the convex MINLP algorithm, a global solution may not be found; however, a solution that reduces the value of the objective function can be determined within a specific timeframe.

5.3 Droop constants determination for intermittent DGs

The active and reactive power references for the two-segment *Q*–*P* droop controller of DGs are identical to the active power output used for the base case of OPF and the reactive power output determined by OPF, respectively. The objective of determining the droop constants is to calculate values that maintain the voltages of the distribution system as low as possible, but higher than their lower bound limits, when the active power output of the DG is different from its reference value.

If a large lower droop constant is used, the voltages of the distribution system increase excessively, as shown in Fig. 4.4, thus degrading the CVR effect. In contrast, an under-voltage violation may occur if a small lower droop constant is used. Therefore, the minimum lower droop constant that ensures no under-voltage violation should be used. For the upper droop constant, the maximum value should be used because the operation characteristics are opposite to those of the lower droop constant. In the proposed method, the droop constants satisfying the requirements are determined through two steps, i.e., 1) initial estimation and 2) correction.

5.3.1 Estimation of initial droop constants

Because the proposed method is passive, the voltage variations due to an active power change of the DG should be compensated for by the DG itself. When the active and reactive power outputs of DG *k* are only different from

their reference values, the voltage magnitude of node *i* can be approximated as

$$|V_i| \approx |V_{i,0}| + \frac{\partial |V_i|}{\partial P_k^{3\phi}}\left(P_k^{3\phi} - P_{k,ref}^{Q-P}\right) + \frac{\partial |V_i|}{\partial Q_k^{3\phi}}\left(Q_k^{3\phi} - Q_{k,ref}^{Q-P}\right), \quad (5.14)$$

where

$V_{i,0}$: initial voltage of node *i*, which is the result of the OPF.

$\frac{\partial |V_i|}{\partial P_k^{3\phi}}$: voltage magnitude sensitivity of node *i* with respect to the three-phase active power of DG *k*

$\frac{\partial |V_i|}{\partial Q_k^{3\phi}}$: voltage magnitude sensitivity of node *i* with respect to the three-phase reactive power of DG *k*.

The calculation method of the sensitivities are presented in Appendix B.

When the lower droop controller is activated (i.e., the active power output is less than the reference value), the approximated voltage magnitude can be written as follows using the lower droop constant.

$$|V_i| \approx |V_{i,0}| + \frac{\partial |V_i|}{\partial P_k^{3\phi}}\left(P_k^{3\phi} - P_{k,ref}^{Q-P}\right) - R_k^{-}\frac{\partial |V_i|}{\partial Q_k^{3\phi}}\left(P_k^{3\phi} - P_{k,ref}^{Q-P}\right). \quad (5.15)$$

The minimum voltage constraint for node *i* is given by

$$V_{i,min} \le |V_{i,0}| + \frac{\partial |V_i|}{\partial P_k^{3\phi}}\left(P_k^{3\phi} - P_{k,ref}^{Q-P}\right) - R_k^{-}\frac{\partial |V_i|}{\partial Q_k^{3\phi}}\left(P_k^{3\phi} - P_{k,ref}^{Q-P}\right) \text{ for all node } i\,. \quad (5.16)$$

By arranging with respect to the droop constant, the constraint for the lower droop constant can be formulated as

$$R_k^- \geq \frac{|V_{i,0}| - V_{i,min}}{\frac{\partial |V_i|}{\partial Q_k^{3\phi}}\left(P_k^{3\phi} - P_{k,ref}^{Q-P}\right)} + \frac{\frac{\partial |V_i|}{\partial P_k^{3\phi}}}{\frac{\partial |V_i|}{\partial Q_k^{3\phi}}} \quad \text{for all node } i \,. \tag{5.17}$$

The maximum value of the right-hand side of the inequality corresponds to the minimum value of the active power because the numerator of the first term and the voltage sensitivities are positive. Therefore, the constraint is modified as

$$R_k^- \geq \frac{|V_{i,0}| - V_{i,min}}{\frac{\partial |V_i|}{\partial Q_k^{3\phi}}\left(P_{k,min}^{3\phi} - P_{k,ref}^{Q-P}\right)} + \frac{\frac{\partial |V_i|}{\partial P_k^{3\phi}}}{\frac{\partial |V_i|}{\partial Q_k^{3\phi}}} \quad \text{for all node } i \,. \tag{5.18}$$

Because the minimum value of the lower droop constants satisfying the constraints should be used, the initial lower droop constant for DG k, $R_{k,ini}^-$, is determined as

$$R_{k,ini}^- = \max_i \left\{ \frac{|V_{i,0}| - V_{i,min}}{\frac{\partial |V_i|}{\partial Q_k^{3\phi}}\left(P_{k,min}^{3\phi} - P_{k,ref}^{Q-P}\right)} + \frac{\frac{\partial |V_i|}{\partial P_k^{3\phi}}}{\frac{\partial |V_i|}{\partial Q_k^{3\phi}}} \right\}. \tag{5.19}$$

The voltage magnitude of node i can be approximated as follows when the upper droop is activated:

$$|V_i| \approx |V_{i,0}| + \frac{\partial |V|_i}{\partial P_k^{3\phi}}\left(P_k^{3\phi} - P_{k,ref}^{Q-P}\right) - R_k^+ \frac{\partial |V|_i}{\partial Q_k^{3\phi}}\left(P_k^{3\phi} - P_{k,ref}^{Q-P}\right). \tag{5.20}$$

The voltage constraint for node i is given by

$$V_{i,min} \leq |V_{i,0}| + \frac{\partial |V_i|}{\partial P_k^{3\phi}}\left(P_k^{3\phi} - P_{k,ref}^{Q-P}\right) - R_k^+ \frac{\partial |V_i|}{\partial Q_k^{3\phi}}\left(P_k^{3\phi} - P_{k,ref}^{Q-P}\right) \quad \text{for all load } i \,. \tag{5.21}$$

By arranging with respect to the upper droop constant, we can obtain

$$R_k^+ \le \frac{|V_{i,0}| - V_{i,min}}{\frac{\partial |V_i|}{\partial Q_k^{3\phi}}\left(P_k^{3\phi} - P_{k,ref}^{Q-P}\right)} + \frac{\frac{\partial |V_i|}{\partial P_k^{3\phi}}}{\frac{\partial |V_i|}{\partial Q_k^{3\phi}}} \quad \text{for all node } i\,. \tag{5.22}$$

The minimum value of the right-hand side of the inequality occurs when the active power output is identical to its maximum value. In this case, the constraint for the upper droop constant is given by

$$R_{k,max}^+ \le \frac{|V_{i,0}| - V_{i,min}}{\frac{\partial |V|_i}{\partial Q_k^{3\phi}}\left(P_{k,max}^{3\phi} - P_{k,ref}^{Q-P}\right)} + \frac{\frac{\partial |V_i|}{\partial P_k^{3\phi}}}{\frac{\partial |V_i|}{\partial Q_k^{3\phi}}} \quad \text{for all node } i\,. \tag{5.23}$$

Because the maximum value of the upper droop constant satisfying the constraint should be used, the initial upper droop constant, $R_{k,ini}^+$, is determined as

$$R_{k,ini}^+ = \min_i \left\{ \frac{|V_{i,0}| - V_{i,min}}{\frac{\partial |V|_i}{\partial Q_k^{3\phi}}\left(P_{k,max}^{3\phi} - P_{k,ref}^{Q-P}\right)} + \frac{\frac{\partial |V_i|}{\partial P_k^{3\phi}}}{\frac{\partial |V_i|}{\partial Q_k^{3\phi}}} \right\}. \tag{5.24}$$

The overall procedure to determine the initial droop constants are shown in Fig. 5.2.

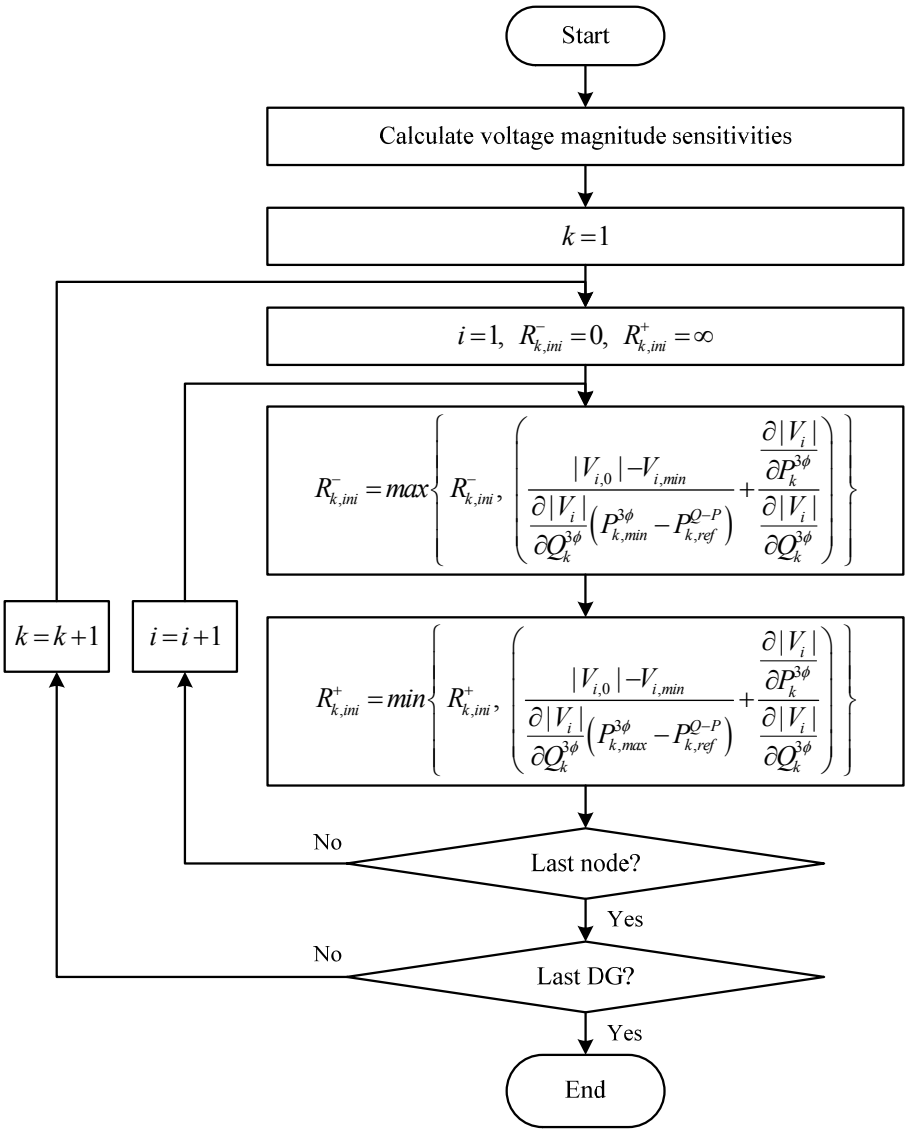

Fig. 5.2 Flow chart for determining the initial droop constants.

5.3.2 Correction of droop constants

Because the initial droop constants are determined with the assumption that the active power output of a single DG changes, an under-voltage violation may occur when the active power outputs of two or more DGs change if the initial droop constants are used directly, as shown in Fig. 5.3. In the figure, the *x*-axis and *y*-axis represent the total active power variation of the DGs, $\Delta P_{total}^{3\phi}$, and the voltage magnitude of node *i*, respectively. When the active power output of a single DG decreases, the voltage is maintained above the minimum limit (the dotted line and dash-dot line in Fig. 5.3). However, if the active power outputs of the two DGs decreases, the voltage can be less than the minimum limit, i.e., the straight line. Therefore, considering the active power output changes of multiple DGs, the droop constants should be corrected to prevent an under-voltage violation.

Because the droop constant correction is the final step in the determining the actual constants, accurate sensitivities should be used to reduce the error caused by the approximation. Figure 5.4 shows the voltage variations of the nodes with respect to the active power output change of the DG with the two-segment droop *Q*–*P* control method. Note that the change in the voltage is not linear. Moreover, the sign of the slope can be changed at the reference active power. Therefore, it is not appropriate to use the voltage sensitivities calculated at a single operating point.

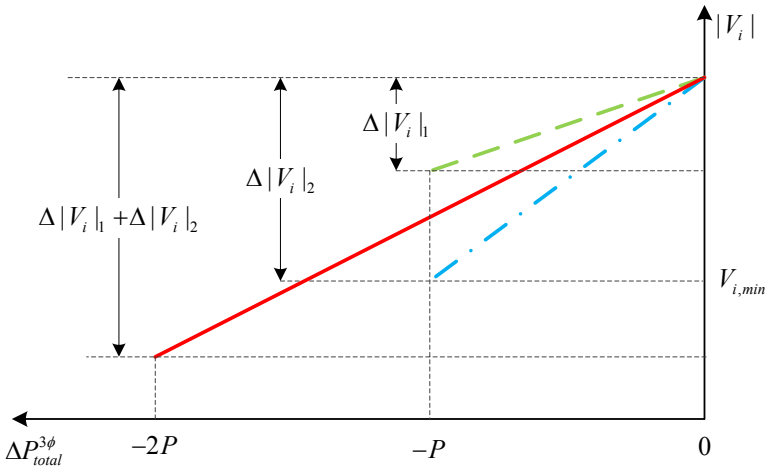

Fig. 5.3 Voltage variations with the initial lower droop constants (dotted line: only the active power output of DG 1 is reduced; dash-dot line: only the active power output of DG 2 is reduced; straight line: the active power outputs of the DGs are equally reduced).

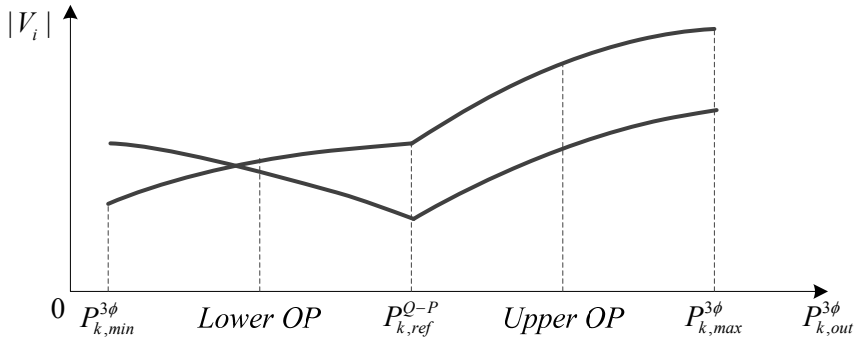

Fig. 5.4 Node voltage variation with respect to the active power output change of a DG with two-segment Q–P droop controller.

To reduce the approximation error, the voltage sensitivities of two operating points, denoted as '*Lower OP*' and '*Upper OP*' in Fig. 5.4, are used. At the '*Lower OP*' point, the active and reactive power outputs of the DGs are given by

$$P_k^{3\phi} = \frac{P_{k,min}^{3\phi} + P_{k,ref}^{Q-P}}{2} \quad \text{for all DG } k \tag{5.25}$$

and

$$Q_k^{3\phi} = Q_{k,ref}^{Q-P} - R_{k,ini}^{-} \frac{P_{k,min}^{3\phi} - P_{k,ref}^{Q-P}}{2} \quad \text{for all DG } k\,. \tag{5.26}$$

The active and reactive power outputs at the '*Upper OP*' point are given by

$$P_k^{3\phi} = \frac{P_{k,ref}^{Q-P} + P_{k,max}^{3\phi}}{2} \quad \text{for all DG } k \tag{5.27}$$

and

$$Q_k^{3\phi} = Q_{k,ref}^{Q-P} - R_{k,ini}^{+} \frac{P_{k,max}^{3\phi} - P_{k,ref}^{Q-P}}{2} \quad \text{for all DG } k\,. \tag{5.28}$$

To distinguish matrices that have the same meaning but are calculated at different operating points, the following notation are used:

- $\frac{\partial |V|}{\partial P_{lower}^{3\phi}}$ and $\frac{\partial |V|}{\partial Q_{lower}^{3\phi}}$: correspond to the voltage magnitude sensitivity matrices with respect to the three-phase active and reactive power outputs of the DGs at the '*Lower OP*' point.

- $\frac{\partial |V|}{\partial P_{upper}^{3\phi}}$ and $\frac{\partial |V|}{\partial Q_{upper}^{3\phi}}$: correspond to the voltage magnitude sensitivity matrices with respect to the three-phase active and reactive power output of the DGs at the '*Upper OP*' point.

Initially, the lower and upper droop constants for each DG are set to corresponding initial constants. And then, the constants are corrected as follows.

A. Minimum voltage estimation for node *i*

From the sensitivities, the gradient of the voltage magnitude for node *i* with respect to the active power output of DG *k* can be obtained as

$$G_{lower,ik} = \frac{\partial |V_i|}{\partial P_{lower,k}^{3\phi}} - R_{k,ini}^{-} \frac{\partial |V_i|}{\partial Q_{lower,k}^{3\phi}} \tag{5.29}$$

and

$$G_{upper,ik} = \frac{\partial |V_i|}{\partial P_{upper,k}^{3\phi}} - R_{k,ini}^{+} \frac{\partial |V_i|}{\partial Q_{upper,k}^{3\phi}}, \tag{5.30}$$

where

$G_{lower,ik}$: gradient of the voltage magnitude for node *i* with respect to the three-phase active power output of DG *k* at '*Lower OP*'

$G_{upper,ik}$: gradient of the voltage magnitude for node *i* with respect to the three-phase active power output of DG *k* at '*Upper OP*'

$\frac{\partial |V_i|}{\partial P_{lower,k}^{3\phi}}$: element of i^{th} row and k^{th} column of $\frac{\partial |V|}{\partial P_{lower}^{3\phi}}$

$\frac{\partial |V_i|}{\partial Q^{3\phi}_{lower,k}}$: element of i^{th} row and k^{th} column of $\frac{\partial |V|}{\partial Q^{3\phi}_{lower}}$

$\frac{\partial |V_i|}{\partial P^{3\phi}_{upper,k}}$: element of i^{th} row and k^{th} column of $\frac{\partial |V|}{\partial P^{3\phi}_{upper}}$

$\frac{\partial |V_i|}{\partial Q^{3\phi}_{upper,k}}$: element of i^{th} row and k^{th} column of $\frac{\partial |V|}{\partial Q^{3\phi}_{upper}}$

Figure 5.5 shows possible trajectories of the voltage magnitude with respect to the active power variation of the DG. From the gradients, the active power output that minimizes the voltage magnitude can be inferred. For instance, the voltage of node *i* is minimized when the active power output of DG *k* is identical to the minimum value, if $G_{ik,lower}$ and $G_{ik,upper}$ are positive, i.e., Case 1.

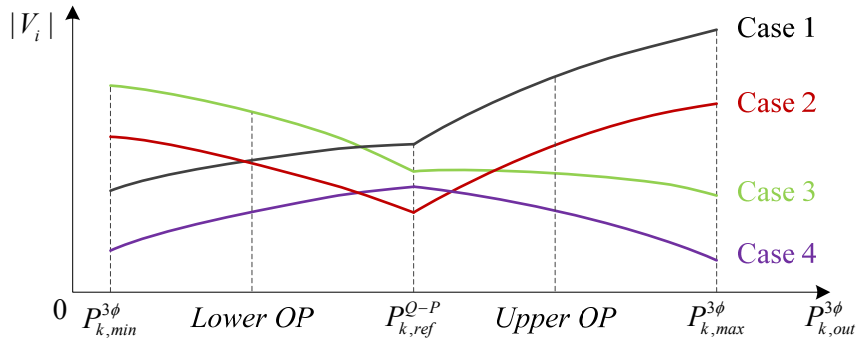

Fig. 5.5 Possible trajectory of the node voltage with the two-segment Q–P droop controller.

Based on the gradients, $\Delta P_{lower,k}^{3\phi}$ and $\Delta P_{upper,k}^{3\phi}$ that are used to estimate the minimum voltage magnitude are determined as follows.

- $G_{lower,ik} \geq 0$, $G_{upper,ik} \geq 0$ (Case 1): $\Delta P_{lower,k}^{3\phi} = P_{k,min}^{3\phi} - P_{k,ref}^{Q-P}$, $\Delta P_{upper,k}^{3\phi} = 0$
- $G_{lower,ik} < 0$, $G_{upper,ik} \geq 0$ (Case 2): $\Delta P_{lower,k}^{3\phi} = 0$, $\Delta P_{upper,k}^{3\phi} = 0$
- $G_{lower,ik} < 0$, $G_{upper,ik} < 0$ (Case 3) : $\Delta P_{lower,k}^{3\phi} = 0$, $\Delta P_{upper,k}^{3\phi} = P_{k,max}^{3\phi} - P_{k,ref}^{Q-P}$
- $G_{lower,ik} \geq 0$, $G_{upper,ik} < 0$ (Case 4) :
  - $G_{lower,ik}(P_{k,min}^{3\phi} - P_{k,ref}^{Q-P}) < G_{upper,ik}(P_{k,max}^{3\phi} - P_{k,ref}^{Q-P})$:

    $\Delta P_{lower,k}^{3\phi} = P_{k,min}^{3\phi} - P_{k,ref}^{Q-P}$, $\Delta P_{upper,k}^{3\phi} = 0$
  - Otherwise

    $\Delta P_{lower,k}^{3\phi} = 0$, $\Delta P_{upper,k}^{3\phi} = P_{k,max}^{3\phi} - P_{k,ref}^{Q-P}$

If $\Delta P_{lower,k}^{3\phi}$ and $\Delta P_{upper,k}^{3\phi}$ are determined for all DGs, the minimum voltage magnitude of node *i* can be estimated as

$$|V_i|_{esti,min} = |V_{i,0}| + \sum_k \left(\frac{\partial |V_i|}{\partial P_{lower,k}^{3\phi}} - R_{k,ini}^{-} \frac{\partial |V_i|}{\partial Q_{lower,k}^{3\phi}} \right) \Delta P_{lower,k}^{3\phi} + \sum_k \left(\frac{\partial |V_i|}{\partial P_{upper,k}^{3\phi}} - R_{k,ini}^{+} \frac{\partial |V_i|}{\partial Q_{upper,k}^{3\phi}} \right) \Delta P_{upper,k}^{3\phi} \quad (5.31)$$

B. Droop constant update for node *i*

If the estimated minimum voltage is less than the minimum limit, the droop constants should be modified to eliminate the under-voltage violation. If the active power output of the DG is smaller than its reference value and thus the

lower droop constant is activated, the lower droop constant should be increased to supply more reactive power. On the contrary, the upper droop constant should be reduced, if the active power output is larger than the reference value. In the proposed method, the droop constants to eliminate the under-voltage violation of node *i* is determined as

$$R_k^- = (1+\alpha)R_{k,ini}^- \tag{5.32}$$

and

$$R_k^+ = (1-\alpha)R_{k,ini}^+, \tag{5.33}$$

where α is a positive constant.

By substituting equations (5.32) and (5.33) into $R_{k,ini}^-$ and $R_{k,ini}^+$ of equation (5.31), respectively, the voltage magnitude of node *i* after the correction, $|V_i|_{corr}$, can be obtained as

$$\begin{aligned} |V_i|_{corr} = |V_{i,0}| + \sum_k \left(\frac{\partial |V_i|}{\partial P_{lower,k}^{3\phi}} - (1+\alpha)R_{k,ini}^- \frac{\partial |V_i|}{\partial Q_{lower,k}^{3\phi}} \right) \Delta P_{lower,k}^{3\phi} \\ + \sum_k \left(\frac{\partial |V_i|}{\partial P_{upper,k}^{3\phi}} - (1-\alpha)R_{k,ini}^+ \frac{\partial |V_i|}{\partial Q_{upper,k}^{3\phi}} \right) \Delta P_{upper,k}^{3\phi} \end{aligned} . \tag{5.34}$$

Using equation (5.31), the voltage can be written as

$$\begin{aligned} |V_i|_{corr} = |V_i|_{esti,min} - \sum_k \left(\alpha R_{k,ini}^- \frac{\partial |V_i|}{\partial Q_{lower,k}^{3\phi}} \right) \Delta P_{lower,k}^{3\phi} \\ + \sum_k \left(\alpha R_{k,ini}^+ \frac{\partial |V_i|}{\partial Q_{upper,k}^{3\phi}} \right) \Delta P_{upper,k}^{3\phi} \end{aligned} . \tag{5.35}$$

The voltage magnitude after the correction has to be greater than or equal to the

minimum voltage limit:

$$V_{i,min} \le |V_i|_{corr} . \tag{5.36}$$

The minimum constraint for α can be formulated as follows by substituting equation (5.35) into equation (5.36) and arranging with respect to α.

$$\alpha \ge \frac{V_{i,min} - |V_i|_{esti,min}}{-\sum_k \left(R^-_{k,ini} \frac{\partial |V_i|}{\partial Q^{3\phi}_{lower,k}} \right) \Delta P^{3\phi}_{lower,k} + \sum_k \left(R^+_{k,ini} \frac{\partial |V_i|}{\partial Q^{3\phi}_{upper,k}} \right) \Delta P^{3\phi}_{upper,k}} \tag{5.37}$$

Since the minimum value of α should be used to maintain the voltage as low as possible, α is determined as

$$\alpha = \frac{V_{i,min} - |V_i|_{esti,min}}{-\sum_k \left(R^-_{k,min} \frac{\partial |V_i|}{\partial Q^{3\phi}_{lower,k}} \right) \Delta P^{3\phi}_{lower,k} + \sum_k \left(R^+_{k,max} \frac{\partial |V_i|}{\partial Q^{3\phi}_{upper,k}} \right) \Delta P^{3\phi}_{upper,k}} . \tag{5.38}$$

Finally, the lower and upper droop constants of DGs are updated as follows according to a droop constant activated.

$$R^-_k = \begin{cases} max\left\{ R^-_k,\ (1+\alpha) R^-_{k,ini} \right\} & \text{if } \Delta P^{3\phi}_{lower,k} < 0 \\ R^-_k & \text{Otherwise} \end{cases} \tag{5.39}$$

$$R^+_k = \begin{cases} min\left\{ R^+_k,\ (1-\alpha) R^+_{k,ini} \right\} & \text{if } \Delta P^{3\phi}_{upper,k} > 0 \\ R^+_k & \text{Otherwise} \end{cases} \tag{5.40}$$

If $\Delta P^{3\phi}_{lower,k}$ is negative, the lower droop constant is activated. Similarly, a positive $\Delta P^{3\phi}_{upper,k}$ means that the upper droop constant is activated. In order to ensure no under-voltage violation for all nodes, the maximum value is selected

for the lower droop constant and the minimum value is selected for the upper droop constant.

C. Overall procedure

The overall procedure of the droop constants correction is shown in Fig. 5.6.

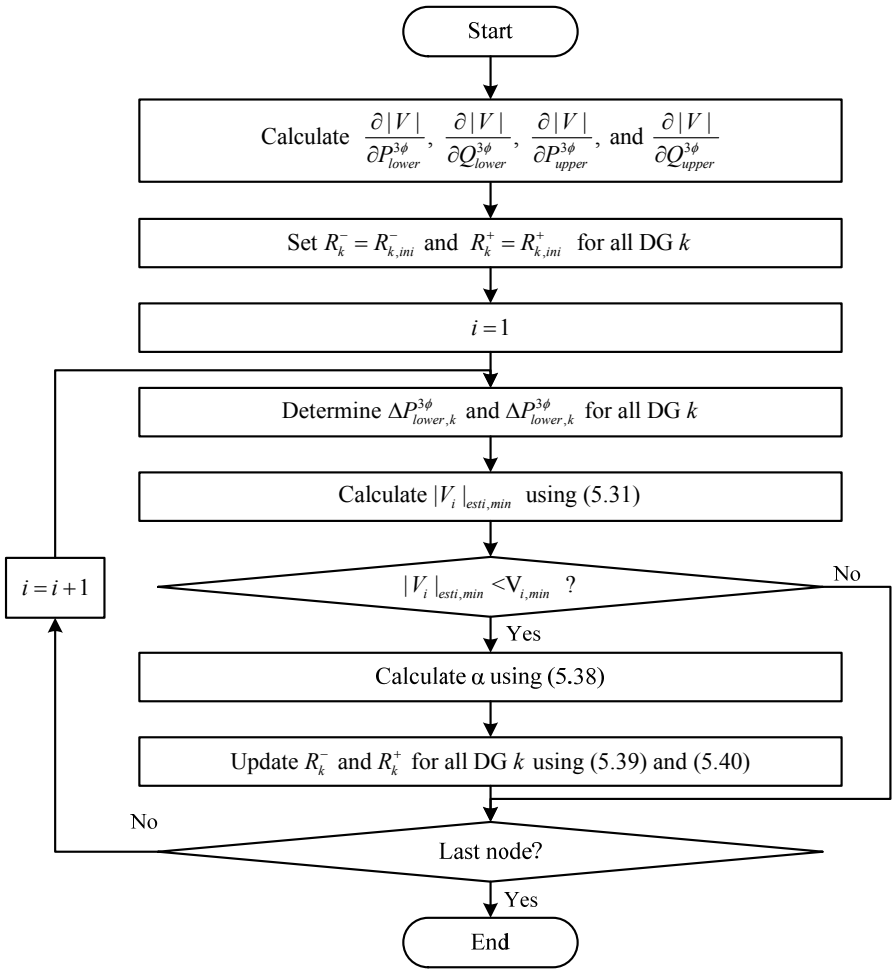

Fig. 5.6 Flow chart for the droop constant correction.

5.4 Illustrative example

5.4.1 Test system

The modified IEEE 13-node test feeder used in Chapter 3, Fig. 3.9, was used for a test system. The real distribution system was represented using a power flow in which the loads were modeled with the ZIP model. The parameters for the load model were identical to those of the original IEEE 13-node test feeder. Information about the voltage regulator and capacitors are summarized in Tables 5.2 and 5.3, respectively.

Table 5.2 Step voltage regulator in the IEEE 13-node test feeder

Device	Node	Tap size	Phases
SVR 1	1-650	0.625 %	A, B, C

Table 5.3 Shunt capacitors in the IEEE 13-node test feeder

Device	Node	Rated kVAr		
		Phase A	Phase B	Phase C
ShC 1	675	200	200	200
ShC 2	611	–	–	100

The DGs were photovoltaic of which the grid interfacing VSC was a GVGC sensing and BPSC type. The major parameters of the DG are shown in Table 3.3. The PDF for the active power output of the DG is formulated by using the beta distribution function:

$$PDF(P_k^{3\phi}) = \begin{cases} \dfrac{\Gamma(a+b)}{\Gamma(a)\Gamma(b)} \left(\dfrac{P_k^{3\phi} - P_{k,min}^{3\phi}}{P_{k,max}^{3\phi} - P_{k,min}^{3\phi}} \right)^{a-1} \left(1 - \dfrac{P_k^{3\phi} - P_{k,min}^{3\phi}}{P_{k,max}^{3\phi} - P_{k,min}^{3\phi}} \right)^{b-1} & \text{if } P_{k,min}^{3\phi} \le P_k^{3\phi} \le P_{k,max}^{3\phi} \\ 0 & \text{otherwise} \end{cases}, \tag{5.41}$$

where $\Gamma(\cdot)$ is the gamma function, and a and b are positive constants. For the PDF shown in Fig. 5.7, a, b, $P_{k,min}^{3\phi}$, and $P_{k,max}^{3\phi}$ are 1, 1.5, 0 kW, and 900 kW, respectively. The expected value of the active power output is 360.0 kW.

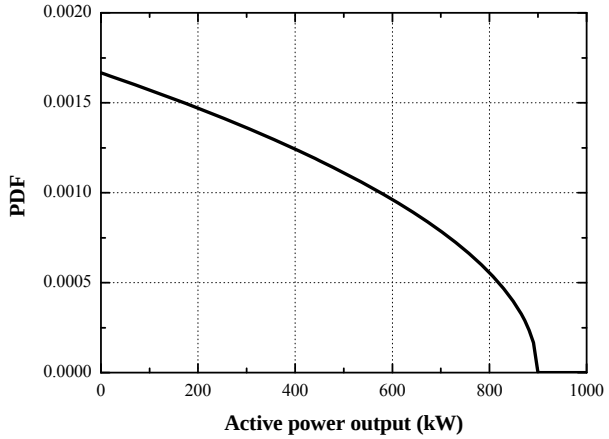

Fig. 5.7 PDF of the active power output for DGs.

The active and reactive power outputs of all DGs were 360 kW and 0 kVAr, respectively. The state of the SVR and ShCs were as follows.

- Tap position of SVR 1: 10 (A), 4 (B), 11 (C)
- State of ShC 1: closed (A), closed (B), closed (C)
- State of ShC 2: closed (C)

Initially, the transmission supplied 2455.6 kW of active power.

The lower and upper bounds of the node voltage were set to 0.96 p.u. and 1.05 p.u., respectively. The average CVR factor used for the objective function of the OPF problem, *w*, was 0.7. The OPF was solved by using the branch and bound method and the sequential quadratic programming method [68]. The voltage sensitivities used to formulate the quadratic program are presented in Appendix B.

5.4.2 CVR results

The reference values determined from the first execution of the CVR function were as follows.

- Tap positions of SVR 1: 4 (A), –2 (B), 6 (C)
- State of ShC 1: closed (A), closed (B), closed (C)
- State of ShC 2: closed (C)
- DG 1: $P_{1,ref}^{Q-P} = 360$ kW, $Q_{1,ref}^{Q-P} = 118.3$ kVAr, $R_1^+ = 0.190$, $R_1^- = 0.472$
- DG 2: $P_{2,ref}^{Q-P} = 360$ kW, $Q_{2,ref}^{Q-P} = 118.3$ kVAr, $R_2^+ = 0.193$, $R_2^- = 0.479$
- DG 3: $P_{3,ref}^{Q-P} = 360$ kW, $Q_{3,ref}^{Q-P} = 65.7$ kVAr, $R_3^+ = 0.195$, $R_3^- = 0.483$

In order to identify the effect of the feedback control, the CVR function was executed again after the references were applied to the volt/var devices. It was assumed that the power consumptions of loads at the rated condition and the active power outputs of DGs were not changed. As a result of the execution of

the CVR function, only the references and droop constants for the DGs were changed as follows.

- DG 1: $P_{1,ref}^{Q-P} = 360$ kW, $Q_{1,ref}^{Q-P} = 118.3$ kVAr, $R_1^+ = 0.154$, $R_1^- = 0.446$
- DG 2: $P_{2,ref}^{Q-P} = 360$ kW, $Q_{2,ref}^{Q-P} = 118.3$ kVAr, $R_2^+ = 0.155$, $R_2^- = 0.452$
- DG 3: $P_{3,ref}^{Q-P} = 360$ kW, $Q_{3,ref}^{Q-P} = 20.3$ kVAr, $R_3^+ = 0.154$, $R_3^- = 0.456$

The voltages of the distribution system before and after the executions of the CVR function are compared in Fig. 5.8. Because the loads were represented with a constant power model, the minimum voltage of the distribution system was slightly higher than the minimum voltage limit after the first execution of the CVR function. However, the minimum voltage was almost identical to the minimum voltage limit as a result of the feedback control, i.e., after the second execution of the CVR function. The average voltage reductions of phase A, phase B, and phase C were 0.033 p.u., 0.032 p.u., and 0.026 p.u., respectively. Due to the decrease of the voltage, the power consumption of the loads were changed as shown in Table 5.3. Consequently, the active power supplied by the transmission system was decreased from 2455.6 kW to 2422.1 kW.

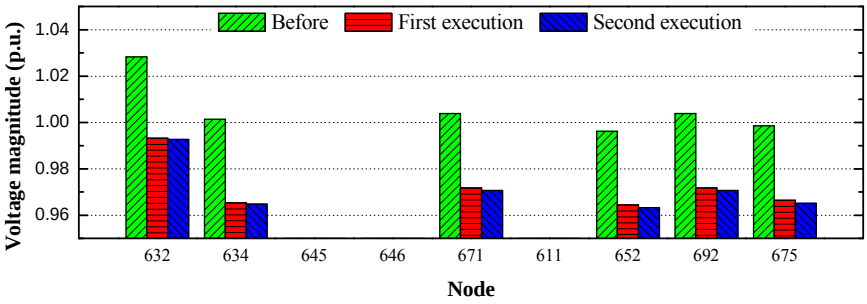

(a) Phase A

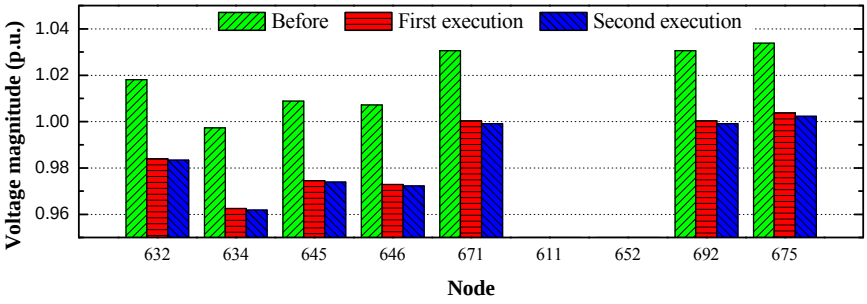

(b) Phase B

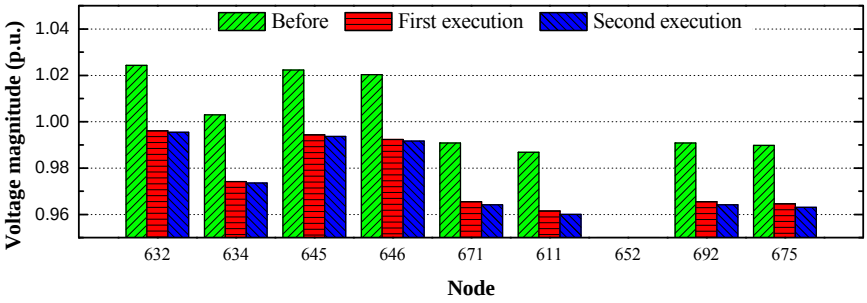

(a) Phase C

Fig. 5.8 Voltage magnitude changes of the load nodes.

Table 5.4 Active power consumption changes of the loads

Node	Model	Active power consumption (kW)					
		Phase A (AB)		Phase B (BC)		Phase C (CA)	
		Before	After	Before	After	Before	After
634	Y-P	160.0	160.0	120.0	120.0	120.0	120.0
645	Y-P	–	–	170.0	170.0	–	–
646	D-Z	–	–	236.7	222.2	–	–
652	Y-Z	127.0	118.8	–	–	–	–
671	D-P	385.0	385.0	385.0	385.0	385.0	385.0
675	Y-P	485.0	485.0	68.0	68.0	290.0	290.0
692	D-I	–	–	–	–	170.7	165.7
611	Y-I	–	–	–	–	167.7	163.2
632	Y-P	17.0	17.0	66.0	66.0	117.0	117.0

* Model: D = delta connection, Y = wye connection, P = constant power, I = constant current, Z = constant impedance

5.4.3 Droop constants determination method

100,000 cases were used to demonstrate the intermittent active power outputs of the DGs. For each case, the active power outputs of the DGs were randomly determined based on the PDF shown in Fig. 5.7. The minimum voltage of the distribution system for each case after the second execution of the CVR function was observed according to the droop constant. The initial droop constants were as follows.

- DG 1: $R_1^+ = 0.366,\ R_1^- = 0.394$
- DG 2: $R_2^+ = 0.369,\ R_2^- = 0.399$
- DG 3: $R_3^+ = 0.367,\ R_3^- = 0.403$

Figure 5.9 shows the minimum voltage of the distribution system when all droop constant were zero, i.e., fixed reactive power control. Due to the intermittent active power outputs of the DGs, the voltage decreased to 0.9466 p.u. in worst case and an under-voltage violation occurred in 49,630 cases (49.6%). Even though the minimum voltage could be increased by using the initial estimated droop constants as shown in Fig. 5.10, an under-voltage violation still occurred in 10,684 cases and the minimum voltage was 0.9560 p.u. in the worst case, as described in the previous section. However, with the corrected droop constants, an under voltage violation never occurred as shown in Fig. 5.11. Moreover, the minimum voltages were maintained slightly higher than the lower bound, 0.96 p.u, as desired.

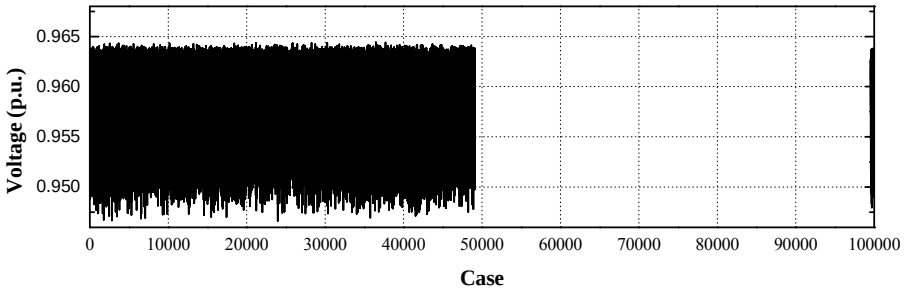

Fig. 5.9 Minimum voltages with zero droop constants.

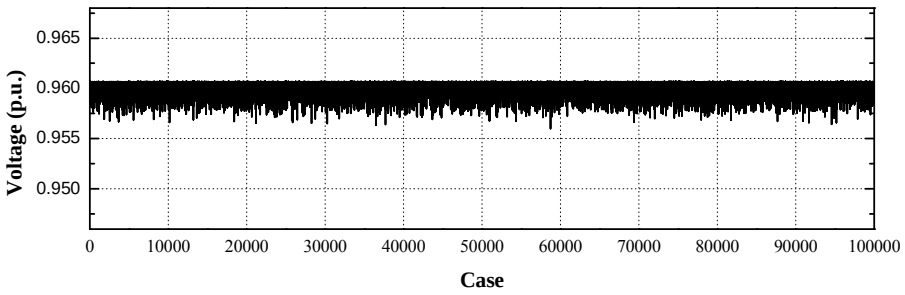

Fig. 5.10 Minimum voltages with initial droop constants.

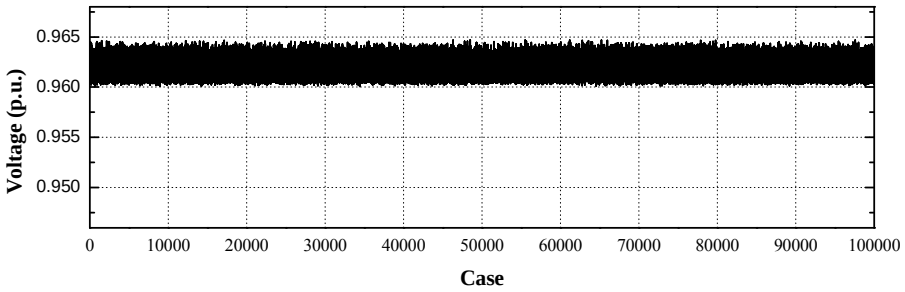

Fig. 5.11 Minimum voltages with corrected droop constants.

Chapter 6. Case Study

6.1 Introduction to the test system

For the test system, the modified IEEE 123-node test feeder shown in Fig. 6.1 was used [63]. Three 1-MW DGs are connected at nodes 66, 250, and 300 through a transformer. The DGs and the transformers are identical to those used in Chapter 4. The total load of the test system is 3,490+*j*1,925 kVA, as summarized in Table 6.1. There are four tap changers, i.e., one OLTC and three SVRs, and four ShCs, as listed in Tables 6.2 and 6.3, respectively. It is assumed that ShC 2, ShC 3, and ShC 4 are fixed capacitors.

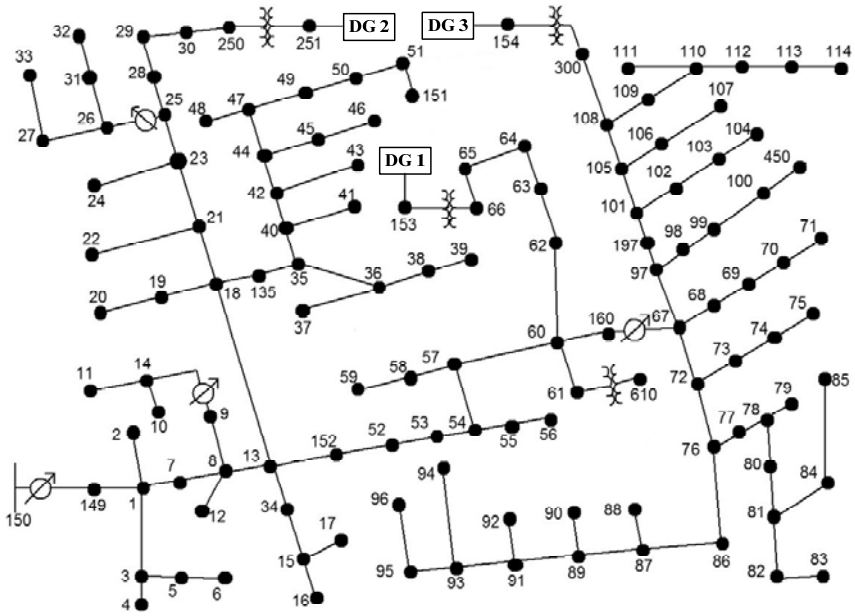

Fig. 6.1 Modified IEEE 123-node test feeder.

The estimated average CVR factor used for the objective function of the OPF, *w*, was set to 0.7. The minimum and maximum voltage limits were 0.96 p.u. and 1.05 p.u., respectively. It was assumed that the power factor of the DG should be between 0.95 lagging and 0.95 leading.

Table 6.1 Loads in the IEEE 123-node test feeder

Load	Number	Power consumption (|*V*| = 1 p.u.)
Constant power	59	1,935 + *j*990 kVA
Constant current	13	705 + *j*430 kVA
Constant impedance	15	850 + *j*500 kVA
Total	87	3,490 + *j*1,920 kVA

Table 6.2 Tap changers in the IEEE 123-node test feeder

Device	Node	Tap size	Phases
OLTC 1	150-149	1.25 %	A, B, C
SVR 1	9-14	0.625 %	A
SVR 2	25-26	0.625 %	A, C
SVR 3	160-67	0.625 %	A, B, C

Table 6.3 Shunt capacitors in the IEEE 123-node test feeder

Device	Node	Rated kVAr		
		Phase A	Phase B	Phase C
ShC 1	83	200	200	200
ShC 2	88	50	–	–
ShC 3	90	–	50	–
ShC 4	92	–	–	50

6.2 Effect of the DG model

In order to identify the effect of the proposed DG model on the CVR, the DG was assumed as a dispatchable DG, and the CVR results using the proposed model and those using the balanced model presented in [49] were compared. A fixed reactive power control method was used for the DGs. According to the active power outputs of the DGs, the following three cases were considered.

Case 1: $P_{DG\,1}^{3\phi} = P_{DG\,2}^{3\phi} = P_{DG\,3}^{3\phi}$ = 360.0 kW

Case 2: $P_{DG\,1}^{3\phi} = P_{DG\,2}^{3\phi} = P_{DG\,3}^{3\phi}$ = 514.3 kW

Case 3: $P_{DG\,1}^{3\phi} = P_{DG\,2}^{3\phi} = P_{DG\,3}^{3\phi}$ = 818.2 kW

The reduction of the active power supplied by the transmission system depends on the initial state of the volt/var control devices. In order to realize the CVR effect when the minimum voltage limit is reduced by 4 %, the initial state was determined using the CVR function, of which the minimum voltage limit was 1.00 p.u. The initial states of the volt/var control devices are shown in Appendix C.1. The initial active powers supplied by the transmission system for Cases 1, 2, and 3 were 2485.9 kW, 2005.0 kW, and 1087.4 kW, respectively.

As noted in previous chapters, the safety margin should be enlarged considering the inaccuracy of the DG model used. In order to determine the safety margin when the balanced model was used, the results of the power flow using the proposed model and the balanced model were compared. Given that the power flow using the proposed model can accurately calculate the system

voltage, the differences in the results can represent the inaccuracy which arises when using the balanced model. Under various load and generation conditions, power flow studies were performed. The results showed that the calculated minimum voltage of the test system when the balanced model was used could be higher than the actual voltage by as much as 0.0023 p.u. Therefore, the minimum voltage of the CVR function using the balanced model was set to 0.9623 p.u. considering the difference.

The references for the volt/var control devices are shown in Appendix C.2. The reductions of the active power supplied by the transmission system are compared in Fig. 6.2. By using the proposed model, additional reductions of the active power supplied were realized; 6.9 kW in Case 1, 6.7 kW in Case 2, and 4.6 kW in Case 3. In other words, the effect of the CVR was improved by 6.8% in average (based on the reductions of the active power supplied using the balanced model).

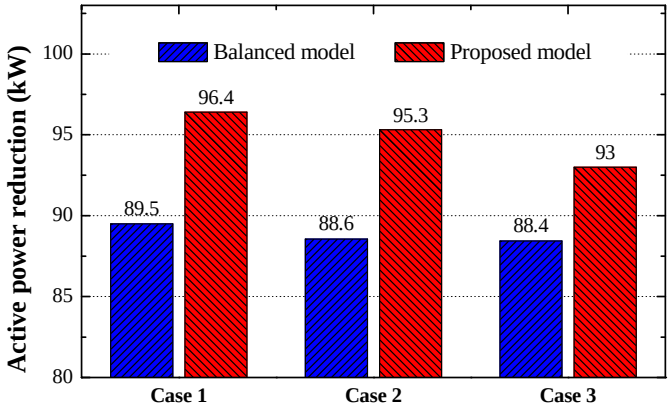

Fig. 6.2 Reduction of the active power supplied according to the DG model.

6.3 Effect of the two-segment *Q–P* droop control method

In this case study, the DGs were assumed to be photovoltaics, i.e., intermittent DGs. In order to identify the improvement in the CVR effect when using the two-segment *Q–P* droop control method, CVR results when using a fixed reactive power control method and a fixed voltage control method were also observed and compared. Since the effect of the reactive power control method on CVR depends on the intermittency of the DG output, three PDFs shown in Fig 6.3 were used. For all PDFs, the minimum and maximum active power outputs are 0 kW and 900 kW, respectively. The expected active power outputs of PDF 1, PDF 2, and PDF 3 are 360.0 kW, 514.3 kW, and 818.2 kW, respectively. PDF 1 refers a very cloudy day, while PDF 3 corresponds to a slightly cloudy day.

According to the active power outputs of the DGs and corresponding PDFs, the following three cases were tested.

Case 1: $P_{DG\,1}^{3\phi} = P_{DG\,2}^{3\phi} = P_{DG\,3}^{3\phi}$ = 360.0 kW, PDF 1 was used.

Case 2: $P_{DG\,1}^{3\phi} = P_{DG\,2}^{3\phi} = P_{DG\,3}^{3\phi}$ = 514.3 kW, PDF 2 was used.

Case 3: $P_{DG\,1}^{3\phi} = P_{DG\,2}^{3\phi} = P_{DG\,3}^{3\phi}$ = 818.2 kW, PDF 3 was used.

Since the active power outputs are same with those for cases of the previous section, the degradation of the CVR effect due to the intermittent active power can be identified by comparing the results.

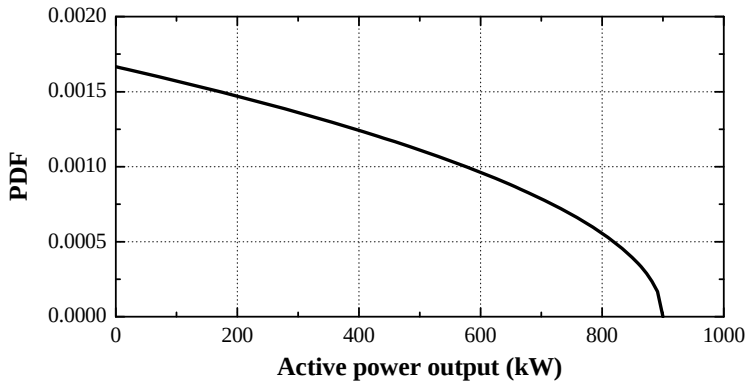

(A) PDF 1

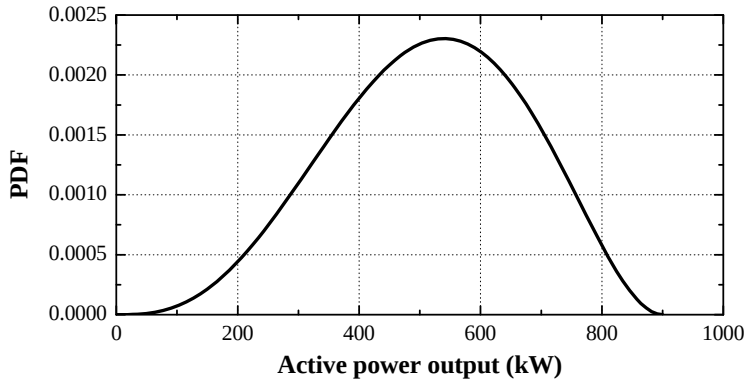

(b) PDF 2

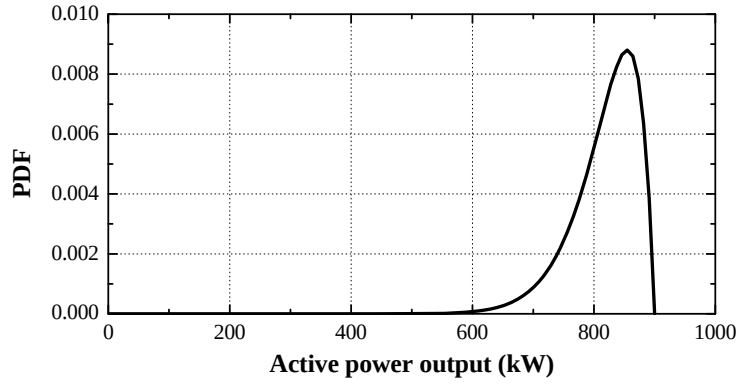

(C) PDF 3

Fig. 6.3 PDFs for active power output of the DGs.

When the fixed reactive power control method or the fixed voltage control method is used with an intermittent DG, an under-voltage violation may occur, as discussed in Chapter 3. Because the stated objective of the CVR is to maintain the voltage within the operational range, the CVR function should determine references which ensure no under-voltage violation. Therefore, the references for these methods were determined as shown in Fig. 6.4. Initially, the minimum voltage limit used for the OPF problem, V_{min}, was set to the actual minimum voltage limit, $V_{min,0}$. The references were determined by solving the OPF. Considering the worst cases, the active powers of the DG were set at their minimum values and the voltages of the distribution system were calculated with the power flow considering the reactive power control method used. If the minimum voltage was lower than the actual minimum voltage limit, the minimum voltage limit used for the OPF problem was increased by 0.0001 p.u. and the references were determined again with the increased minimum voltage limit. If the fixed voltage control method is used, an under voltage violation can occur when the active power output of the DG is increased. Therefore, the voltages when the active power outputs of the DGs were equal to their maximum values were also checked.

In the worst case, the references for the fixed reactive power control method and the fixed voltage method were determined by solving 284 OPFs (Case 2) and 31 OPFs (Case 2), respectively. Meanwhile, the references for the two-segment *Q–P* droop control method were determined by solving a single OPF for all cases. The references for the volt/var control devices are shown in Appendix C.3. In order to demonstrate the effects of intermittent active power

in DGs, 100,000 active power sets were generated based on the PDF for each case, and the CVR results for each set were observed.

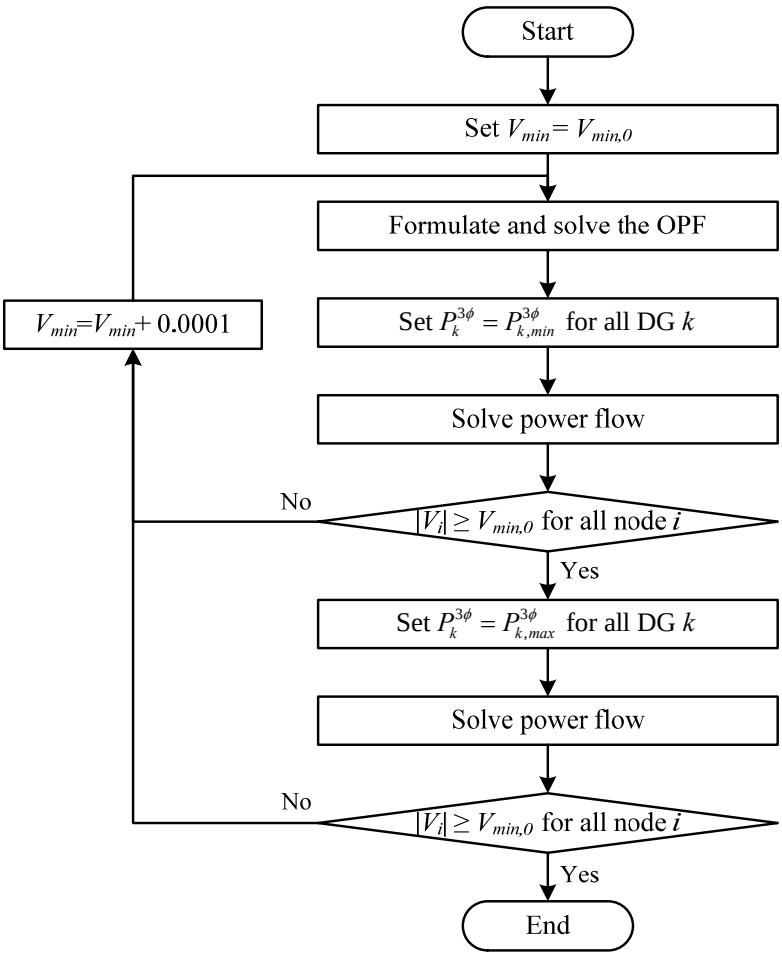

Fig. 6.4 Flow chart of the CVR function for the fixed reactive power control method and the fixed voltage control method.

The reduction of the active power supplied by the transmission system are compared in Fig. 6.5. The active power refers to average values. If the reactive power outputs of the intermittent DGs were not adjusted according to the active power output, i.e., fixed reactive control method, the active power supplied was only reduced by 64.5 kW in Case 1. Because 96.4 kW of the active power supplied was reduced when the DGs were dispatchable, as shown in Fig 6.2, it can be inferred that the CVR effect was degraded by 33 % due to the intermittent active power. Despite the fact that the fixed voltage control method, an active method, was used, the reduction only increased to 87.9 kW. However, by adopting the two-segment *Q–P* droop control method, the reduction was increased to 96.3 kW, which was nearly identical to the result of the dispatchable DG case. In other words, in Case 1, the CVR effect was improved by 49.3 % with respect to the result using the fixed reactive power control method and 9.6 % with respect to the result using the fixed voltage control method. From the results of Cases 2 and 3, it can be also identified that the CVR effect was improved by using the two-segment *Q–P* droop control method.

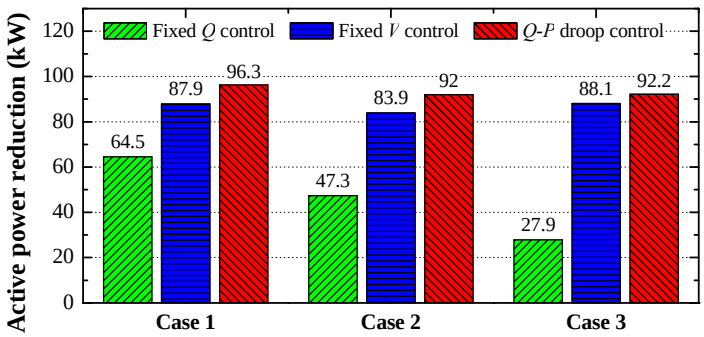

Fig. 6.5 Reduction of the active power supplied according to reactive power control method.

6.4 Effect of the active power determination method

To identify the effect of the active power determination method, two cases were examined and the results were compared. In Case 1, measured active power outputs of the intermittent DGs were used to generate a base case for the OPF problem. Meanwhile, expected values for the active power of intermittent DGs did in Case 2, which corresponds to the proposed method. In both cases, the proposed DG model was used in the CVR function and the two-segment *Q*–*P* droop control method was adopted for the DGs. The initial state of the tap changes and ShC were identical to those of Case 1 used in the previous section. The execution cycle of the CVR function was assumed to be five minutes. The total active power consumption of the loads at the rated condition (i.e., V=1.0 p.u.) and the active power outputs of the DGs were changed as shown in Fig. 6.6 and Fig. 6.7, respectively.

In all cases, the references for ShC 1, OLTC 1, and SVR 1 were not changed. In Case 1, the references for the other SVRs varied, as shown in Fig. 6.8 and total number of tap changes was 17. However, the number of tap changes was reduced to 8 in Case 2, as shown in Fig. 6.9. As noted earlier, an increase in the number of tap changes increases the operating cost of a distribution system. Therefore, the operating cost can be reduced by using the proposed active power determination method (i.e., Case 2).

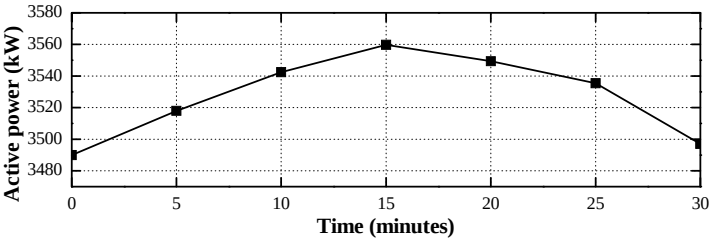

Fig. 6.6 Active power consumption of the loads.

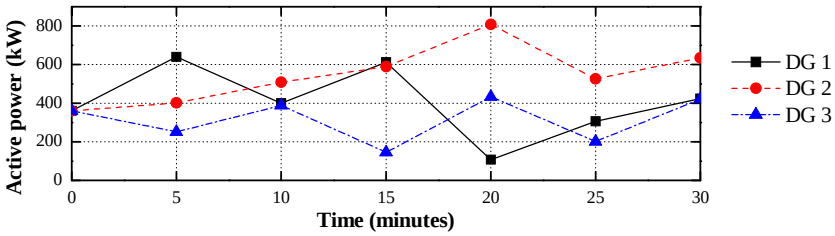

Fig. 6.7 Active power output of the intermittent DGs.

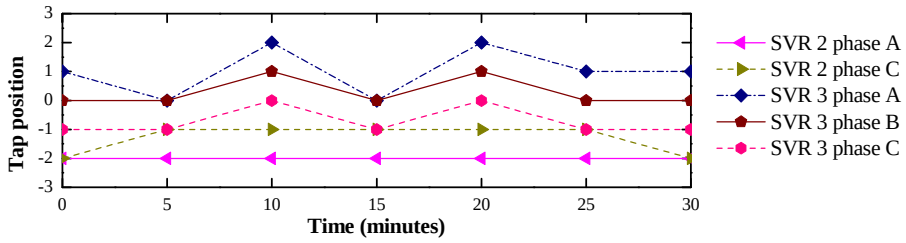

Fig. 6.8 References for SVRs: Case 1.

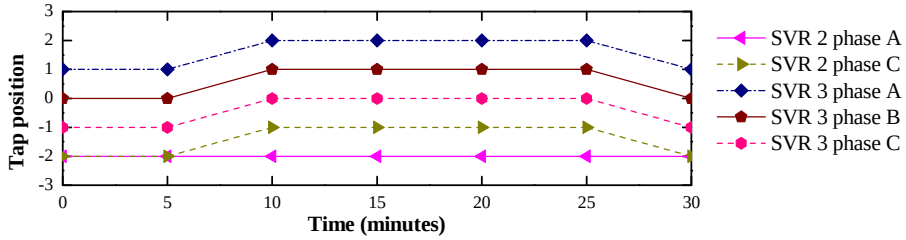

Fig. 6.9 References for SVRs: Case 2.

Chapter 7. Conclusions and Future Extensions

7.1 Conclusions

This dissertation has presented a new conservation voltage reduction (CVR) method for distribution systems considering distributed generators (DGs).

The CVR concept and implementation methods have been reviewed. A network-model-based CVR method is adopted in this dissertation, as this type of method is preferred as a CVR method for next-generation distribution management systems (DMSs). With the network-model-based method, the references for volt/var control devices are determined with an optimal power flow (OPF), after which these references are sent to the volt/var control device through a communication system. In order to ensure that the voltages delivered to customers exceed a specific level, the minimum voltage limit used for the OPF should be larger than the actual limit considering errors. It was identified that inaccuracy in the DG model and the intermittent active power output of the DG can degrade the CVR effect by increasing the minimum voltage limit used for the OPF. Moreover, the operational cost of the distribution system can increase due to the frequent switching operation of mechanical-switch-based volt/var control devices if the measured active power of the intermittent DG is used to generate the base case of OPF. Therefore, this dissertation has proposed steady-state models for DGs, a reactive power control method, and a network-model-based CVR method to

improve the CVR effect by reducing the adverse impact of DGs.

Unified models of a three-phase VSC for an unbalanced steady-state analysis have been proposed. Given that the characteristics of the primary energy source can be negligible for a steady-state analysis, the models capably represent three-wire VSC-interfaced DGs. The factors that determine the output of the VSC under an unbalanced operating condition have been identified as the active and reactive power references, the power control strategy, the output filter, the voltage and current sensor positions. In this dissertation, five power control strategies and three types of output filters have been considered. Based on the sensor positions, two equivalent circuit models consisting of an equivalent three-phase current source (ETCS) with impedance have been proposed. The output current of the ETCS has been formulated as a function of the active and reactive power references and the terminal voltage. With the unified model, 35 three-wire VSC types can be represented. The accuracy of the proposed models has been verified by comparing the results of a power flow study to those obtained from a PSCAD simulation. With the proposed models, the voltage of the test system can be calculated accurately within an error level of 0.025 % (0.00025 p.u.).

A two-segment *Q–P* droop control method has been proposed to reduce the adverse effect of the intermittent DG on the CVR. The performance of the conventional reactive power control methods has been tested under an unbalanced operating condition considering the CVR. The results have shown that the reactive power should be controlled with two different objectives according the active power output to improve the CVR effect. If the active

power is lower than a specific value, the reactive power should be adjusted to prevent an under-voltage violation. Otherwise, the reactive power should be controlled to decrease the voltages of the distribution system but should be higher than the minimum voltage limit. Based on these requirements, the two-segment *Q–P* droop control method has been proposed. The relationship between the active and reactive power is represented by two line segments determined by the active and reactive power references and the lower and upper droop constants. If the active power output is lower than its reference value, the lower droop constant and the references determine the reactive power. Otherwise, the upper droop constant and the references serve in this function. Because the droop constants should reflect the state of the distribution system, they are determined by the CVR function in the DMS.

A method to determine the droop constants has also been proposed. The droop constant is determined based on the optimal state given by the OPF. In order to reduce the computational burden, an approximation method using the voltage sensitivities has been adopted. Assuming that the active power of only a DG is varied, the droop constants satisfying the requirements are estimated for each DG. Next, the droop constants are corrected considering the active power variation of multiple DGs. From a numerical test, it has been verified that the droop constants are determined properly.

In order to prevent frequent switching operations, a method to generate the base case of the OPF has been proposed. With this method, the expected value of the active power for intermittent DGs is used to generate the base case instead of the measured value. The effectiveness of this method has been

identified in a numerical test.

Finally, the effects of the proposed models and methods have been verified in a case study using a modified IEEE 123-node test feeder with three DGs. In order to identify the improvement, the results were compared to those using conventional models and methods. The comparisons have shown that the CVR effect can be improved by using the proposed models and methods.

7.2 Future Extensions

The proposed methods will be extended considering the following subjects:

- This dissertation proposed models of a three-wire VSC for an unbalanced steady-state analysis. Because various types of converters can be used for a DG interface system, models for other types should be developed.

- If references for volt/var control devices are determined based on only measured load data, a reference for a mechanical-switch-based device can be changed in a short time. Although the CVR effect is improved, the overall operating costs of the distribution system can increase due to frequent switching operations. It is expected that the load forecast data can be used to solve this problem.

- The two-segment *Q*–*P* droop control method can be used for other objectives for VVC with an appropriate droop constant method.

Bibliography

[1] P. P. Barker and R.W. de Mello, “Determining the impact of distributed generation on power systems: Part 1—Radial distribution systems,” in *Proc. IEEE Power Eng. Soc. Summer Meeting*, vol. 3, Seattle, WA, Jul. 16–20, 2000, pp. 1645–1656.

[2] C. Masters, “Voltage rise the big issue when connecting embedded generation to long overhead 11 kV lines,” *Inst. Elect. Eng. Power Eng. J.*, pp. 5–12, Feb. 2002.

[3] P. Carvalho, P. F. Correia, and L. Ferreira, “Distributed reactive power generation control for voltage rise mitigation in distribution networks,” *IEEE Trans. Power Syst.*, vol. 23, no. 2, pp. 766–772, May 2008.

[4] Z. Wang and J. Wang, “Review on implementation and assessment of conservation voltage reduction,” *IEEE Trans. Power Syst.*, vol. 29, no. 3, pp. 1306–1315, May 2014.

[5] “Advanced Distribution Management System,” available online at <http://www.schneider-electric-dms.com/media/SEDMS%20ADMS%20SW%20short%20overview.pdf>

[6] A. P. S. Meliopoulos, E. Polymeneas, Zhenyu Tan, Renke Huang, and Dongbo Zhao, “Advanced distribution management system,” *IEEE Trans. Smart Grid*, vol. 4, no. 4, pp. 2109–2117, Dec. 2013.

[7] I.-K. Song, S.-Y. Yun, S.-C. Kwon, and N.-H. Kwak, “Design of smart distribution management system for obtaining real-time security analysis and predictive operation in Korea,” *IEEE Trans. Smart Grid*, vol. 4, no. 1,

pp. 375–382, Mar. 2013.

[8] Jiang Wu and Xiaohong Guan, “Coordinated multi-microgrids optimal control algorithm for smart distribution management system,” *IEEE Trans. Smart Grid*, vol. 4, no. 4, pp. 2174–2181, Dec. 2013.

[9] ANSI Standard C 84.1–1995, *Electrical Power Systems and Equipment–Voltage Rating.*

[10] CSA Standard CAN3–C235–83, *Preferred Voltage Levels for AC Systems, 0 to 50,000 V.*

[11] Technical report: *Green Circuits: Distribution Efficiency Case Studies,* available online at <http://www.epri.com/abstracts/Pages/ProductAbstract.aspx?ProductId=000000000001023518>.

[12] R. Preiss and V. Warnock, “Impact of voltage reduction on energy and demand,” *IEEE Trans. Power App. Syst.*, vol. PAS–97, no. 5 pp. 1665–1671, Sep./Oct. 1978.

[13] D. Lauria, “Conservation voltage reduction (CVR) at Northeast utilities,” *IEEE Trans. Power Del.*, vol. 2, pp. 1186–1191, 1987.

[14] J. De Steese, S. Merrick, and B. Kennedy, “Estimating methodology for a large regional application of conservation voltage reduction,” *IEEE Trans. Power Syst.*, vol. 5, pp. 862–870, 1990.

[15] D. Kirschner, “Implementation of conservation voltage reduction at Commonwealth Edison,” in *Proc. IEEE PES 1990Winter Meeting*, Atlanta, GA, USA, 1990.

[16] B. Kennedy and R. Fletcher, “Conservation voltage reduction (CVR) at

Snohomish county PUD," *IEEE Trans. Power Syst.*, vol. 6, pp. 986–998, 1991.

[17] A. Dwyer, R. E. Nielsen, J. Stangl, and N. S.Markushevich, "Load to voltage dependency tests at BC hydro," *IEEE Trans. Power Syst.*, vol. 10, pp. 709–715, 1995.

[18] B. Williams, "Distribution capacitor automation provides integrated control of customer voltage levels and distribution reactive power flow," in *Proc. IEEE Power Industry Computer Application Conf.*, 1995, 1995, pp. 215–220.

[19] Technical report: *Distribution Efficiency Initiative*, available online at < https://www.leidos.com/NEEA-DEI_Report.pdf>

[20] W. Sunderman, "Conservation voltage reduction system modeling, measurement, and verification," in *Proc. 2012 IEEE PES Transmission and Distribution Conf. Expo. (T&D)*, 2012, pp. 1–4.

[21] T. A. Short and R.W. Mee, "Voltage reduction field trials on distributions circuits," in *Proc. 2012 IEEE PES Transmission and Distribution Conf. Expo. (T&D)*, 2012, pp. 1–6.

[22] S.-R. Nam, S.-H. Kang, J.-H. Lee, S.-J. Ahn, and J.-H. Choi, "Evaluation of the Effects of nationwide conservation voltage reduction on peak-load saving using SOMAS data," *Energies*, vol. 6, no. 12, pp. 6322–6334, Dec. 2013.

[23] M. Farivar, C. R. Clarke, S. H. Low, and K. M. Chandy, "Inverter var control for distribution systems with renewables," in *Proc. IEEE Smart Grid Communication Conf.*, Oct. 2011.

[24] M. Farivar, R. Neal, C. Clarke, and S. H. Low, “Optimal inverter VAR control in distribution systems with high PV penetration,” in *Proc. IEEE PES General Meeting*, Jul. 2012.

[25] M. Manbachi, M. Nasri, B. Shahabi, H. Farhangi, A. Palizban, and S. Arzanpour et al., “Real-time adaptive VVO/CVR topology using multi-agent system and IEC 61850-based communication protocol,” *IEEE Trans. Sustain. Energy*, vol. 5, no. 2, pp. 587–596, 2014.

[26] R. Singh, F. Tuffner, J. Fuller, and K. Schneider, “Effects of distributed energy resources on conservation voltage reduction (CVR),” in *Proc. 2011 IEEE PES General Meeting*, 2011, pp. 1–7.

[27] Y. J. Kim, S. J. Ahn, P. I. Hwang, G. C. Pyo, and S. I. Moon, “Coordinated control of a DG and voltage control devices using a dynamic programming algorithm,” *IEEE Trans. Power Syst.*, vol. 28, no. 1, pp. 42–51, Feb. 2013.

[28] H.-G. Yeh, D. F. Gayme, and S. H. Low, “Adaptive VAR control for distribution circuits with photovoltaic generators,” *IEEE Trans. Power Syst.*, vol. 27, pp. 1656–1663, 2012.

[29] J. M. Carrasco, L. G. Franquelo, J. T. Bialasiewicz, E. Galván, R. P. Guisado, andM. A. Prats et al., “Power-electronic systems for the grid integration of renewable energy sources: A survey,” *IEEE Trans. Ind. Electron.*, vol. 53, pp. 1002–1016, 2006.

[30] Technical report: *Protection Coordination Planning with Distributed Generation*, available online at <https://www.nrcan.gc.ca/sites/www.nrcan.gc.ca/files/canmetenergy/files/p

ubs/2007-149e.pdf>

[31] IEEE Standard 1547™-2003, *IEEE Standard for Interconnecting Distributed Resources with Electric Power Systems*.

[32] Available online at <http://cyber.kepco.co.kr/ckepco/front/jsp/CY/H/C/CYHCHP00801.jsp>

[33] P. Kundur, *Power System Stability and Control*, McGraw Hill, 1994.

[34] Technical report: *Evaluation of Conservation Voltage Reduction (CVR) on a National Level*, available online at <http://www.pnl.gov/main/publications/external/technical_reports/PNNL-19596.pdf>

[35] M. J. Krok and S. Gene, "A coordinated optimization approach to Volt/VAr control for large power distribution networks," in *Proc. Amer. Control Conf. (ACC)*, 2011, 2011, pp. 1145–1150.

[36] C. McCarthy and J. Josken, "Applying capacitors to maximize benefits of conservation voltage reduction," in *Proc. Rural Electric Power Conf.*, 2003, 2003, pp. C4-1–C4-5.

[37] J. Triplett and S. Kufel, "Implementing CVR through voltage regulator LDC settings," in *Proc. 2012 IEEE Rural Electric Power Conf.*, 2012, pp. B2-1–B2-5.

[38] M. A. Peskin, P. W. Powell, and E. J. Hall, "Conservation voltage reduction with feedback from advanced metering infrastructure," in *Proc. 2012 IEEE PES Transmission and Distribution Conf. Expo.*, 2012, pp. 1–8.

[39] R. Neal, "The use of AMI meters and solar PV inverters in an advanced Volt/VAr control system on a distribution circuit," in *Proc. 2010 IEEE*

PES Transmission and Distribution Conf. Expo., 2010, pp. 1–4.

[40] R. Belvin and T. Short, “Voltage reduction results on a 24-kV circuit,” in *Proc. 2012 IEEE PES Transmission and Distribution Conf. Expo.*, 2012, pp. 1–4.

[41] E. Baran and M. Y. Hsu, “Volt/Var control at distribution substations,” *IEEE Trans. Power Syst.*, vol. 14, pp. 312–318, Feb. 1999.

[42] Available online at
< http://cialab.ee.washington.edu/nwess/2012/talks/uluski.pdf >

[43] I. Roytelman, B. Wee, and R. Lugtu, “Volt/Var control algorithm for modern distribution management system,” *IEEE Trans. Power Syst.*, vol. 10, pp. 1454–1460, 1995.

[44] S. Bose, D. F. Gayme, S. Low, and M. K. Chandy, “Optimal power flow over tree networks,” in *Proc. 49th Annual Allerton Conf.*, 2011, pp. 1342–1348.

[45] M. S. Chen and W. E. Dillon, “Power system modeling,” *IEEE Proceedings*, vol. 62, no. 7, pp. 901–915, July 1974.

[46] M. Z. Kamh and R. Iravani, “Unbalanced model and power flow analysis of microgrids and active distribution systems,” *IEEE Trans. Power Del.*, vol. 25, no. 4, pp. 2851–2858, Oct. 2010.

[47] K. Mahmoud, M. Abdel-Akher, and M. Orabi, “Induction generator model for unbalanced distribution power-flow analysis,” *Energy Conversion Congress and Exposition*, pp. 2786-2790, Sept. 2010.

[48] M. Z. Kamh and R. Iravani, “Three-phase steady-state model of type-3 wind generation unit—Part I: Mathematical models,” *IEEE Trans. Sustain.*

Energy, vol. 2, no. 4, pp. 477–486, Oct. 2011.

[49] S. M. Moghaddas-Tafreshi and E. Mashhour, "Distributed generation modeling for power flow studies and a three-phase unbalanced power flow solution for radial distribution systems considering distributed generation," *Elect. Power Syst. Res.*, vol. 79, no. 4, pp. 680–686, Apr. 2009.

[50] M. Z. Kamh and R. Iravani, "A unified model of three-phase electronically-coupled distributed energy resources for power-flow analysis," *IEEE Trans. Power Del.*, vol. 26, no. 2, pp. 899–909, Apr. 2011.

[51] P. I. Hwang, S. I. Moon, and S. J. Ahn, "A vector-controlled distributed generator model for a power flow based on a three-phase current injection method," *Energies*, vol. 6, no. 8, pp. 4269–4287, Aug. 2013.

[52] A. Panosyan, R. Walling, E.-M Bärthlein, and R. Witzmann, "Reactive power compensation of self-induced voltage variations," in *Proc. 2012 CIRED workshop*, 2012, pp.1–4.

[53] J. W. Smith, W. Sunderman, R. Dugan, and B. Seal, "Smart inverter volt/var control functions for high penetration of PV on distribution systems," in *Proc. IEEE Power Systems Conf. Expo.*, 2011, pp. 1–6.

[54] R. Teodorescu, M. Liserre, and P. Rodriguez, *Grid Converters for Photovoltatic and Wind Power System*, Wiley-IEEE Press, 2011.

[55] R. H. Lasseter, et. al, "Control and design of microgrid components," PSERC Final project reports, Jan. 2006.

[56] A. J. Roscoe, S. J. Finney, and G. M. Burt, "Tradeoffs between AC power quality and DC bus ripple for 3-Phase 3-wire inverter-connected devices within microgrids," *IEEE Trans. Power Electron.*, vol. 26, no. 3, pp. 674–

688, Mar. 2011.

[57] F. Wang, J. L. Duarte, and M. A. M. Hendrix, “Pliant active and reactive power control for grid-interactive converters under unbalanced voltage dips,” *IEEE Trans. Power Electron.*, vol. 26, no. 5, pp. 1511–1521, May 2011.

[58] P. Rodriguez, A. V. Timbus, R. Teodorescu, M. Liserre, and F. Blaabjerg, “Flexible active power control of distributed power generation systems during grid faults,” *IEEE Trans. Ind. Electron.*, vol. 54, no. 5, pp. 2583–2583, Oct. 2007.

[59] P. Rodriguez, A. Timbus, R. Teodorescu, M. Liserre, and F. Blaabjerg, “Reactive power control for improving wind turbine system behavior under grid faults,” *IEEE Trans. Power Electron.*, vol. 24, no. 7, pp. 1798–1801, Jul. 2009.

[60] M. Castilla, J. Miret, J. L. Sosa, J. Matas, and L. Garc´ıa de Vicuna, “Grid fault control scheme for three-phase photovoltaic inverters with adjustable power quality characteristics,” *IEEE Trans. Ind. Electron.*, vol. 25, no. 12, pp. 2930–2940, Dec. 2010.

[61] J. A. Suul, “Control of Grid Integrated Voltage Source Converters under Unbalanced Conditions,” *Ph.D. dissertation*, Dept. Elec. Power Eng., Norwegian University of Science and Technology, Trondheim, Norway, 2012

[62] C. S. Cheng and D. Shirmohammadi, “A three-phase power flow method for real-time distribution system analysis,” *IEEE Trans. Power Syst.*, vol. 10, pp. 671–679, May 1995.

[63] M. Simoes, A. Reznik, A. Al Durra, and S.M. Muyeen, “LCL filter design and performance analysis for grid interconnected systems,” IEEE Trans. Ind. Appl., vol. 50, no. 2, pp. 1225–1232, Mar. 2014.

[64] Distribution test feeders, available online at < http://ewh.ieee.org/soc/pes/dsacom/testfeeders/index.html >

[65] A. Bracale, P. Caramia, G. Carpinelli, Di Fazio AR, and G. Ferruzzi, “A Bayesian method for short-term probabilistic forecasting of photovoltaic generation in smart grid operation and control,” *Energies*, vol. 6, no. 2, pp. 733–747, Feb. 2013.

[66] A. J. Wood, B. F. Wollenberg, *Power Generation, Operation, and Control*, John Wiley & Sons, Inc., 1996.

[67] Advanced inverters for distributed PV, available online at <http://www.clean-coalition.org/site/wp-content/uploads/2013/10/CC_ PV_AI_Paper_Final_Draft_v2.5_05_13_2013_AK.pdf >

[68] P. Venkataraman, *Applied Optimization with MATLAB Programming*, Wiley, 2009.

[69] G. W. Stagg, *Computer Methods in Power System Analysis*, McGraw Hill, 1968.

Appendix A. Results of VSC Model Verification

A.1 Single node system

Table A.1 Maximum differences of DG output currents between the PSCAD simulation and the power flow: Cases 1 and 2 for the single node system

VSC type		Case 1 (%)			Case 2 (%)		
		Model 1	**Model 2**	**Proposed**	**Model 1**	**Model 2**	**Proposed**
GVGC	VC	10.615	2.900	0.278	10.791	3.453	0.258
	PNSC	2.777	9.746	0.001	1.536	13.000	0.001
	AARC	4.384	12.320	0.046	4.747	13.128	0.055
	BPSC	3.118	10.751	0.026	3.121	13.082	0.028
	SRFPIC	3.035	10.766	0.056	3.065	13.115	0.057
GVCC	VC	12.556	5.344	0.248	10.888	4.151	0.065
	PNSC	4.585	11.387	0.002	1.678	13.061	0.005
	AARC	5.409	14.518	0.049	4.620	12.992	0.056
	BPSC	5.015	12.943	0.029	3.047	13.044	0.031
	SRFPIC	4.926	12.957	0.056	3.107	13.076	0.058
CVGC	VC	10.743	2.791	0.269	10.948	3.177	0.152
	PNSC	2.805	9.456	0.003	1.544	12.572	0.001
	AARC	4.401	11.939	0.047	4.747	12.717	0.054
	BPSC	3.132	10.368	0.025	3.121	12.670	0.028
	SRFPIC	3.048	10.382	0.057	3.065	12.705	0.058
CVCC	VC	12.651	5.418	0.187	10.939	3.984	0.090
	PNSC	4.652	11.031	0.001	1.628	12.681	0.004
	AARC	5.462	14.171	0.049	4.665	12.629	0.055
	BPSC	5.066	12.593	0.029	3.005	12.681	0.031
	SRFPIC	4.983	12.614	0.051	3.058	12.721	0.066

Appendix A

Table A.2 Maximum differences of DG output currents between the PSCAD simulation and the power flow: Cases 3 and 4 for the single node system

VSC type		Case 3 (%)			Case 4 (%)		
		Model 1	**Model 2**	**Proposed**	**Model 1**	**Model 2**	**Proposed**
GVGC	VC	8.911	2.777	0.375	7.648	0.449	0.189
	PNSC	2.699	12.203	0.003	2.777	4.817	0.001
	AARC	4.866	9.646	0.051	4.383	6.539	0.047
	BPSC	3.124	10.757	0.030	3.120	5.052	0.026
	SRFPIC	3.117	10.762	0.058	3.035	5.064	0.056
GVCC	VC	9.648	4.990	0.230	9.488	2.493	0.109
	PNSC	4.766	11.197	0.005	4.537	5.605	0.001
	AARC	5.027	11.441	0.050	5.361	8.575	0.049
	BPSC	4.880	11.303	0.032	4.967	7.080	0.029
	SRFPIC	4.962	11.380	0.055	4.877	7.093	0.057
CVGC	VC	8.894	2.768	0.341	7.877	0.499	0.207
	PNSC	2.672	11.887	0.004	2.893	4.521	0.002
	AARC	4.846	9.344	0.051	4.456	6.189	0.047
	BPSC	3.110	10.455	0.029	3.176	4.680	0.025
	SRFPIC	3.104	10.462	0.056	3.091	4.693	0.058
CVCC	VC	9.628	4.859	0.359	9.612	2.810	0.237
	PNSC	4.709	10.858	0.006	4.811	5.340	0.001
	AARC	4.983	11.114	0.051	5.578	8.376	0.049
	BPSC	4.836	10.977	0.032	5.177	6.856	0.028
	SRFPIC	4.913	11.048	0.049	5.097	6.879	0.049

Table A.3 Maximum differences of DG output currents between the PSCAD simulation and the power flow: Cases 5 and 6 for the single node system

VSC type		Case 5 (%)			Case 6 (%)		
		Model 1	**Model 2**	**Proposed**	**Model 1**	**Model 2**	**Proposed**
GVGC	VC	5.826	0.466	0.061	4.663	0.414	0.211
	PNSC	1.538	6.103	0.003	2.695	6.430	0.006
	AARC	4.748	6.223	0.056	4.869	4.709	0.054
	BPSC	3.122	6.179	0.029	3.126	5.058	0.032
	SRFPIC	3.065	6.210	0.058	3.116	5.060	0.057
GVCC	VC	5.898	0.840	0.082	6.278	2.637	0.136
	PNSC	1.718	6.115	0.005	4.808	6.389	0.007
	AARC	4.578	6.050	0.056	5.069	6.645	0.053
	BPSC	3.086	6.100	0.032	4.922	6.501	0.034
	SRFPIC	3.148	6.128	0.058	5.007	6.585	0.056
CVGC	VC	5.877	0.551	0.050	4.586	0.454	0.135
	PNSC	1.569	5.682	0.002	2.596	6.162	0.014
	AARC	4.752	5.866	0.057	4.790	4.428	0.055
	BPSC	3.124	5.822	0.029	3.079	4.836	0.036
	SRFPIC	3.066	5.853	0.058	3.065	4.845	0.056
CVCC	VC	5.729	0.836	0.063	6.282	2.423	0.154
	PNSC	1.516	5.878	0.004	4.584	5.937	0.017
	AARC	4.761	5.876	0.057	4.893	6.242	0.054
	BPSC	3.092	5.925	0.031	4.751	6.102	0.038
	SRFPIC	3.049	5.969	0.072	4.822	6.172	0.046

A.2 Modified IEEE 13-node test feeder

Table A.4 Maximum current and voltage differences between the PSCAD simulation and the power flow: Case 1 for the modified IEEE 13-node test feeder

VSC type		DG current difference (%)			Node voltage difference (%)		
		Model 1	**Model 2**	**Proposed**	**Model 1**	**Model 2**	**Proposed**
GVGC	VC	7.302	1.083	0.168	0.297	0.056	0.009
	PNSC	2.492	5.737	0.009	0.170	0.398	0.003
	AARC	5.306	8.476	0.046	0.245	0.473	0.001
	BPSC	3.834	7.090	0.023	0.209	0.437	0.003
	SRFPIC	3.853	7.073	0.003	0.212	0.440	0.001
GVCC	VC	11.298	5.648	0.333	0.732	0.518	0.014
	PNSC	6.644	10.016	0.007	0.645	0.873	0.003
	AARC	9.169	12.743	0.050	0.716	0.944	0.001
	BPSC	7.851	11.382	0.029	0.683	0.911	0.003
	SRFPIC	7.837	11.368	0.036	0.685	0.912	0.002
CVGC	VC	6.792	0.443	0.208	0.269	0.051	0.011
	PNSC	3.003	5.439	0.011	0.188	0.336	0.005
	AARC	5.902	8.021	0.137	0.187	0.414	0.005
	BPSC	4.341	6.527	0.020	0.149	0.376	0.005
	SRFPIC	4.360	6.509	0.004	0.152	0.379	0.001
CVCC	VC	10.826	5.423	0.377	0.674	0.449	0.017
	PNSC	6.216	9.574	0.010	0.585	0.813	0.005
	AARC	8.772	12.333	0.048	0.657	0.885	0.003
	BPSC	7.440	10.958	0.028	0.624	0.852	0.005
	SRFPIC	7.438	10.956	0.051	0.625	0.853	0.003

Table A.5 Maximum current and voltage differences between the PSCAD simulation and the power flow: Case 2 for the modified IEEE 13-node test feeder

VSC type		DG current difference (%)			Node voltage difference (%)		
		Model 1	**Model 2**	**Proposed**	**Model 1**	**Model 2**	**Proposed**
GVGC	VC	5.159	0.683	0.117	0.218	0.039	0.012
	PNSC	2.957	8.480	0.003	0.364	0.455	0.003
	AARC	5.129	7.941	0.056	0.325	0.416	0.002
	BPSC	3.982	8.306	0.028	0.348	0.439	0.004
	SRFPIC	4.011	8.283	0.004	0.351	0.442	0.000
GVCC	VC	4.947	1.613	0.200	0.658	0.484	0.015
	PNSC	3.338	8.882	0.009	0.841	0.933	0.003
	AARC	5.108	7.899	0.057	0.797	0.888	0.002
	BPSC	4.086	8.488	0.034	0.823	0.914	0.003
	SRFPIC	4.137	8.457	0.053	0.825	0.916	0.002
CVGC	VC	5.244	0.615	0.107	0.181	0.059	0.013
	PNSC	2.874	8.392	0.005	0.319	0.410	0.005
	AARC	5.255	7.969	0.122	0.282	0.396	0.006
	BPSC	4.027	8.256	0.027	0.303	0.395	0.005
	SRFPIC	4.057	8.230	0.004	0.306	0.398	0.002
CVCC	VC	4.874	1.655	0.157	0.615	0.437	0.015
	PNSC	3.431	8.980	0.006	0.796	0.887	0.005
	AARC	4.992	8.037	0.056	0.752	0.843	0.004
	BPSC	3.965	8.623	0.031	0.778	0.869	0.005
	SRFPIC	4.002	8.601	0.071	0.780	0.871	0.003

Table A.6 Maximum current and voltage differences between the PSCAD simulation and the power flow: Case 3 for the modified IEEE 13-node test feeder

VSC type		DG current difference (%)			Node voltage difference (%)		
		Model 1	**Model 2**	**Proposed**	**Model 1**	**Model 2**	**Proposed**
GVGC	VC	4.932	1.116	0.167	0.197	0.046	0.015
	PNSC	4.384	8.730	0.009	0.531	0.535	0.003
	AARC	3.768	8.142	0.058	0.380	0.384	0.002
	BPSC	4.145	8.501	0.034	0.458	0.462	0.004
	SRFPIC	4.175	8.531	0.004	0.461	0.465	0.000
GVCC	VC	6.614	5.155	0.234	0.596	0.489	0.013
	PNSC	8.148	12.323	0.013	1.010	1.015	0.003
	AARC	7.262	11.477	0.054	0.854	0.858	0.003
	BPSC	7.765	11.957	0.036	0.934	0.939	0.004
	SRFPIC	7.794	11.985	0.060	0.936	0.940	0.003
CVGC	VC	5.211	0.500	0.193	0.243	0.058	0.013
	PNSC	4.080	8.365	0.006	0.480	0.485	0.004
	AARC	3.541	7.925	0.143	0.336	0.409	0.006
	BPSC	3.796	8.168	0.033	0.408	0.412	0.005
	SRFPIC	3.827	8.198	0.006	0.411	0.416	0.002
CVCC	VC	6.102	4.739	0.180	0.547	0.435	0.015
	PNSC	7.666	11.862	0.012	0.958	0.962	0.004
	AARC	6.814	11.050	0.054	0.803	0.808	0.004
	BPSC	7.309	11.522	0.035	0.883	0.887	0.005
	SRFPIC	7.320	11.532	0.076	0.884	0.888	0.004

Appendix B. Voltage Sensitivity Matrices

B.1 Power injection sensitivity matrices with respect to the three-phase power of a DG

Power injection sensitivity matrices represent the relationship between the three-phase active and reactive power outputs of DGs and the node injection powers and consist of four matrices:

$\frac{\partial P}{\partial P_{DGs}^{3\phi}}, \frac{\partial Q}{\partial P_{DGs}^{3\phi}}$: active and reactive power injection sensitivity matrices with respect to three-phase active power outputs of DGs

$\frac{\partial P}{\partial Q_{DGs}^{3\phi}}, \frac{\partial Q}{\partial Q_{DGs}^{3\phi}}$: active and reactive power injection sensitivity matrices with respect to three-phase reactive power outputs of DGs.

Fig. B.1 shows a simple radial system with two DGs and corresponding active power injection sensitivity matrix. The structure of the other matrices are identical to that of the active power injection sensitivity matrix. Since each node is a three-phase node and there are three nodes excluding the slack node, the number of rows is 9. The number of column is identical to the number of DGs. In the matrix, only the elements corresponds to nodes connected to DGs are non-zero, *i.e.*, sub-matrices $\frac{\partial P_3}{\partial P_1^{3\phi}}$ and $\frac{\partial P_4}{\partial P_2^{3\phi}}$.

Appendix B

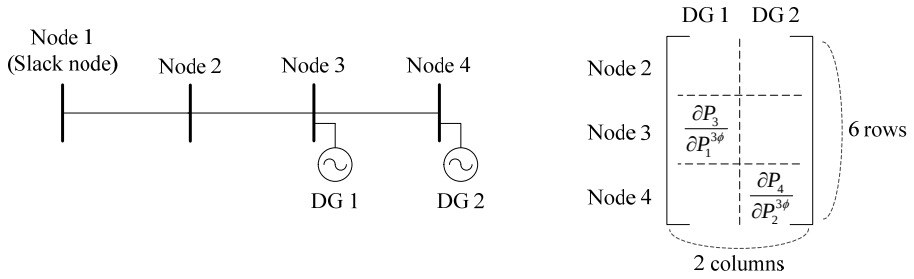

Fig. B.1 Structure of power injection sensitivity matrices

The complex power injected by the equivalent three-phase current source (ETCS), which represents DG *k* and is connected node *i*, is given by

$$\begin{bmatrix} S_i^a \\ S_i^b \\ S_i^c \end{bmatrix} = diag(V_i) \begin{bmatrix} V_i^a & 0 & 0 \\ 0 & V_i^b & 0 \\ 0 & 0 & V_i^c \end{bmatrix} I_g^* \quad , \tag{B.1}$$

where the superscription *a*, *b*, and *c* denote phase A, phase B, and phase C, respectively, and $diag(V_i)$ is defined as

$$diag(V_i) = \begin{bmatrix} V_i^a & 0 & 0 \\ 0 & V_i^b & 0 \\ 0 & 0 & V_i^c \end{bmatrix}. \tag{B.2}$$

From equation (B.1), the sub-matrices can be formulated. For example,

$$\frac{\partial P_i}{\partial P_k^{3\phi}} = \frac{\partial}{\partial P_k^{3\phi}} \mathrm{Re}\left\{ \begin{bmatrix} S_i^a \\ S_i^b \\ S_i^c \end{bmatrix} \right\} = \mathrm{Re}\left\{ \frac{\partial}{\partial P_k^{3\phi}} \left(diag(V_i) I_g^* \right) \right\} \tag{B.3}$$

$$\frac{\partial Q_i}{\partial P_k^{3\phi}} = \frac{\partial}{\partial P_k^{3\phi}} \mathrm{Im}\left\{ \begin{bmatrix} S_i^a \\ S_i^b \\ S_i^c \end{bmatrix} \right\} = \mathrm{Im}\left\{ \frac{\partial}{\partial P_k^{3\phi}} \left(diag(V_i) I_g^* \right) \right\} \tag{B.4}$$

where Re{·} and Im{·} are real and imaginary part operators. By substituting equations (3.67)–(3.70) into the grid current, I_g, the sub-matrices can be written with respect to the three-phase active and reactive power references. For example, $\frac{\partial P_i}{\partial P_k^{3\phi}}$ for the voltage-controlled VSC is written as

$$\frac{\partial P_i}{\partial P_k^{3\phi}} = \mathrm{Re}\left\{ \frac{\partial}{\partial P_k^{3\phi}} \left(diag(V_i) \left(\alpha \frac{P_{ref}^{3\phi} - jQ_{ref}^{3\phi}}{\left(V_i^*\right)^t E} E + \beta \frac{V_i^t T V_i^*}{\left(V_i^*\right)^t E} E - \gamma T V_i \right)^* \right) \right\}, \quad \text{(B.5)}$$

where V_i is the voltage vector of node i and given by

$$V_i = \begin{bmatrix} V_i^a & V_i^b & V_i^c \end{bmatrix}^t. \quad \text{(B.6)}$$

Because the three-phase active and reactive power outputs are identical to corresponding references in the steady-state, equation (B.5) can be modified as

$$\begin{aligned} \frac{\partial P_i}{\partial P_k^{3\phi}} &= \mathrm{Re}\left\{ \frac{\partial}{\partial P_k^{3\phi}} \left(diag(V_i) \left(\alpha \frac{P_k^{3\phi} - jQ_k^{3\phi}}{\left(V_i^*\right)^t E} E + \beta \frac{V_i^t T V_i^*}{\left(V_i^*\right)^t E} E - \gamma T V_i \right)^* \right) \right\}. \quad \text{(B.7)} \\ &= \mathrm{Re}\left\{ \frac{\alpha}{V_i^t E^*} diag(V_i) E^* \right\} \end{aligned}$$

Finally, we can obtain all sensitivity matrices as follows.

- Voltage-controlled VSC

$$\frac{\partial P_i}{\partial P_k^{3\phi}} = \frac{\partial P_i}{\partial Q_k^{3\phi}} = \mathrm{Re}\left\{ \frac{\alpha}{V_i^t E^*} diag(V_i) E^* \right\} \quad \text{(B.8)}$$

$$\frac{\partial Q_i}{\partial P_k^{3\phi}} = \frac{\partial Q_i}{\partial Q_k^{3\phi}} = \mathrm{Im}\left\{ \frac{\alpha}{V_i^t E^*} diag(V_i) E^* \right\} \quad \text{(B.9)}$$

Appendix B

- Current-controlled VSC with PNSC

$$\frac{\partial P_i}{\partial P_k^{3\phi}} = \mathrm{Re}\left\{ \frac{-\alpha}{\left(V_i^t\right)^* MV_i} diag(V_i) MV_i^* \right\} \tag{B.10}$$

$$\frac{\partial Q_i}{\partial P_k^{3\phi}} = \mathrm{Im}\left\{ \frac{-\alpha}{\left(V_i^t\right)^* MV_i} diag(V_i) MV_i^* \right\} \tag{B.11}$$

$$\frac{\partial P_i}{\partial Q_k^{3\phi}} = \mathrm{Re}\left\{ \frac{\alpha}{\left(V_i^t\right)^* MV_i} diag(V_i) TV_i^* \right\} \tag{B.12}$$

$$\frac{\partial Q_i}{\partial Q_k^{3\phi}} = \mathrm{Im}\left\{ \frac{\alpha}{\left(V_i^t\right)^* MV_i} diag(V_i) TV_i^* \right\} \tag{B.13}$$

- Current-controlled VSC with AARC

$$\frac{\partial P_i}{\partial P_k^{3\phi}} = \mathrm{Re}\left\{ \frac{\alpha}{\left(V_i^t\right)^* TV_i} diag(V_i) TV_i^* \right\} \tag{B.14}$$

$$\frac{\partial Q_i}{\partial P_k^{3\phi}} = \mathrm{Im}\left\{ \frac{\alpha}{\left(V_i^t\right)^* TV_i} diag(V_i) TV_i^* \right\} \tag{B.15}$$

$$\frac{\partial P_i}{\partial Q_k^{3\phi}} = \mathrm{Re}\left\{ \frac{\alpha}{\left(V_i^t\right)^* TV_i} diag(V_i) MV_i^* \right\} \tag{B.16}$$

$$\frac{\partial Q_i}{\partial Q_k^{3\phi}} = \mathrm{Im}\left\{ \frac{\alpha}{\left(V_i^t\right)^* TV_i} diag(V_i) MV_i^* \right\} \tag{B.17}$$

- Current-controlled VSC with BPSC or SRFPIC

$$\frac{\partial P_i}{\partial P_k^{3\phi}} = \mathrm{Re}\left\{ \frac{\alpha}{\left(V_i^t\right)^* A V_i} diag(V_i) A^* V_i^* \right\} \tag{B.18}$$

$$\frac{\partial Q_i}{\partial P_k^{3\phi}} = \mathrm{Im}\left\{ \frac{\alpha}{\left(V_i^t\right)^* A V_i} diag(V_i) A^* V_i^* \right\} \tag{B.19}$$

$$\frac{\partial P_i}{\partial Q_k^{3\phi}} = \mathrm{Re}\left\{ \frac{j\alpha}{\left(V_i^t\right)^* A V_i} diag(V_i) A^* V_i^* \right\} \tag{B.20}$$

$$\frac{\partial Q_i}{\partial Q_k^{3\phi}} = \mathrm{Im}\left\{ \frac{j\alpha}{\left(V_i^t\right)^* A V_i} diag(V_i) A^* V_i^* \right\} \tag{B.21}$$

B.2 Voltage sensitivity matrices with respect to the three-phase power of a DG

Using the power injection sensitivity matrices, the voltage sensitivity matrices are calculated as

$$\frac{\partial \theta}{\partial P_{DGs}^{3\phi}} = \left[\frac{\partial \theta}{\partial P} \quad \frac{\partial \theta}{\partial Q}\right]\left[\frac{\partial P}{\partial P_{DGs}^{3\phi}} \quad \frac{\partial Q}{\partial P_{DGs}^{3\phi}}\right]^t \tag{B.22}$$

$$\frac{\partial \theta}{\partial Q_{DGs}^{3\phi}} = \left[\frac{\partial \theta}{\partial P} \quad \frac{\partial \theta}{\partial Q}\right]\left[\frac{\partial P}{\partial Q_{DGs}^{3\phi}} \quad \frac{\partial Q}{\partial Q_{DGs}^{3\phi}}\right]^t \tag{B.23}$$

$$\frac{\partial |V|}{\partial P_{DGs}^{3\phi}} = \left[\frac{\partial |V|}{\partial P} \quad \frac{\partial |V|}{\partial Q}\right]\left[\frac{\partial P}{\partial P_{DGs}^{3\phi}} \quad \frac{\partial Q}{\partial P_{DGs}^{3\phi}}\right]^t \tag{B.24}$$

$$\frac{\partial |V|}{\partial Q_{DGs}^{3\phi}} = \left[\frac{\partial |V|}{\partial P} \quad \frac{\partial |V|}{\partial Q}\right]\left[\frac{\partial P}{\partial Q_{DGs}^{3\phi}} \quad \frac{\partial Q}{\partial Q_{DGs}^{3\phi}}\right]^t \tag{B.25}$$

where

$\frac{\partial \theta}{\partial P_{DGs}^{3\phi}}$, $\frac{\partial \theta}{\partial Q_{DGs}^{3\phi}}$: voltage angle sensitivity matrices with respect to three-phase active and reactive power outputs of DGs

$\frac{\partial \theta}{\partial P}$, $\frac{\partial \theta}{\partial Q}$: voltage angle sensitivity matrices with respect to active and reactive power injections

$\frac{\partial |V|}{\partial P_{DGs}^{3\phi}}$, $\frac{\partial |V|}{\partial Q_{DGs}^{3\phi}}$: voltage magnitude sensitivity matrices with respect to three-phase active and reactive power outputs of DGs

$\frac{\partial |V|}{\partial P}$, $\frac{\partial |V|}{\partial Q}$: voltage magnitude sensitivity matrices with respect to active and reactive power injections

The voltage angle and magnitude sensitivity matrices with respect to the active and reactive power injections can be obtained from the inverse matrix of Jacobian matrix. For three-phase analysis, the bus admittance matrix used to calculate the Jacobian matrix is calculated using the primitive admittance matrix and the bus incidence matrix [69].

Appendix C. Detailed Data of Case Study

C.1 Initial state of the volt/var control devices

Table C.1 Initial reactive power outputs of DGs

Case	DG 1	DG 2	DG 3
1	12.0 kVAr	118.3 kVAr	−118.3 kVAr
2	124.9 kVAr	169.0 kVAr	107.0 kVAr
3	268.9 kVAr	268.9 kVAr	169.6 kVAr

Table C.2 Initial state of ShC 1

Case	Phase A	Phase B	Phase C
1	Closed	Closed	Closed
2	Closed	Open	Closed
3	Open	Open	Open

Table C.3 Initial tap positions

Device	Case 1			Case 2			Case 3		
	Phase A	Phase B	Phase C	Phase A	Phase B	Phase C	Phase A	Phase B	Phase C
OLTC 1	4	2	3	4	2	3	3	2	2
SVR 1	−3	–	–	−3	–	–	−1	–	–
SVR 2	−1	–	−1	−1	–	−1	−1	–	0
SVR 3	1	−1	0	1	−1	0	0	2	0

C.2 References of the volt/var control devices for the effect of the DG model

C.2.1 Balanced model

Table C.4 Reactive power references for DGs: balanced model

Case	DG 1	DG 2	DG 3
1	44.7 kVAr	118.3 kVAr	−113.4 kVAr
2	150.5 kVAr	169.0 kVAr	136.8 kVAr
3	234.4 kVAr	268.9 kVAr	75.4 kVAr

Table C.5 References for ShC 1: balanced model

Case	Phase A	Phase B	Phase C
1	Closed	Closed	Closed
2	Closed	Open	Closed
3	Open	Open	Open

Table C.6 References for tap changers: balanced model

Device	Case 1			Case 2			Case 3		
	Phase A	Phase B	Phase C	Phase A	Phase B	Phase C	Phase A	Phase B	Phase C
OLTC 1	1	−1	0	0	−1	−1	0	−2	−1
SVR 1	−3	–	–	−2	–	–	−2	–	–
SVR 2	−1	–	−1	−1	–	0	−1	–	0
SVR 3	1	−1	0	0	2	0	1	0	2

C.2.2 Proposed model

Table C.7 Reactive power references for DGs: proposed model

Case	DG 1	DG 2	DG 3
1	80.1 kVAr	118.3 kVAr	23.5 kVAr
2	150.2 kVAr	169.0 kVAr	91.2 kVAr
3	265.5 kVAr	267.2 kVAr	185.4 kVAr

Table C.8 References for ShC 1: proposed model

Case	Phase A	Phase B	Phase C
1	Closed	Closed	Closed
2	Closed	Closed	Closed
3	Open	Closed	Closed

Table C.9 References for tap changers: proposed model

Device	Case 1			Case 2			Case 3		
	Phase A	Phase B	Phase C	Phase A	Phase B	Phase C	Phase A	Phase B	Phase C
OLTC 1	1	−2	0	0	−2	−1	0	−3	−2
SVR 1	−4	–	–	−2	–	–	−2	–	–
SVR 2	−2	–	−2	−1	–	0	−1	–	0
SVR 3	1	0	−1	1	−1	0	3	−1	−1

C.3 References of the volt/var control devices for the effect of the two-segment *Q–P* droop control method

C.3.1 Fixed reactive power control

Table C.10 Reactive power references for DGs: fixed reactive power control

Case	DG 1	DG 2	DG 3
1	64.2 kVAr	104.7 kVAr	3.2 kVAr
2	169.0 kVAr	151.5 kVAr	149.7 kVAr
3	184.7 kVAr	223.8 kVAr	251.1 kVAr

Table C.11 References for ShC 1: fixed reactive power control

Case	Phase A	Phase B	Phase C
1	Closed	Closed	Closed
2	Open	Open	Closed
3	Open	Open	Open

Table C.12 References for tap changers: fixed reactive power control

Device	Case 1			Case 2			Case 3		
	Phase A	Phase B	Phase C	Phase A	Phase B	Phase C	Phase A	Phase B	Phase C
OLTC 1	2	−1	1	2	0	0	2	0	1
SVR 1	−4	–	–	−3	–	–	−2	–	–
SVR 2	−2	–	−2	−1	–	0	−1	–	−1
SVR 3	1	0	−1	3	2	0	2	0	2

C.3.2 Fixed voltage control

Table C.13 Voltage references for DGs: fixed voltage control

Case	DG 1	DG 2	DG 3
1	0.9726 p.u.	0.9744 p.u.	0.9767 p.u.
2	0.9755 p.u.	0.9793 p.u.	0.9767 p.u.
3	0.9806 p.u.	0.9795 p.u.	0.9763 p.u.

Table C.14 References for ShC 1: fixed voltage control

Case	Phase A	Phase B	Phase C
1	Closed	Closed	Closed
2	Closed	Open	Closed
3	Open	Open	Open

Table C.15 References for tap changers: fixed voltage control

Device	Case 1			Case 2			Case 3		
	Phase A	Phase B	Phase C	Phase A	Phase B	Phase C	Phase A	Phase B	Phase C
OLTC 1	1	−2	0	0	−1	−1	0	−2	−1
SVR 1	−4	–	–	−2	–	–	−2	–	–
SVR 2	−2	–	−1	−1	–	0	−1	–	−1
SVR 3	1	1	0	0	2	1	1	0	1

C.3.3 Two-segment *Q–P* droop control

Table C.16 References for DGs: two-segment Q–P droop control

Case	References	Distributed generator		
		DG 1	DG 2	DG 3
1	P_{ref}^{Q-P} (kW)	360.0	360.0	360.0
	Q_{ref}^{Q-P} (kVAr)	80.1	118.3	23.5
	R^{+} (kVAr/kW)	0.4087	0.4173	0.3686
	R^{-} (kVAr/kW)	0.5109	0.5157	0.5684
2	P_{ref}^{Q-P} (kW)	514.3	514.3	514.3
	Q_{ref}^{Q-P} (kVAr)	150.2	169.0	91.2
	R^{+} (kVAr/kW)	0.4256	0.4288	0.4763
	R^{-} (kVAr/kW)	0.7132	0.7164	0.6835
3	P_{ref}^{Q-P} (kW)	818.2	818.2	818.2
	Q_{ref}^{Q-P} (kVAr)	265.5	267.2	185.4
	R^{+} (kVAr/kW)	0.3931	0.3918	0.4571
	R^{-} (kVAr/kW)	0.16640	0.6694	0.6888

Table C.17 References for ShC 1: two-segment Q–P droop control

Case	Phase A	Phase B	Phase C
1	Closed	Closed	Closed
2	Closed	Closed	Closed
3	Open	Closed	Closed

Table C.18 References for tap changers: two-segment Q–P droop control

Device	Case 1			Case 2			Case 3		
	Phase A	Phase B	Phase C	Phase A	Phase B	Phase C	Phase A	Phase B	Phase C
OLTC 1	1	−2	0	0	−2	−1	0	−3	−2
SVR 1	−4	–	–	−2	–	–	−2	–	–
SVR 2	−2	–	−2	−1	–	0	−1	–	0
SVR 3	1	0	−1	1	−1	0	3	−1	−1

국 문 초 록

최근 분산전원의 배전계통 연계가 지속적으로 증가하고 있다. 분산전원의 연계는 공급 신뢰도를 향상시킬 수 있으며 송배전 손실과 투자 비용을 감소시킬 수 있다. 하지만, 태양광발전과 같이 출력변동이 심한 분산전원의 연계는 배전계통 전압관리에 새로운 문제를 유발한다. 이에 따라 분산전원을 포함한 배전계통의 안정적이며 경제적인 운영을 위하여 정보통신기술과 전력기술을 융합한 차세대 배전계통 운영시스템이 도입되고 있다. 차세대 배전계통 운영시스템에서는 배전계통의 다양한 정보를 취득하고 분석할 수 있으며, 분산전원을 포함한 배전계통 운영자원의 원격제어가 가능하다.

Conservation voltage reduction (CVR)은 배전계통의 전압 및 무효전력 제어기법 중 하나로 배전계통에서 소비되는 에너지를 감소시키는 것을 목적으로 한다. 네트워크 모델 기반 CVR 기법은 중앙제어 방식으로 CVR을 구현하는 기법으로 배전계통 운영시스템에서 주기적으로 최적 조류계산을 이용하여 전압 및 무효전력 제어기기들의 지령값을 도출한다. 네트워크 모델 기반 CVR 기법을 사용면 CVR 효과를 극대화할 수 있음에도 불구하고, 구현을 위해 통신 인프라 시스템과 추가적인 배전계통 해석 프로그램이 필요하기 때문에 현재는 많이 사용되고 있지 않다. 하지만, 차세대 배전계통 운영시스템에서는 네트워크 모델 기반 CVR 기법을 구현하기 위한 기본적인 기능을 제공하기 때문에 네트워크 모델 기반 CVR 기법은 차세대 배전계통 운영시스템에서 사용될 것으로 전망되고 있다. 따라서, 본 논문에서는 분산전원을 포함한 배전계통의 네트워크 모델 기반 CVR 기법에 대한 연구를 진행하였다.

분산전원의 연계가 네트워크 모델 기반 CVR에 미치는 영향을 분석하였다. CVR은 배전계통의 전압을 낮게 제어하기 때문에 부하의 변동이나 네트워크 모델의 오차로 인하여 발생할 수 있는 저전압을

방지하기 위해 최적 조류계산에서 사용되는 전압의 하한을 실제 하한보다 높게 설정한다. 최적 조류계산에서 사용되는 전압 하한이 실제 하한에 가까울수록 CVR 효과는 향상된다. 분산전원이 연계되는 경우, 최적 조류계산에서 사용되는 전압 하한은 분산전원 모델의 오차를 반영하여 증가되어야 한다. 또한, CVR 기능의 실행 주기 사이에 분산전원의 출력 변동으로 발생할 수 있는 저전압을 방지하기 위해 전압 하한은 증가되어야 한다. 따라서, 분산전원을 포함한 배전계통의 CVR 효과를 향상시키기 위해서는 정확한 분산전원의 모델과 분산전원의 출력변동으로 발생할 수 있는 저전압을 방지하기 위한 분산전원의 로컬 제어기법이 필요하다.

정상상태 해석에서 분산전원은 일반적으로 분산전원 연계시스템의 모델만으로 모델링한다. 본 논문에서는 분산전원의 연계시스템으로 많이 사용되는 전압형 컨버터의 3상 정상상태 모델을 제안하였다. 컨버터의 상별 출력은 유·무효전력 지령값, 필터 임피던스, 연계지점의 전압, 센서 위치, 출력 제어 기법에 의해 결정된다. 이를 반영하여 전류원을 포함한 두 개의 등가회로와 전류원의 출력 전류식을 제안하였다. 제안한 모델을 사용한 조류계산의 결과와 PSCAD 시뮬레이션의 결과를 비교하여 모델의 정확도를 검증하였다.

CVR 실행 주기 사이의 분산전원 출력 변동으로 발생할 수 있는 저전압을 방지하고 CVR 효과를 향상시키기 위해 분산전원의 새로운 무효전력 제어기법을 제안하였다. 제안된 기법은 전압 측정값을 사용하지 않는 기법으로 일반적인 분산전원의 배전계통 연계기준을 만족시킨다. 제안한 기법에서 유효전력과 무효전력의 관계는 유·무효전력 지령값과 두 개의 droop 계수에 의해 결정되는 두 개의 선분으로 나타내어진다.

본 논문에서는 제안한 분산전원 모델과 무효전력 제어기를 고려한 배전계통 운영시스템의 CVR 기능을 제안하였다. 제안한 CVR 기능의 목적은 송전계통으로부터 유입되는 유효전력을 최소화시키는 전압 및 무효전력 제어기기들의 지령값과 제안한 무효전력 제어기의 droop 계수를 계산하는 것이다. 기존의 네트워크 모델 기반 CVR

기법과 동일하게 제안한 CVR 기능에서는 최적 조류계산을 이용하여 지령값을 도출한다. 하지만, 전압 및 무효전력 제어기기들의 빈번한 지령값 변동을 방지하기 위해 최적 조류계산에서 분산전원의 출력 측정값 대신에 확률밀도함수의 기댓값을 사용하였다. 한편, droop 계수는 최적 조류계산에서 도출된 배전계통의 최적 상태와 전압 민감도를 사용하여 계산된다.

마지막으로 3기의 분산전원을 포함한 IEEE 123-node test feeder를 이용한 사례연구를 통해 제안한 기법들을 사용함으로써 CVR 효과가 향상됨을 확인하였다.

주요어:

분산전원, 배전계통 운영시스템, 전압 및 무효전력 제어, 드룹 제어

학 번: 2006 - 21324